Kinematic and Kinetic Gait Analysis to Quantify Locomotor Function in Pre-Clinical Models of the Rodent Hindlimb

---

A Thesis

Presented to:

the faculty of the School of Engineering and Applied Science

University of Virginia

---

in partial fulfillment of the requirements for the degree

Master of Science

by

W. Brody Hicks

May 2023

APPROVAL SHEET

This thesis is submitted in partial fulfillment of the requirements for the degree of

Master of Science (Mechanical and Aerospace Engineering)

Author Signature: 

This Thesis has been read and approved by the examining committee:

Committee Chair: Richard W. Kent, PhD

Committee Member: George J. Christ, PhD

Committee Member: Matthew B. Panzer, PhD

Accepted for the School of Engineering and Applied Science:

Jennifer L. West, School of Engineering and Applied Science
May 2023

Abstract

The rodent hindlimb is a popular animal model for evaluating the effects of various musculoskeletal pathologies in a pre-clinical setting. Furthermore, rodent gait analyses have become a preferred strategy for identifying and quantifying the functional impacts of these pathologies. However, many of the currently utilized methods in rodent gait analysis are limited, providing only surface level insights into gait compensation strategies and pathologic movement function. In human motion analysis, joint kinematics and kinetics are the gold standard metric for evaluating movement function in both normal and pathologic populations, as they provide mechanistic insights into the underlying causes behind movement patterns. The ability to utilize these methods in rodent studies will elucidate specific functional deficits caused pathology and offer a more robust evaluative metric for quantifying the efficacy of proposed treatment strategies. Thus, the purpose of this thesis was to develop the necessary tools to measure 3-D joint kinematics and kinetics during rodent gait in order to provide a more comprehensive analysis of both healthy and pathologic rodent gait.

3-D motion capture and concurrent ground reaction force (GRF) data were collected on healthy Lewis rats during over-ground walking. This data was implemented into a custom musculoskeletal model of the rodent hindlimb to quantify 3-D joint kinematics and kinetics for normal rodent walking. The resulting normative dataset demonstrated significant variability in the rodents' self-selected walking speeds, consistent with variability reported in the literature. A follow-up study was performed to investigate the effects of walking speed on gait parameters. Linear regression equations were presented, describing the relationships between walking speed and several kinematic, kinetic, and spatiotemporal gait parameters. Additionally, these relationships were used to develop a normalization scheme which minimizes variability in the presentation of kinematic and kinetic curves. Finally, the developed methodologies were utilized to evaluate functional impacts of two different hindlimb volumetric muscle loss injury models and quantify the treatment efficacy of a regenerative therapeutic. The results from this study demonstrated the usability of a motion capture and musculoskeletal modeling approach for providing detailed insights into injury response and recovery. This information can be leveraged into the development of treatment strategies focused on optimizing functional outcomes.

Acknowledgements

I would like to thank all those who have contributed their time and effort toward supporting me during my graduate work at the University of Virginia in pursuit of a M.S. in Mechanical Engineering. Specifically, I would like to acknowledge the members of my thesis examination committee: Dr. Rich Kent, Dr. George Christ, and Dr. Matthew Panzer, as well as my advisor, Dr. Shawn Russell. You have each provided invaluable feedback throughout this process, and I could not have completed this work without your expertise.

I would also like to thank Evan Dooley, Michael Rariden, and Xiao Hu for their friendship, support, and feedback on both a technical and personal level. In addition, I would like to thank Anna Workman, Caroline Nealon, Christian Tessman, Sydney Shriver, Olivia Sergent, and the numerous other members of the Motion Analysis and Motor Performance Lab and Laboratory of Regenerative Therapeutics for their help performing surgeries, collecting data, and providing assistance during data processing/analysis.

Table of Contents

List of Figures

1. Introduction

The rodent hindlimb is a popular animal model for evaluating a diverse set of musculoskeletal pathologies in a pre-clinical setting. Currently, there is a significant amount of research utilizing rodent models to investigate the efficacy of potential treatments before they are ready for clinical implementation. Because many of these pathologies result in significant functional impairments, rodent locomotion analyses have emerged as a preferred strategy for providing deeper insight into locomotor deficits and quantifying functional recovery. The ability to quantify and assess the specific functional deficits caused by a particular pathology is a critical step toward expediting the development of interventions to treat these pathologies.

In the clinic, human gait evaluations quantifying joint kinematics and kinetics serve as the gold-standard practice for analyzing movement pathology. Gait is often studied because it demonstrates the most basic, repeatable level of functional movement and can be reliably analyzed. Even still, normal walking is a sophisticated motion, incorporating complex movement dynamics and limb coordination. These complexities are further confounded by the addition of gait pathologies, where loss of function results in deviation from typical movement patterns. Joint kinetics outline the driving forces behind movement patterns, and are of critical importance for robustly quantifying compensation strategies after injury and evaluating the effectiveness of different treatments. While gait kinematics and kinetics have long been the gold-standard metrics in the clinic, they have been sparsely implemented in pre-clinical analyses of rodent locomotion. As a result, many of these studies are unable to offer specific insight into causes of gait adaptations. Incorporating these best practices into pre-clinical studies of rodent locomotion will allow for the use of comprehensive gait analyses that could illuminate the causes and effects of functional deficits and inform the development of interventions geared toward the restoration of

biomechanical function.

With this in mind, this thesis is focused on the development of the necessary tools to quantify and evaluate joint kinematics and kinetics during both healthy and pathologic rodent gait. This was accomplished by:

1. Applying gold standard 3-D motion capture and musculoskeletal modeling techniques to detect and quantify differences in gait between healthy and injured animals.
2. Developing a comprehensive database of kinematics and kinetics for healthy rat gait.
3. Using these methods to characterize changes in gait patterns when interventions are performed to treat injured (volumetric muscle loss) animals.

This work will ultimately provide insight into the development of advanced therapies and treatment strategies designed to restore biomechanical function.

2. Background & Literature Review

2.1 Musculoskeletal Modeling for Gait Analysis

In human movement research, gait analyses are useful tool for studying movement and quantifying functional deficits resulting from a particular injury or pathology. Several human studies have utilized comprehensive analyses of walking as a metric of functional movement quality (Robbins et al., 2016; Slater et al., 2017). Furthermore, dynamic musculoskeletal modeling approaches offer the ability to simulate internal joint information, providing detailed insights into the underlying causes of abnormal movement patterns. Specifically, inverse dynamic simulations utilize body segment kinematics and measured ground reaction forces to calculate a set of generalized forces necessary to match the accelerations obtained from inverse kinematics (Seth et al., 2011). Musculoskeletal simulation platforms such as OpenSim (Delp et al., 2007) have utilized a series of computational methods to further deconstruct joint moments determined from inverse dynamics in order to better understand the neuromuscular control strategies which produces coordinated movement. For example, static optimization methods work to distribute joint moments across a series of redundant muscle actuators by minimizing muscle activation, as described in (Crowninshield, 1978; Crowninshield & Brand, 1981; Kaufman et al., 1991; Seth et al., 2011). As a result, static optimization can provide accurate information regarding individual muscle forces which contribute to joint moments and the requisite muscle activations needed to achieve those muscle forces. In addition, algorithms such as computed muscle control simulations utilize static optimization, along with feedforward and feedback controls, in order compute a set of muscle excitations that drive a musculoskeletal model to match experimentally computed kinematics (Thelen et al., 2003; Thelen & Anderson, 2006). Clearly, musculoskeletal modeling simulation frameworks provide advanced

computational methodologies that are critical for thorough analyses of the mechanisms behind certain movement pathologies.

It has been shown that there are many similarities between the human lower extremity and the rodent hindlimb (Burkholder et al., 1994; DeLaurier et al., 2008). For this reason, rats are among the most common laboratory animals used in research into human movement and locomotion. Rats have been used to study a diverse set of movement pathologies in a pre-clinical setting, such as volumetric muscle loss (Aurora et al., 2014; Dienes et al., 2019; Passipieri et al., 2017; Wu et al., 2012), nerve injury (Allbright et al., 2018; Choe et al., 2011; Cooney et al., 2016; Kemp et al., 2013), ligament injury (Akamatsu et al., 2014; Black et al., 2011; Komatsu et al., 2016; Maerz et al., 2015), and osteoarthritis (Allen et al., 2012; Hamilton et al., 2015; Lakes & Allen, 2016). There is a significant amount of research underway geared toward designing and testing treatments for these pathologies by evaluating the recovery of movement function after some intervention. However, musculoskeletal modeling frameworks are only sparsely applied to these research arenas.

Applying the state-of-the-art gait analysis and musculoskeletal modeling methods to evaluate functional recovery in rats requires a model capable of providing insight into the mechanisms of gait adaptations. Johnson et al. (2008) developed a 3-D musculoskeletal model of the rodent hindlimb by experimentally determining hindlimb joint center locations and limb geometries via dissection. In addition, their study also determined the origin and insertion points for 39 hindlimb muscles and evaluated changes in muscle moment arms over a range of physiologically relevant joint angles. Finally, they examined how postural changes would alter the function of select muscles, finding that a transition from quadrupedal to bipedal posture significantly affected muscle function in a number of hindlimb muscles. In a later study, Johnson

et al. incorporated a lumped-parameter model of muscle (Schutte et al., 1993; Thelen et al., 2003; Zajac, 1989), combining muscle architectural measurements obtained from dissected rats with parameter values in the literature to calculate the following muscle-specific parameters: maximum isometric force, maximum shortening velocity, optimal fiber length, pennation angle at optimal length, and tendon slack length (Johnson et al., 2011). The physiological and morphological parameters of the model were validated by comparing EMG data collected during locomotion experiments to muscle activations obtained from static optimization simulations performed in OpenSim (Delp et al., 2007; Johnson et al., 2011; Kaufman et al., 1991).

While the Johnson et al. model is a necessary step toward a dynamic musculoskeletal model for evaluation rat motion, this model did not provide bio-fidelic inertial parameters for the body segments. While others have done this in for mice (Charles et al., 2018), no one has reported the inertial properties of the relevant bodies necessary for use in a musculoskeletal model of the rat hindlimbs. Inertial forces are an important component of inverse dynamic calculations, and as such, it is necessary to define proper body segment inertial parameters before evaluating resulting joint moments. To this end, prior work in the UVA Laboratory of Regenerative Therapeutics has compiled limb anthropometry from the fresh cadavers of a group of 17 female Lewis rats (**Figure 1**). The hindlimbs were scanned, weighed, and segmented to obtain mass, center of mass, and moments of inertia for each of the hindlimb body segments. These inertial characteristics were applied to an augmented version of the Johnson rat hindlimb model (Dienes et al., 2019) prior to inverse dynamic calculations in order to compute the first set of 3-D hindlimb joint moments for the rat during normal locomotion (Dienes & Hicks et al., 2022). More information on the specific processes for obtaining hindlimb inertial parameters can be found in **Chapter 3**.

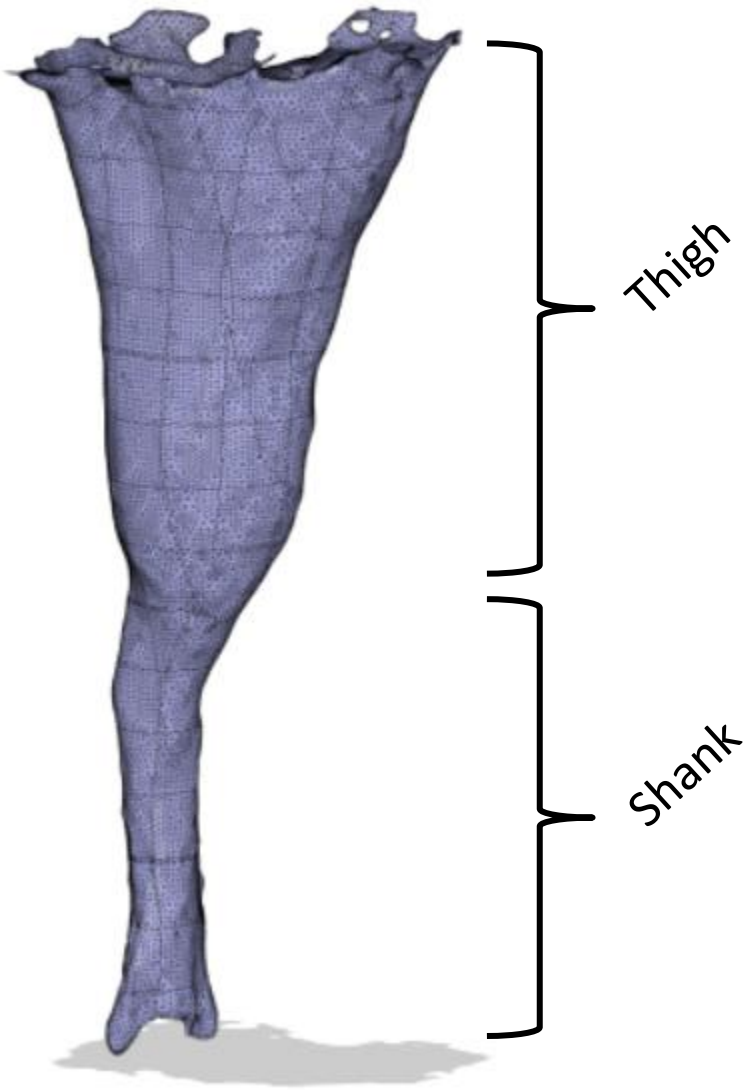

Figure 1: Representative 3-D reconstruction of the thigh and shank of a scanned rat hindlimb.

Musculoskeletal modeling simulation results are heavily dependent on the data used as input into the model. To obtain joint moments from inverse dynamics, one must know all joint motion as well as the external loads (e.g. ground reaction forces) that produce that joint motion. In human movement analysis, the current gold-standard method for obtaining motion and forces is 3-D motion capture with concurrent ground reaction force measurement. In order to apply these best practices to analyze rat locomotion, it is necessary to address the unique challenges that arise in rodent motion capture that are not present in human data collection. When collecting 3-D motion capture data on humans, several reflective markers are placed on bony, anatomical landmarks to track the motion of each desired body segment. Reflective markers are placed on bony landmarks to minimize the skin and soft tissue artifacts and allow for optimal body segment tracking. In rodents, the significant skin and soft tissue artifact present in the hindlimb presents a challenge for tracking the motion of the knee.

(Bauman & Chang, 2010) demonstrated the significant effects that skin and soft tissue artifacts have on kinematics of the hindlimb during treadmill gait. They compared differences sagittal plane kinematics between 2-D X-ray fluoroscopy, skin-derived marker positions, and triangulation of the knee joint center position, reporting that skin-derived methods yield high kinematic errors when compared to bone-derived methods. X-ray fluoroscopy is the highest accuracy method for calculating joint kinematics as it allows for direct tracking of the skeletal anatomy, and as such, deviations from bone-derived kinematics should be taken with a grain of salt. Although the approach utilized in this work employs skin-derived methods for measuring body segment motion, the hindlimb kinematics reported in this thesis compare favorably to Bauman and Chang's bone-derived kinematics, while also providing information about non-sagittal planes of motion (**Figure 2**). Furthermore, Bauman and Chang's fluoroscopy method

examined rodent gait in 2-D, considering only the sagittal plane. This work has demonstrated that rodent gait incorporates significant out-of-plane motion (e.g. hip abduction) (Dienes & Hicks et al., 2022), which is not accounted for in 2-D methods. Failure to account for these out-of-plane kinematics in 2-D fluoroscopy likely explains the increased excursion observed in the knee in the proposed 3-D methods.

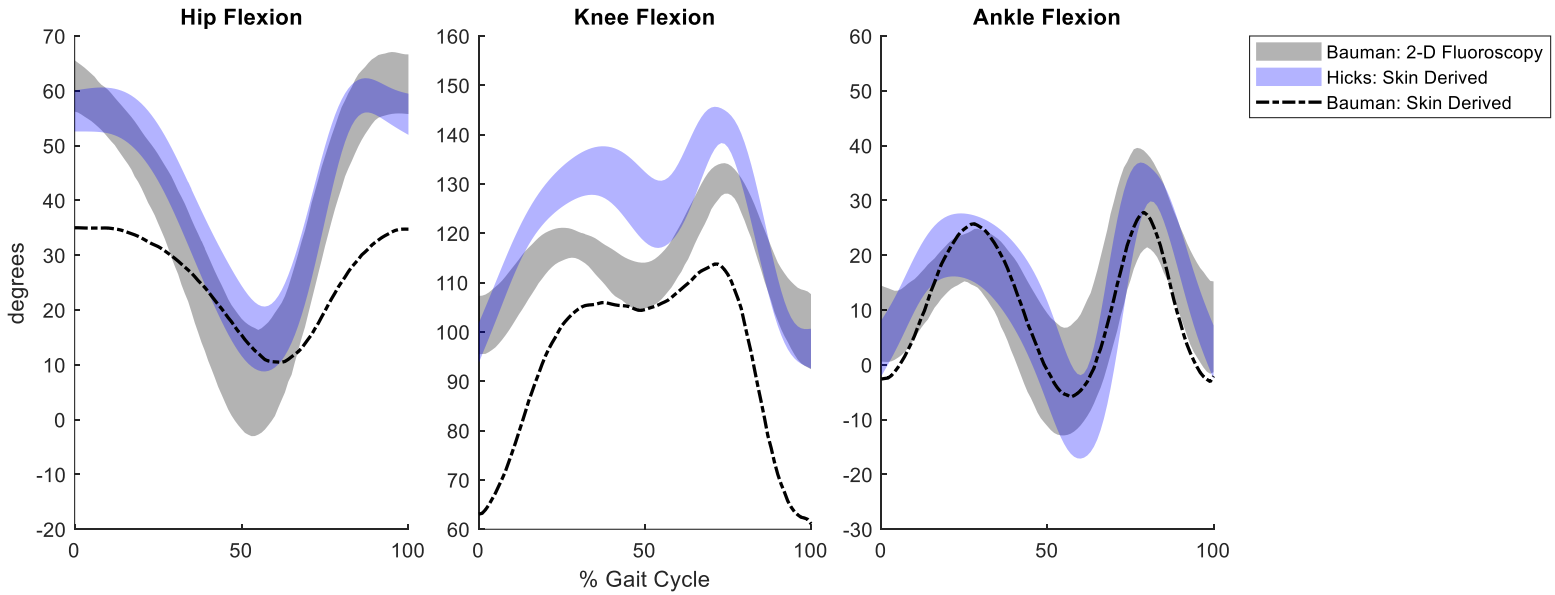

Figure 2: Comparison of healthy sagittal plane hip, knee, and ankle kinematics versus X-ray fluoroscopy and skin-derived kinematics from Bauman et al (2010). Data was mined using Graph Grabber software (V2.0.2, Quintessa Ltd., Oxfordshire, UK) and transformed from joint extension angles to joint flexion angles. Ankle kinematics were transformed to account for difference in definition of neutral position between models.

2.2 Introduction to Quadruped Gait

Quadrupedal locomotion is characterized by distinctly different limb coordination sequences and foot contact patterns that bipedal locomotion. In human locomotion, ambulation methods are typically defined as walking, skipping, hopping, and running. In four-legged locomotion, the introduction of ground contact with the forelimbs increases the number of gaits utilized by quadruped species. Similarly to humans, quadruped gaits are precisely differentiated by their distinct combinations of limb-support patterns. Hildebrand (1989) characterized vertebrate quadruped gaits as a continuum which is traversed situationally by many mammalian and reptilian species and which typically shifts with walking speed. Prior studies have also shown that transitions between gaits naturally occur at different speeds in rats (Gillis & Biewener, 2001).

There is agreement in the literature regarding the distinction of the many forms of quadruped gaits (Alexander, 1984; Gambariāǹ, 1974; Hildebrand, 1980, 1989; Hoyt & Taylor, 1981). The common terminologies used to denote the distinct gaits characterized by different limb-support sequences in order of increasing speed are as follows: walk, amble, trot, pace, canter, transverse gallop, rotary gallop, bound, and pronk (Alexander, 1984). Some mammalian species also perform a pronking gait, in which all four limbs leave the ground at the same time, similar to hopping or bounding in humans (Alexander, 1984). Alexander (1984) diagrammed the typical relative phases of the feet during each distinct quadrupedal gait (see **Figure 3**). It should be noted that the walk and amble consist of the same foot-fall pattern, with amble occurring at faster speeds and resulting primarily in dual limb-support, as opposed to triple limb-support in walking (Alexander, 1984). As such, for the purpose of this thesis, “walking” or “lateral sequence walking” will be used interchangeably to refer to both walking and ambling gait.

Hildebrand (1989) also pointed out that different species avoid some gaits on the continuum in accordance with anatomical constraints and economy of effort, as the maneuverability and stability that a given gait provides will be dependent on body type. Alexander (1984) also addresses this phenomenon, pointing out that differences in typical posture between reptiles, cursorial mammals, and non-cursorial mammals results in different gait selection. It is critical to understand the distinction between gaits, as changes in symmetry, limb placement, or timing of gait events that occur with different gaits could be misidentified as gait pathology if not considered.

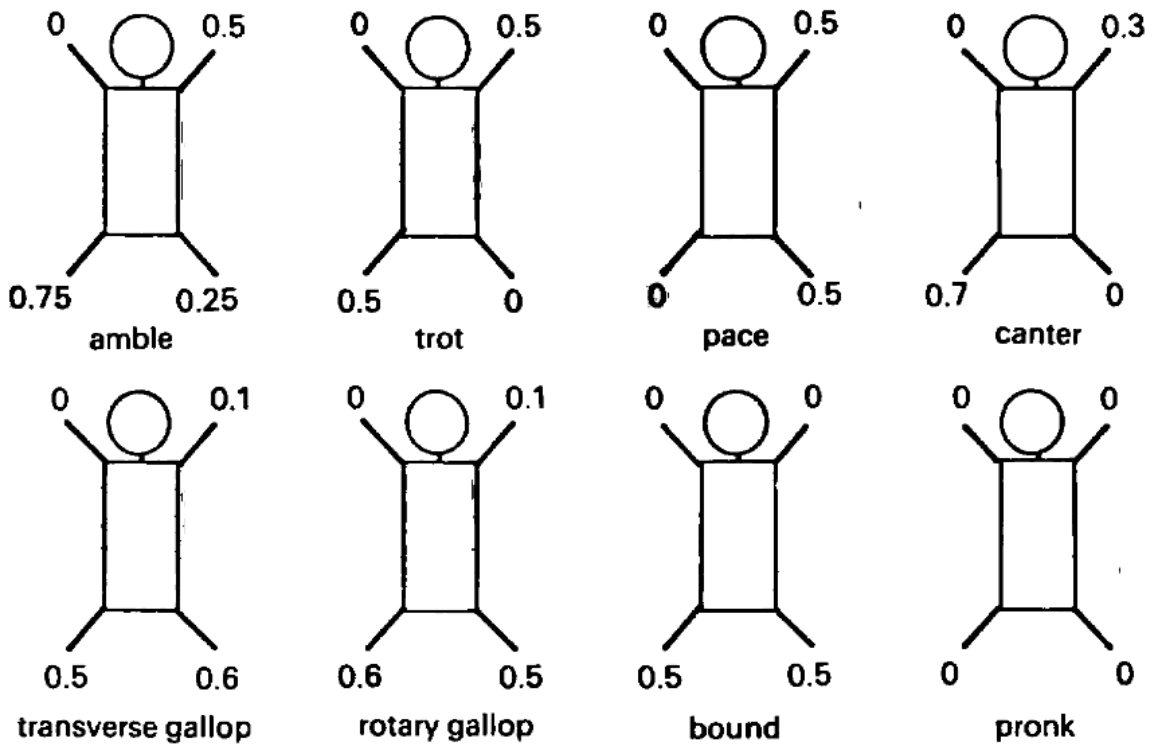

Figure 3: Figure adapted from Alexander et. al (1984). Diagrams of quadrupedal running gaits showing typical relative phases of the feet interacting with the ground throughout a gait cycle.

(Gillis & Biewener, 2001) reported that rats primarily use lateral sequence walking, trotting, and transverse galloping gait at slow, intermediate, and fast speeds, respectively. The foot strike sequence and limb support pattern for each gait is shown in **Figure 4**, in accordance with the method used by Hildebrand (1980) to visualize temporal gait sequences in quadrupeds. Furthermore, Gillis and Biewener described speed intervals at which their rats transitioned between gaits: lateral sequence walk (17-48 cm/s), trot (59-71 cm/s), and gallop (60-122 cm/s). Interestingly, there is a notable break between the speeds for the walk and trot phases, as well as a notable overlap between the speeds for the trot and gallop phases. These results make more sense when visualizing the change from one gait to another as a continuum (Hildebrand, 1989) rather than a discrete shift at a given speed. Size-differences and limb length discrepancies between their study animals is also a potential reason for the overlapping bins, where larger animals are able to maintain a slower gait at faster speeds and a smaller animal would need to transition to a faster gait to maintain that speed. Because of this, it is likely that the treadmill speed chosen to elicit a particular gait was animal-dependent, resulting in discontinuities in the reported bins. Due to the changes in step timing and limb placement between gaits, the resulting joint kinematics were shown to vary with each gait. Gillis and Biewener demonstrated this inter-gait variability by evaluating sagittal plane joint angles at the hip and knee for each gait. However, their study did not discuss any potential intra-gait kinematic variability that may exist within a particular gait phase. The large speed bins presented for each gait phase suggest that there could be a subtle transitioning effects within a gait that have not yet been characterized in the literature. The work presented in **Chapter 4** addresses this in detail.

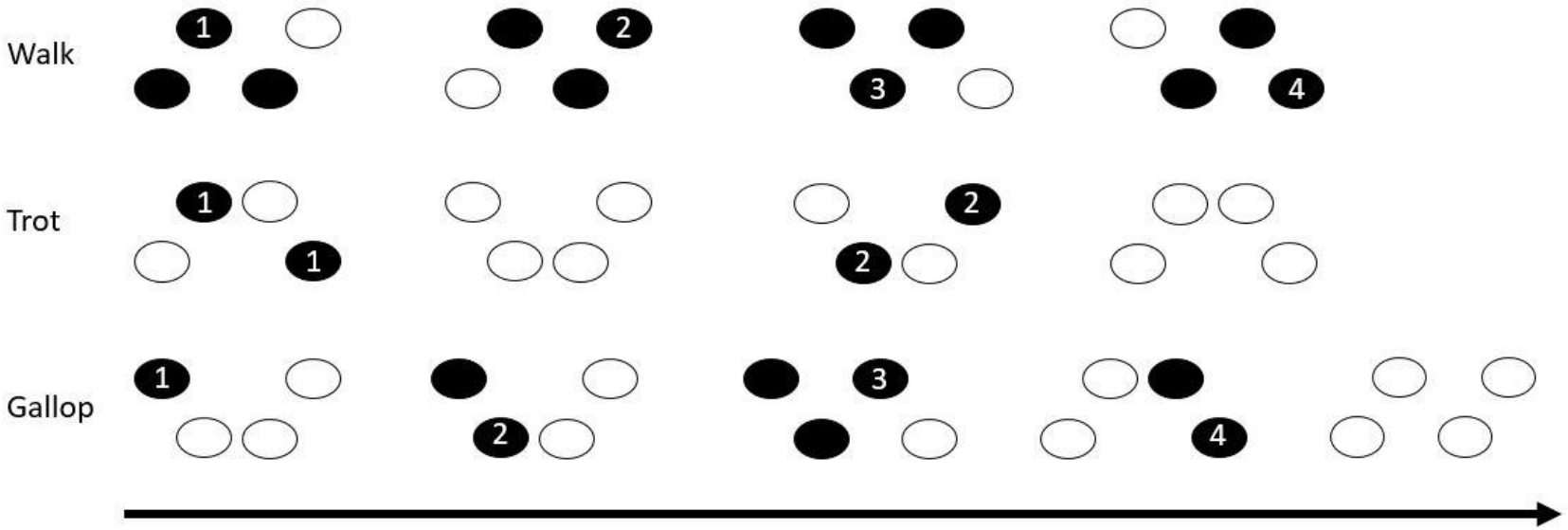

Figure 4: Limb support diagram for the lateral sequence walk, trot, and transverse gallop gaits used by rats during normal locomotion. Arrow indicates the direction of travel.

The complexities of quadrupedal locomotion are further exacerbated by the distinction between plantigrade, digitigrade, and unguligrade locomotion. These types of locomotion are solely based on the limb anatomy of the animal in question. Plantigrade refers to species that place the full length of their foot on the ground during each stride, such as humans, bears, or kangaroos. Digitigrade locomotion is performed by species that ambulate on their toes, such as canines or felines. Finally, unguligrade locomotion is performed by species that walk on hooves, such as equine species. It is important to note that during normal walking, the rat hindlimbs undergo digitigrade locomotion, spending most of stance in toe-support (Bennett et al., 2012). Understanding the specifics of rat locomotion are critical to developing realistic musculoskeletal models that can closely mimic the natural ranges of motion achieved by the rat during gait.

2.3 Rodent Gait Analysis in the Literature

2.3.1 Spatiotemporal Parameters

Due to the parallels between human and rat gait, studies evaluating the characteristics of rat locomotion have become popular for analyzing the effects of various conditions impacting locomotor function. Analyses of spatiotemporal gait parameters (STPs) such as stride length, walking speed, cadence, or stride time have been used to characterize changes in gait resulting from a variety of pathologies. Specifically, researchers have used STPs to characterize gait changes after osteoarthritis (Allen et al., 2011, 2012; Bonnet et al., 2015; Clarke et al., 1997; Ferland et al., 2011; Kloefkorn et al., 2015), rheumatoid arthritis (Berryman et al., 2009), spinal contusion (Beare et al., 2009; Bhimani et al., 2017), spinal cord injury (Alluin et al., 2011; Neckel et al., 2013), peripheral nerve lesion (Bennett et al., 2012), tibialis anterior volumetric muscle loss (Dienes et al., 2019), Parkinson's disease (Vlamings et al., 2007), and more. Additionally, STPs have been used to provide descriptive information about normal locomotion

(Canu & Garnier, 2009; Clarke & Parker, 1986; Garnier et al., 2008; Perrot et al., 2011).

Parameters such as stride length, stride time, cadence, velocity, duty factor, and step width have been well characterized in the literature for both healthy and pathologic rodent gait. Several proprietary systems have been developed to aid in the quantification of STPs, such as Digigait™, CatWalk (Hamers et al., 2001), and TreadScan™. More basic methods, such as recorded video or paw-print mapping with ink, have also been utilized to measure temporal or spatial parameters, respectively.

It can be difficult to contextualize STPs, because they are often interdependent on one other. For example, locomotion speed has been shown to be a confounder for other STPs in both normal and pathologic rodent gait (Herbin et al., 2007; Koopmans et al., 2007; Pereira et al., 2006). The relationships between speed and STPs such as stride length, stride time, cadence, and stance/swing have been well documented in the literature over a wide range of speeds. Specifically, it has been shown that faster speeds are driven by increased stride length and increased cadence (Batka et al., 2014; Clarke & Parker, 1986; Hruska et al., 1979). Stance time has also been shown to decrease as speed increases (Hruska et al., 1979). However, there is some debate in the literature about the dependence of swing time on speed. Some studies report that swing time decreases as speed increases, while other studies report no dependence on speed. A more detailed analysis of speed dependence on typically reported STPs was presented in (Batka et al., 2014). Prior research has also demonstrated large intra-animal and inter-animal speed variability in both normal and pathologic animals (Cendelín et al., 2010; Dienes et al., 2022; Koopmans et al., 2007). This could be due to the fact that the introduction of pathology has been shown to affect speed in both human and rodent gait (Koopmans et al., 2005; Mountney et al., 2013). Furthermore, Gillis and Biewener (2001) have demonstrated a significant speed

variability within normal walking gait, with fast walking speeds approximately 3x faster than slow walking speeds. As a result, it can be difficult to use STPs alone to quantify gait adaptations resulting from pathology. One of the primary purposes of this work is to provide a method to help dissect which gait changes occur due to spatiotemporal changes (specifically, walking speed), and which gait changes occur due to pathology (**Chapter 4**).

In addition, STPs have been shown to be dependent on a number of factors, including sex, age, weight, species, training history, and pathology (Dellon & Dellon, 1991; Koopmans et al., 2005; McIlwain et al., 2001; Wooley et al., 2009). Furthermore, a lack of reporting of animal size (i.e. limb length) presents additional challenges into the comparison of spatiotemporal data across experiments. In addition, not all studies reporting STPs consider gait phase when reporting parameters, so some results present in the literature may be muddled by the presence of data from multiple gait phases.

Some experiments analyzing rat locomotion control for speed by employing the use of a treadmill (Bauman & Chang, 2010; Dienes et al., 2019; Pereira et al., 2006). The use of a treadmill allows the researcher to apply a set speed across a study, which offers a convenient method for the standardization of some STPs. However, multiple studies have reported differences in STPs and hindlimb joint kinematics with treadmill walking when compared to over-ground walking, which they attribute to differences in proprioceptive and vestibular inputs (Herbin et al., 2007; Neckel, 2015; Pereira et al., 2006). For this reason, over-ground walking is typically preferred to forced-velocity walking, as it more closely approximates natural walking.

In summary, spatiotemporal analyses are useful for providing surface-level insight into the presence of gait pathology. However, they are often limited in the depth of analysis available from the results they produce, as they only provide information about the foot contacting the

ground. As a result, it is not possible to determine specific movement patterns or gait adaptations from STPs alone. Hence, different methods are needed to examine the impacts of a pathology in a systemic fashion.

2.3.2 Joint Kinematics

Joint kinematics are also frequently reported as a study parameter in rat locomotion analyses for both treadmill and over ground walking. For example, Alluin et al. (2011) investigated locomotor recovery in rodents with spinal cord injuries (SCI) using hindlimb joint kinematics, establishing a baseline of recovery after SCI necessary to evaluate the effectiveness of various therapeutic strategies in later experiments. Similarly, Dienes et al. (2019) examined quantified kinematic gait compensations after tibialis anterior volumetric muscle loss injuries. Several studies have characterized the joint kinematic response following peripheral nerve injury (Bauman & Chang, 2013; Bennett et al., 2012; Chang et al., 2009). Furthermore, several studies have quantified kinematics in normal populations, establishing a baseline for evaluating different injury models in comparative studies (Bauman & Chang, 2010; Canu & Garnier, 2009; Dienes et al., 2022; Filipe et al., 2006; Pereira et al., 2006; Thota et al., 2005). However, methodological differences between reported kinematics often lead to high variability in published datasets. There are several different methods typically used to quantify gait kinematics. As previously stated, Bauman et al. used 2-D X-ray fluoroscopy to describe differences between bone-derived kinematics and standard optical kinematics methods. This study presented the effects that incorrectly approximating joint center locations could have on resulting kinematics. However, many of the optical methods described in the literature involve detailed processes of marker digitization as opposed to established motion tracking software and an associated rigid-body model (Allen et al., 2012; Bennett et al., 2012; Pereira et al., 2006). Small changes in joint

approximations during this step will ultimately compound kinematic errors. Furthermore, many of these marker digitization methods result in 2-D kinematics and as such, are only able to examine sagittal plane kinematics. Utilizing 3-D motion capture technology offers the ability to examine joint angles in other planes of motion.

There are several other reasons that may explain kinematic variability in the literature. For instance, several experiments contain small group sizes and low volume of analyzed gait cycles (Andrada et al., 2013; Bennett et al., 2012) . This could be due to behavioral non-compliance in study animals, or limitations in data collection capabilities. Furthermore, comparison across different gait phases may also contribute to kinematic variability in the literature (Bauman & Chang, 2013; Gillis & Biewener, 2001). As stated, this thesis addresses and characterizes the intra-phase kinematic variability present when analyzing gait cycles at different walking speeds. Finally, each group has different criteria for including or excluding gait cycles from their analysis. In order to standardize the dataset, gait cycles exhibiting non-steady state behavior (e.g. rearing, stopping, jolting, turning, or sniffing) were removed. Other groups may have used different criteria to select gait cycles, which could also contribute to lack of agreement between kinematic curves.

2.3.3 Joint Kinetics

Studies evaluating kinetics (joint moments) during gait are less popular, likely due to increased efforts in both data collection and computational modeling required to obtain kinetics. To date, only a handful of groups have quantified joint kinetics during rodent locomotion (Andrada et al., 2010; Bennett et al., 2012). Still, gait kinetics are of critical importance for providing specific insights into the mechanisms of certain gait pathologies. While spatiotemporal and kinematic analyses offer important context towards the interpretation of gait results, they

alone are insufficient for addressing the underlying causes of gait pathology or describing why gait changes occur in the ways they do.

Joint kinetics provide a unique insight into the internal loads experienced during motion, which can be used to inform the design of therapeutics to treat pathologies. Despite the comprehensive benefits of quantifying joint kinetics, only a handful of groups have accurately reported kinetics during rodent locomotion. (Bennett et al., 2012) reported sagittal plane kinetics in the hip, knee, and ankle to address locomotor compensation strategies after peripheral nerve lesion, reporting significant changes in both timing and magnitude of the joint moments produced after gastrocnemius denervation. They demonstrated how the injured rats altered their gait in order to reduce loading on the hindlimb joints, and cited the inability of the gastrocnemius to actively contract as a reason for a delayed ankle plantarflexion moment during stance. While this study provides the most comprehensive analysis of pathologic gait compensation strategies, their 2-D kinematic data collection and reporting of results in the sagittal plane alone fail to address compensations that occur in non-sagittal planes. Andrada et al. (2010, 2013) reported joint moments for the hindlimbs and forelimbs during walking and climbing, commenting on the increased power demand to support locomotion at steeper inclines, with the purpose of applying their results into the design of biologically inspired climbing robots. However, they did not report the joint kinematics for their dataset, so it is difficult to contextualize the significance of their results.

The research in this thesis was conducted in part to develop a robust method for collecting, modeling, and comprehensively analyzing rodent gait kinetics by utilizing the current best practices in motion capture and musculoskeletal modeling. By reporting 3-D kinetics in this analyses, this work can provide deeper insight into the driving forces behind movement patterns

during gait, as well as more effectively analyze and interpret gait changes in movement that result from loss of function after injury.

2.4 An Introduction to Volumetric Muscle Loss

Additionally, this thesis applies the aforementioned analysis to quantify gait adaptations resulting from volumetric muscle loss (VML). VML is defined as the traumatic or surgical loss of skeletal muscle which results in functional impairment (Grogan & Hsu, 2011). VML can be caused by a variety of circumstances, including sport injuries, combat injuries, surgical procedures, disease, and congenital abnormalities. In VML, the musculoskeletal damage and tissue loss often exceeds the skeletal muscle's intrinsic capacity for regeneration, resulting in permanent functional deficits (Carnes & Pins, 2020; Dienes et al., 2019). Current clinical treatments for VML have demonstrated limited efficacy in restoring muscle function or improving muscle strength (Aurora et al., 2014; Garg et al., 2015). As a result, significant preclinical research is being done to develop therapies for regeneration of lost muscle volume. These different treatment strategies have incorporated combinations of hydrogels, scaffolds, and exercise regimens to aid in recovery of muscle volume (Corona et al., 2013; Dziki et al., 2016; Grasman et al., 2015; Passipieri et al., 2019; X. Wu et al., 2012). Specifically, significant research has gone in to the development of a tissue engineered muscle repair (TEMR) construct (Corona et al., 2012, 2013; Machingal et al., 2011).

The typical methods for quantifying functional recovery in rodents with volumetric muscle loss injuries have primarily focused on force production capability of the injured area (Aurora et al., 2014; Corona et al., 2013; Garg et al., 2015; Mintz et al., 2016; Passipieri et al., 2017). While these studies provide important information regarding force production and reconstitution of muscle volume, they typically focus on the target area in isolation and do not

provide a comprehensive functional evaluation. Furthermore, several human movement studies have demonstrated that improved force generation does not necessarily lead to increased movement function (Buchner et al., 1997; Damiano et al., 2010, 2013; Damiano & Abel, 1998; Topp et al., 1993). As a result, it is necessary to incorporate a robust alternative for evaluating functional recovery that goes beyond quantification of force production ability. To address this, the work presented in this thesis applies a 3-D motion capture and musculoskeletal modeling approach to analyze movement function during gait in rats with VML injuries and treated with TEMR construct. In addition, the analysis of functional recovery in treated rats will provide meaningful insight into the future development of therapies to treat VML.

3. Comprehensive Dynamic and Kinematic Analysis of the Rodent Hindlimb During Over Ground Walking

Disclaimer: some passages have been quoted verbatim from [Dienes, J.*, Hicks, B.*, Slater, C., Jansen, K., Christ, G. J., & Russell, S. D., **Comprehensive dynamic and kinematic analysis of the rodent hindlimb during over ground walking**. *Scientific Reports, 12*(1), 19725. https://doi.org/10.1038/s41598-022-20288-3 *These authors contributed equally to this work.

3.1 Introduction

The rat hindlimb is a frequently utilized model system for studying diverse conditions/pathologies spanning volumetric muscle loss (Aurora et al., 2014; Corona et al., 2013; Passipieri et al., 2017; X. Wu et al., 2012), nerve injury (Allbright et al., 2018; Choe et al., 2011; Cooney et al., 2016; Kemp et al., 2013), ligament injury (Akamatsu et al., 2014; Black et al., 2011; Komatsu et al., 2016; Maerz et al., 2015), and osteoarthritis (Allen et al., 2012; Hamilton et al., 2015; Lakes & Allen, 2016). These studies have been very effective in demonstrating the translational potential of regenerative therapeutics, changing the approach to pre-clinical research from evaluating only the local impact of an injury or treatment to evaluating the entire systemic response. These advances have opened the door to numerous future studies in the realm of regenerative therapeutics and rehabilitation that are designed to better understand and predict the outcomes of musculoskeletal pathologies modeled in the rat hindlimb.

In this setting, spatiotemporal parameters (Allen et al., 2011, 2012; Berryman et al., 2009; Bonnet et al., 2015; Lakes & Allen, 2016; Pereira et al., 2006; Schmidt & Fischer, 2011; Simjee et al., 2007) and ground reaction forces (GRFs) (Allen et al., 2012; Andrada et al., 2010, 2013; Howard et al., 2000; Muir & Whishaw, 1999a, 1999b; Roemhildt et al., 2010; Webb et al., 2011) utilize well characterized methodologies, are easy data to obtain, and have both been collected on rats during over-ground walking. These methods are the most sensitive to detecting

changes in rat walking mechanics and weight distribution and have been shown to provide insight into compensation mechanisms related to spinal and knee injuries. Joint kinematics have also been investigated extensively, but there is a lack of congruence in the literature due to vast methodological differences. These inconsistencies include small group sizes, low volumes of analyzed gait cycles, and highly variable data collection and reconstruction protocols, each of which can contribute to the range of outcomes observed in the kinematic literature. But despite the broad differences in the literature, kinematics have been used on a case-by-case basis to evaluate changes in joint motion due to arthritis, spinal injury, or varied walking conditions.

As such, kinematics are an incredibly useful evaluative tool. However, muscle moments (kinetics) are the driving force behind movement patterns, and to date kinetics have not been reliably calculated in rodent models and researchers have primarily relied on spatiotemporal parameters, ground reaction forces (GRFs) , or 1-D kinematics (joint angles) (Alluin et al., 2011; Bauman & Chang, 2013; Bennett et al., 2012; Canu & Garnier, 2009; Garnier et al., 2008; Pereira et al., 2006) to quantify gait changes. In this regard, 3-D kinetics have long been the gold standard of human motion capture and movement analysis, and if these methods are effectively applied to rats then pathological effects and treatment efficacy can be more extensively evaluated. Kinetics offer insight into neuromuscular recruitment strategies and joint loading that no other analysis can provide. Kinetics are the gold standard for human motion analysis for that reason, they allow you to see how the muscles and joints in a system are working to actuate a motion and quantify the forces being experienced at each of the joints. They also provide insight into joint loading, compensation patterns, joint power, and efficiency of motion that would otherwise be undetectable.

The ability to calculate this data for pre-clinical rat models of any neuromusculoskeletal

pathology will be beneficial. However, this work is specifically relevant to the continued efforts to expand the application of multiscale biomechanical metrics for improved evaluation of volumetric muscle loss (VML) injury and repair. Here improved maximum isometric torque has been the primary evaluative metric, even though increases in this measure alone do not necessarily result in improved functional outcomes (Buchner et al., 1997; Damiano et al., 2010, 2013; Damiano & Abel, 1998; Topp et al., 1993). With the large volume of pre- clinical studies being performed on the rat hindlimb to assess muscle, nerve, tendon, and joint injuries, kinetic insight into the extent of injury and the road to recovery would be instrumental in fine-tuning rehabilitative and regenerative therapies.

The primary objective of this study was to develop the necessary modeling methods, as well as a robust database for thorough analysis of the rat hindlimb during normal over-ground walking. To this end, this work added all the previously described metrics to the newly developed method for calculating 3-D joint-by-joint kinetics. Because of the overall utility of spatiotemporal parameters and GRFs, these metrics were reported within the normative database. In short, in this report, advanced motion capture and modeling techniques were implemented to capture concurrent marker and GRF data for rat locomotion. Then, 3D joint kinetic data was calculated, which represents a breakthrough in rodent gait analysis. The current findings confirm and extend previous work, and have major implications for improved treatment of extremity trauma. Specifically, utilizing the information obtained from this more comprehensive biomechanical approach, including thorough kinetic analysis, has the potential to maximize functional recovery and minimize the adoption of compensatory gait patterns by providing detailed insight into the true mechanisms responsible for diminished function following various injuries and pathologies.

3.2 Methods

3.2.1 Experimental Outline

A total of 24 female Lewis rats (Charles River Laboratories) weighing 180.0 ± 7.8 g at 12 weeks of age were tasked with walking on a 2.7 m instrumented walkway. Motion data was collected and analyzed using a combination of Vicon Nexus motion capture software and OpenSim musculoskeletal modeling. Concurrent GRF data was acquired from these trials using ATI Nano43 sensors with a load range ± 9 N (ATI Industrial Automation NC), load cells were mounted with top plates (85 × 50 mm) flush to the walkway surface. Trials were excluded if the rats stopped in the middle of the collection volume, turned around, accelerated below or beyond a lateral sequence walk (17 cm/s < walking velocity < 48 cm/s) (Gillis & Biewener, 2001). Spatiotemporal parameters were acquired from marker positions calculated by Vicon Nexus. Kinetics were calculated by performing inverse dynamics to combine the joint angle and GRF data in the OpenSim model (Dienes et al., 2019; Johnson et al., 2008). Spatiotemporal parameters, joint kinematics, GRFs, joint moments, and joint powers were compiled and averaged to create a normative database for rodent gait. Data presented represents a mean of 8.6 ± 3.6 steps/rat averaged for kinematic and spatiotemporal calculations and a mean of 2.1 ± 1.1 averaged foot strikes recorded on the force plates per rat for kinetic calculations.

3.2.2 Animal Care

This study was conducted in compliance with the Animal Welfare Act, the Implementing Animal Welfare Regulations, in accordance with the principles of the Guide for the Care and Use of Laboratory Animals, and in accordance with ARRIVE guidelines. The University of Virginia Animal Care and Use Committee approved all animal procedures. Animals were pair housed in a vivarium accredited by the American Association for the Accreditation of Laboratory Animal

Care, and they were provided with food and water ad libitum.

3.2.3 Acquisition of Motion Data and Ground Reaction Forces

Rats were briefly anesthetized with 2–3% isoflurane in 100% oxygen prior to motion capture and shaved to allow proper placement of the motion capture marker set (Dienes et al., 2019) illustrated in **Figure 5**. 3 mm and 5 mm reflective markers were placed on the bony landmarks of the left anterior superior iliac crest (LASI), right anterior superior iliac crest (RASI), spine (L6 vertebra), tail (5th caudal vertebra), hip, lateral knee, ankle, and distal end of the fifth metatarsal. Rats were allowed to recover from anesthesia on a heated mat before being placed in the instrumented walkway. Marker data was collected using a 7-camera setup (Vicon, Oxford Metrics, Oxfordshire, ENG) collecting at 200 Hz and GRF data was collected at 1000 Hz. A threshold of 0.07 N, normal to the surface, was used to define foot contact and toe off for each step. After data collection the animals were returned to the vivarium.

3.2.4 Limb Morphometrics and MoI/CoM Calculations

We have previously developed a kinematic model for the rat hindlimb (Johnson et al., 2008), but in order to calculate accurate kinetic data, it is necessary to have both GRF data and inertial data of the rat limbs. To determine inertial parameters, rat limb morphometrics were compiled from the fresh cadavers of 17 female Lewis rats of the same strain, lot, and provider. For each segment of the hindlimb (thigh, shank, foot), lengths (joint center to joint center), and masses were measured, normalized by body weight, and averaged (n = 34 limbs) to obtain morphometric data. Normalized data was then scaled to extrapolate values for animals of different body weights. This data was used to inform accurate weights for each limb segment within the OpenSim model prior to scaling of the model to each individual rat. Centers of mass (CoM) and moments of inertia (MoI) were determined by performing laser surface scans of the

left and right hindlimbs of a representative sample of 5 female Lewis rats. The scans were meshed, smoothed, and reconstructed using Meshmixer software (Autodesk, USA). Reconstructed limbs were then converted to solids and segmented into thigh, shank, and foot sections using Fusion 360 software. Segment masses were extrapolated based on the body weight of the scanned animal and equations determined from the rat limb morphometric database. Once these parameters were established, CoM and 3-D MoI data for each limb segment was calculated by Fusion 360 (Autodesk, USA). CoM and MoI values were normalized to body weight and limb length then averaged so they could be applied to animals over a range of sizes. These inertial measurements were added to the OpenSim model prior to performing inverse kinematics and inverse dynamics.

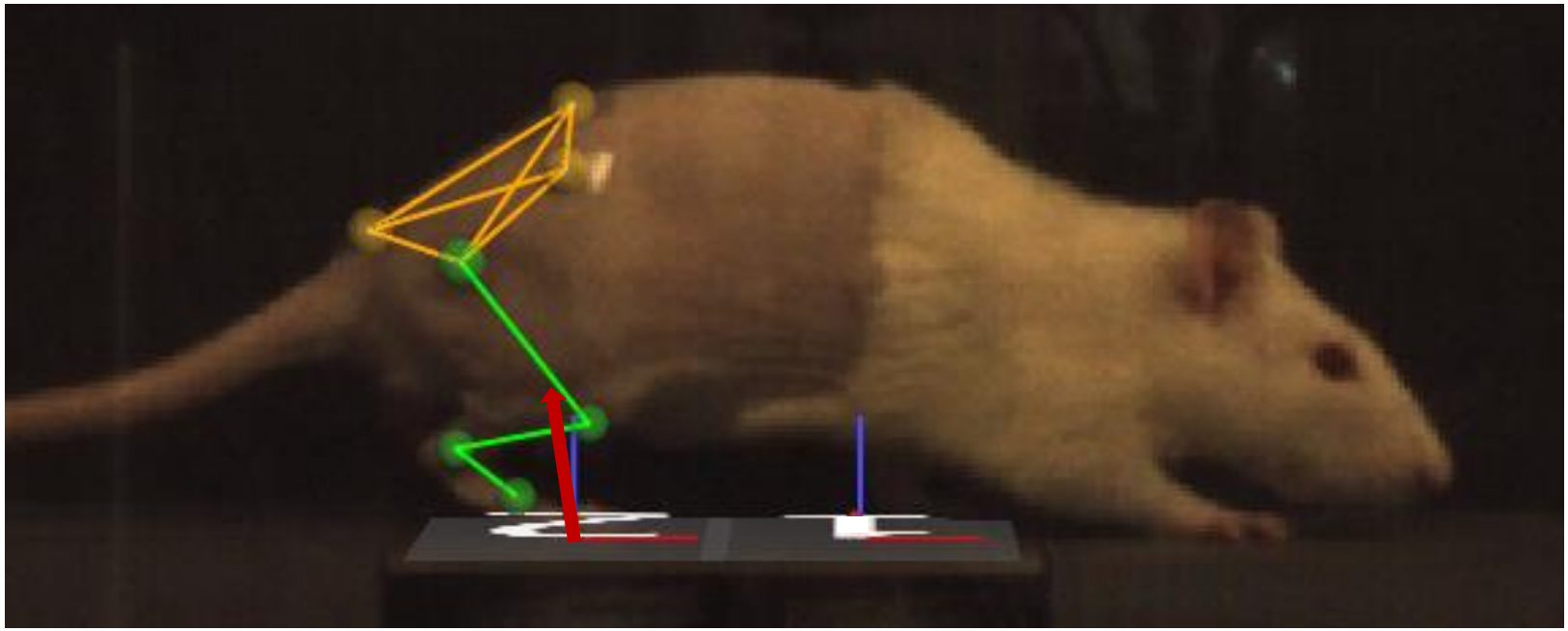

Figure 5: Vicon Nexus 2.7.1 3-D overlay of motion capture marker placements. 3 mm markers were applied to the lateral knee, ankle, and fifth metatarsal (TOE) of the female Lewis rats. 5 mm markers were applied to the spine, hip, right anterior superior iliac crest (RASI), and the tail. Motion capture data was collected at 200 Hz and ground reaction force (GRF) data was collected at 1000 Hz. Data was reconstructed using Vicon Nexus 2.7.1 resulting in overlays of joint positions and GRF vector projections as shown above.

3.2.5 Inverse Kinematics

Gait events and marker identification was completed in Nexus (Vicon, Oxford Metrics, Oxfordshire, ENG) and marker position data was lowpass filtered at 15 Hz (fourth order, two-way Butterworth). Inverse kinematic modeling was performed in OpenSim using a validated rat hindlimb kinematic model (Dienes et al., 2019; Johnson et al., 2008). Calculated CoM and MoI data for the limb segments of each rat was programmed into the kinematic model prior to modeling any walkway trials. This model consisted of four segments (pelvis, femur, tibia, foot) and each joint was modeled as free, ball, revolute, and revolute, respectively. This facilitated a full 3D analysis of hip and pelvis kinematics and kinetics while reducing the number of motion markers required. The knee and ankle joint were limited to flexion and extension due to their small size and marker placement limitations.

3.2.6 Inverse Dynamics

Kinetics were calculated using inverse dynamics by pairing 3D GRF data with con-currently captured motion data using a validated rat hindlimb kinematic model in OpenSim (Johnson et al., 2008). For all simulations the segment coordinates and their relationship to bony landmarks were defined in the method of Johnson (Johnson et al., 2008). In addition, all joint angles were calculated using a Sagittal, Frontal, Transverse Euler sequence. Calculated CoM and MoI data for the limb segments of each rat was programmed into the kinematic model prior to modeling any walkway trials. Marker data and measured GRFs were extracted from Nexus for each trial. Marker data was lowpass filtered at 15 Hz and GRFs were lowpass filtered at 100 Hz (fourth order, two-way Butterworth). This data was then imported into OpenSim and models were run using the inverse dynamics solver, using the methods of Winter (Winter, 2009), resulting in 3D joint moments at the hip and sagittal plane joint moments at the knee and ankle.

Kinetics for each rat were normalized by dividing the net internal load calculated at each joint by each rat's body mass, which was recorded at the time of collection. Utilizing the joint moments and the sagittal plane joint kinematic data, power absorption/dissipation at each joint was calculated in the sagittal plane over the whole stride using Eq. (1).

$$P = M\omega \tag{1}$$

where P is joint power, M is joint moment, and ω is joint angular velocity.

3.3 Results

We successfully collected morphometric, spatiotemporal, kinematic, and 3D ground reaction force data on twenty-four 12-week old female Lewis rats. The joint angles, joint moments, and power data are reported over a full gait cycle, heel strike to heel strike of the right leg.

3.3.1 Spatiotemporal Parameters and Morphometrics

Morphometric data for segment lengths as well as spatiotemporal parameters for stride length, velocity, cadence, and stance percentage are shown in **Table 1**.

Parameter	Value
Stride Length (mm)	122.4 ± 4.8
Velocity (cm/sec)	30.3 ± 3.4
Cadence (steps/min)	294.2 ± 30.7
Stance Percentage (%)	63.9 ± 3.6
Thigh Segment Length (mm)	31.5 ± 2.7
Shank Segment Length (mm)	32.3 ± 2.2
Foot Segment Length (mm)	35.9 ± 2.2

Table 1: Spatiotemporal parameters and morphometric measurements.

3.3.2 Kinematics

Kinematic trajectories of each joint are reported in **Figure 6**. The mean pelvis excursions were 6.90 ± 2.46 degrees pitch, 20.86 ± 3.57 degrees roll and 21.90 ± 3.25 degrees yaw. The

ranges of motion for hip flexion, adduction, and rotation were 54.0 ± 7.7, 10.1 ± 3.8, and 30.1 ± 5.9 degrees. The average maximum flexion of the hip was 50.1 ± 5.3 degrees. The ranges of motion for knee and ankle flexion were 40.6 ± 8.2 and 30.0 ± 9.9 degrees. Average maximum flexions for the knee and ankle were 142.7 ± 4.4 and 48.6 ± 3.8 degrees.

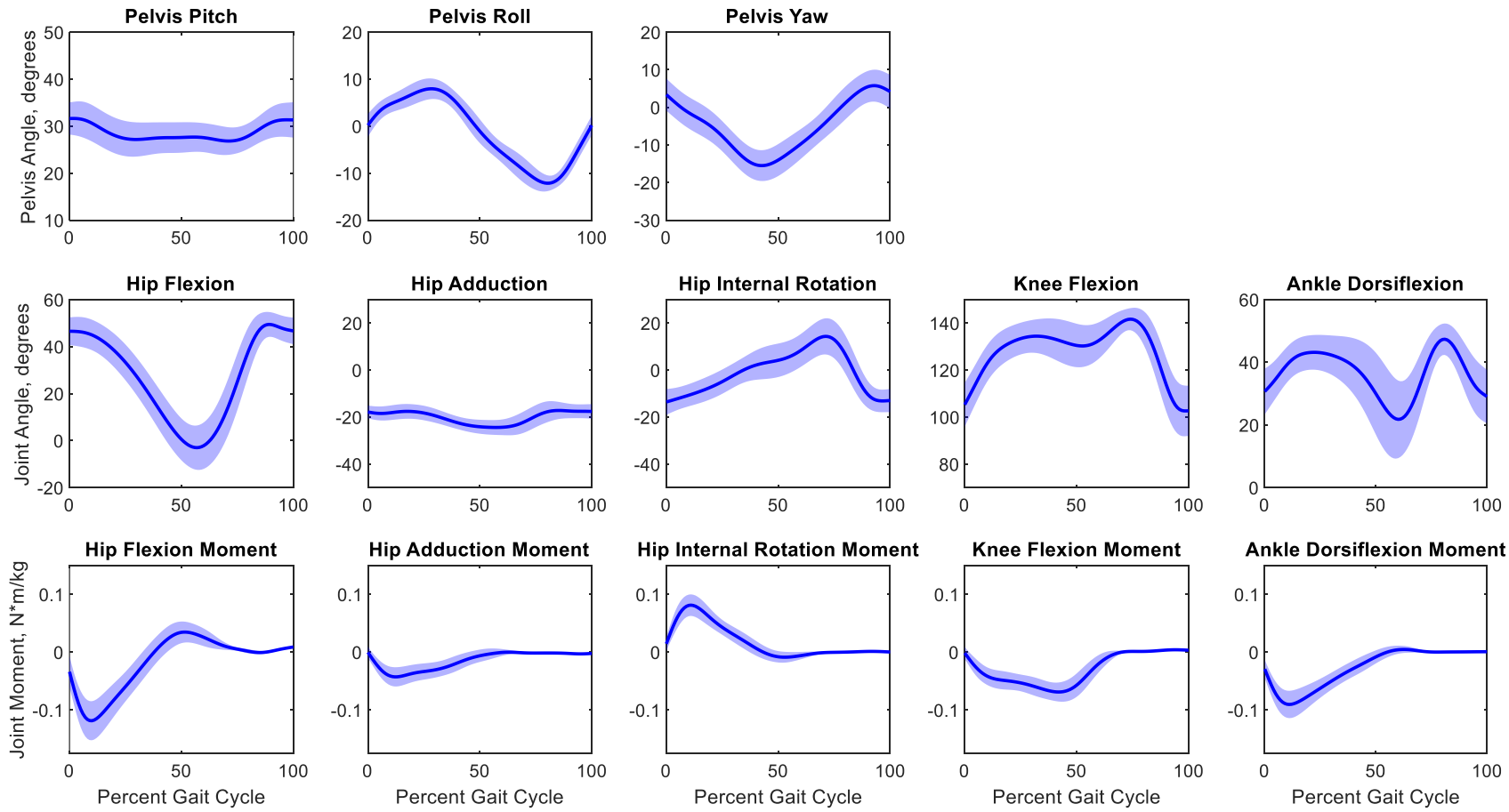

Figure 6: Kinematic (joint angles, top 2 rows) and kinetic (joint moments, bottom row) curves for healthy female Lewis rats. Curves are shown as mean +/- 1SD for pelvic rotation, hip flexion angle/moment, hip adduction angle/moment, hip internal rotation angle/moment, knee flexion angle/moment, and ankle dorsiflexion angle/moment

3.3.3 Ground Reaction Forces

GRFs measured from the load cells are shown in **Figure 7**. The average peak anterior and posterior forces were -1.298 ± 0.697 N/kg and 0.499 ± 0.384 N/kg. The average peak medial and lateral forces were 0.047 ± 0.077 N/kg and -1.092 ± 0.319 N/kg. The average peak vertical force was 6.628 ± 0.758 N/kg.

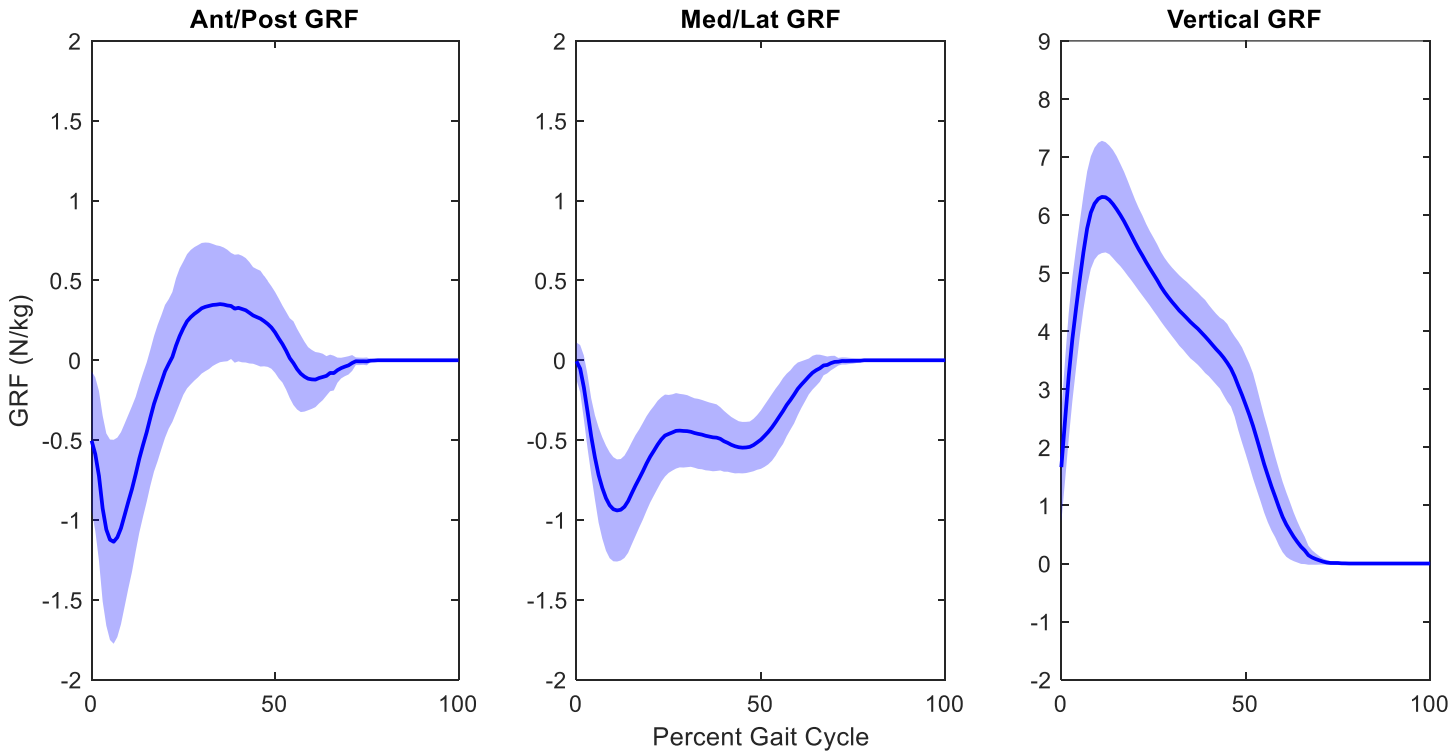

Figure 7: Ground reaction force (GRF) curves for healthy female Lewis rats. Curves are shown as mean +/- 1SD for all three axes (x, y, z). The X-axis is represented by the anterior/posterior forces, the Y-axis is represented by the medial/lateral forces, and the Z-axis is represented by the vertical forces. Data was compiled from load-cell footstrikes from 24 female Lewis rats.

3.3.4 Joint Moments and Power

Joint moments calculated from concurrently recorded joint kinematics and GRFs are shown in **Figure 6**, **Figure 8** shows a stick diagram for a typical gait cycle. The average peak flexion and extension moments about the hip were 0.040 ± 0.016 and -0.122 ± 0.035 Nm/kg. The average peak adduction and abduction moments about the hip were 0.005 ± 0.006 and -0.045 ± 0.016 Nm/kg. The average peak internal rotation moment about the hip was 0.084 ± 0.019 Nm/kg. The average peak extension moment about the knee was -0.072 ± 0.016 Nm/kg. The average peak flexion and extension moments about the ankle were 0.007 ± 0.005 and -0.093 ± 0.023 Nm/kg. Power, in the sagittal plane, was calculated from joint moments and angular velocity data extracted from kinematics, and the results are shown in **Figure 9**. Average peak generation and absorption power for the hip was 0.326 ± 0.147 W/kg and -0.226 ± 0.126 W/kg. Average peak generation and absorption power for the knee was 0.200 ± 0.187 W/kg and -0.316 ± 0.128 W/kg. Average peak generation and absorption power for the ankle was 0.100 ± 0.061 W/kg and -0.374 ± 0.221 W/kg.

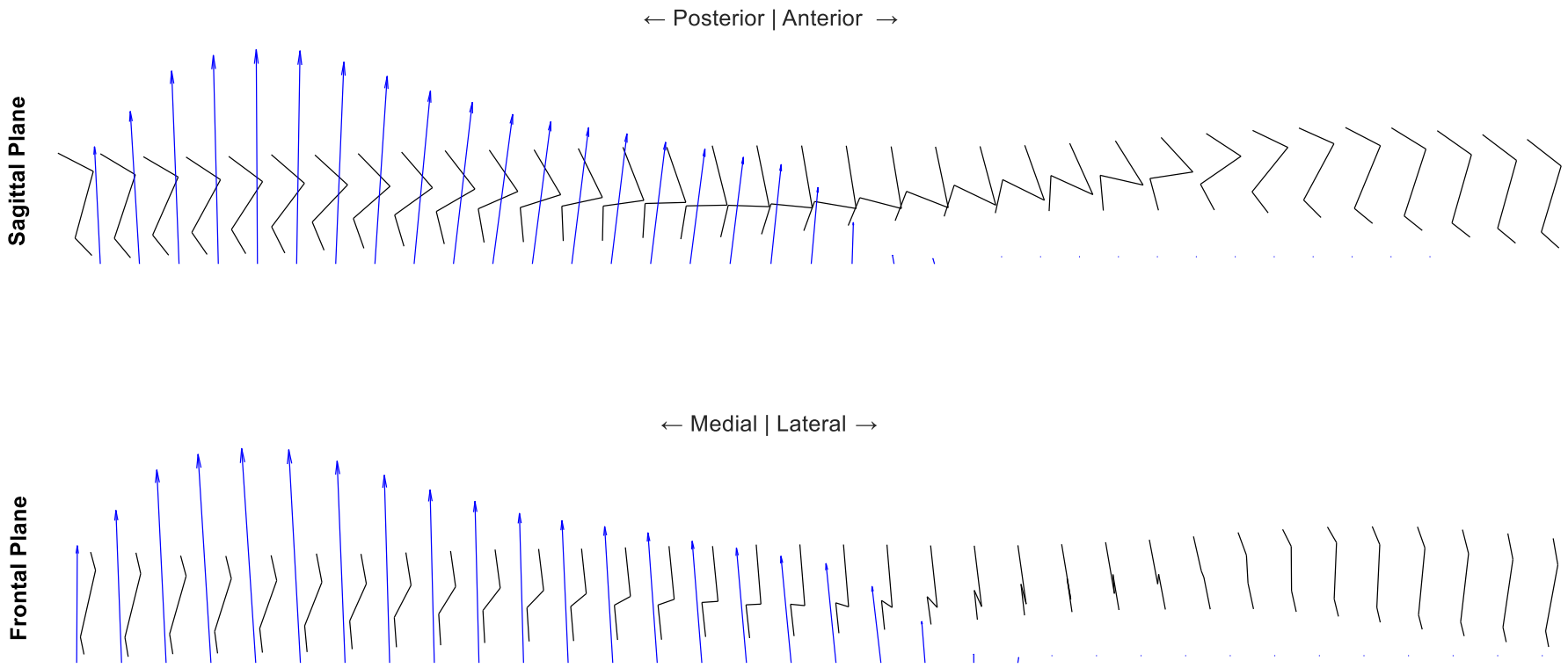

Figure 8: Stick figure of sagittal (top) and frontal (bottom) joint configurations and ground reaction force. One typical stride shown, initial heel strike to final heel strike.

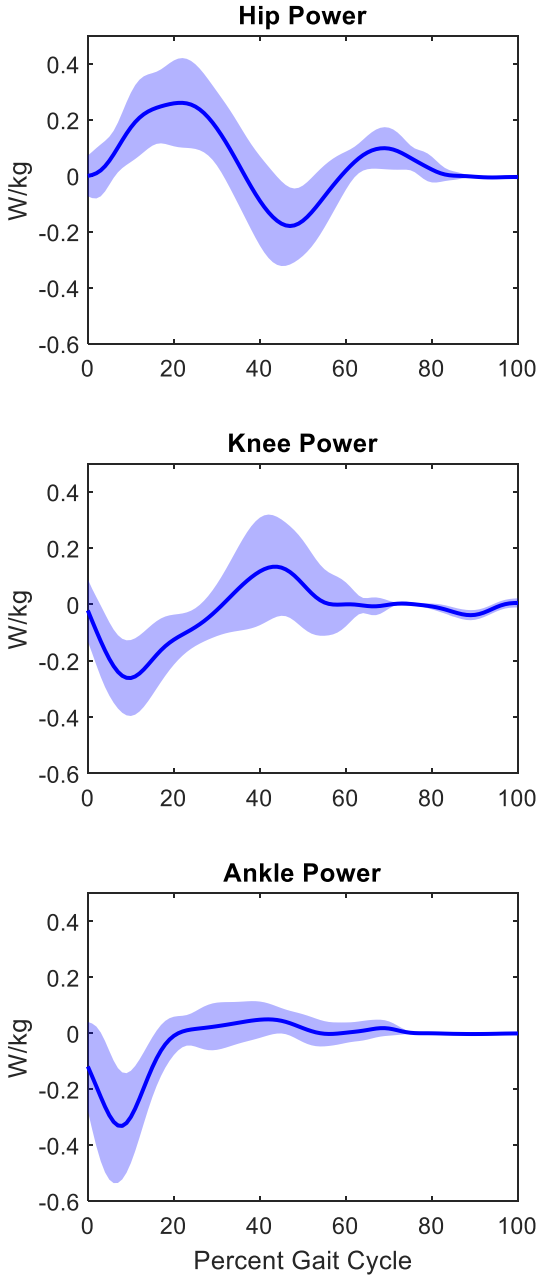

Figure 9: Joint power curves for healthy female Lewis rats. Curves are shown as mean +/- 1SD for all three joints (hip, knee, ankle) for 24 healthy female Lewis rats. All power plots represent the sagittal plane (i.e. flexion/extension) in W/kg.

3.4 Discussion

The methods and data developed in this work should expand the scope for evaluation of pre-clinical rat studies to include any neuromusculoskeletal pathology of interest modeled in the rat hindlimb. Moreover, this analysis can now be accomplished at a much deeper level of biomechanical and physiological detail. This is the first study to report 3D kinematics and 3D kinetics from concurrently recorded motion capture marker and GRF data. This work also compiled data from a larger cohort of animals than previous kinematic or kinetic studies (24 vs. an average of 11) (Allen et al., 2011; Alluin et al., 2011; Balbinot et al., 2018; Bauman & Chang, 2013; Bennett et al., 2012; Dienes et al., 2019; DiGiovanna et al., 2016; Filipe et al., 2006; Garnier et al., 2008, 2008; Gravel et al., 2010; João et al., 2010; Nakahata et al., 2018; Nica et al., 2017; Pereira et al., 2006; Perrot et al., 2011; Schmidt & Fischer, 2011; Thota et al., 2005). As such, this dataset is able to more rigorously describe the expected variance across the population for typical hindlimb data.

The current study also extends previous work that has documented measurable kinematic differences after surgical creation of VML injuries (Dienes et al., 2019). More specifically, the methods developed herein will allow for the expansion of biomechanical analyses to the 3-D kinetic implications of these injuries; including but not limited to, changes in motor control, neuromuscular recruitment patterns, and compensation strategies in response to VML injury or other musculoskeletal pathologies. As such, the impacts of various conditions/pathologies and their treatments can now be analyzed on both a joint-by-joint and systemic basis, providing a complete picture of the response to injury, as well as the recovery timeline. Furthermore, these new kinetic measures promote the linking of functional recovery at the whole animal level (motion) to observations at the cell and tissue level (both histology and muscle contractility) –

providing unprecedented multiscale biomechanical insight into the mechanisms responsible for both VML-related functional deficits, as well as mechanisms of functional recovery upon application of regenerative therapeutics.

3.4.1 Spatiotemporal Parameters

Though kinematics and kinetics were the primary outcomes of this study, spatiotemporal parameters remain important metrics. Spatiotemporal data includes parameters such as stride length, velocity, cadence, and time in swing, stance, and double vs. single support, all of which have been successfully calculated for both treadmill and over-ground walking (Allen et al., 2011, 2012; Andrada et al., 2013; Bennett et al., 2012; Berryman et al., 2009; Boettger et al., 2009; Bonnet et al., 2015; Clarke et al., 1997; Coulthard et al., 2003; Ferland et al., 2011; Fu et al., 2012; Górska et al., 2007; Kloefkorn et al., 2015; Lakes & Allen, 2016; Pereira et al., 2006; Schmidt & Fischer, 2011; Simjee et al., 2007). This data is important to evaluate because it is the most sensitive to changes in gait mechanics, despite providing little insight to the mechanisms driving the change. From the list above, walking speed and step length are the best identifiers of gait abnormalities, but they offer little insight to underlying cause. Recorded values (shown in **Table 1**) are similar to previously reported values for rat walking, demonstrating that the rats in this study were moving at a reasonable self-selected pace. Specifically, the average walking speed of 30.3 ± 3.4 cm/s falls well within the range of previously published literature values for healthy walking of 22–71 cm/s (Allen et al., 2011; Andrada et al., 2013; Coulthard et al., 2003; Górska et al., 2007; Kloefkorn et al., 2015; Pereira et al., 2006; Schmidt & Fischer, 2011; Simjee et al., 2007). In addition, the mean stance percentage of 63.9 ± 3.6% compares favorably to a range of 60–73.9% (Berryman et al., 2009.; Clarke et al., 1997; Coulthard et al., 2003; Górska et al., 2007; Kloefkorn et al., 2015; Pereira et al., 2006), as well as mean stride length of 122.4 ±

4.8 mm, when compared to a reported range of 82.5–150mm (Allen et al., 2011; Boettger et al., 2009; Bonnet et al., 2015; Clarke et al., 1997; Coulthard et al., 2003; Pereira et al., 2006; Simjee et al., 2007).

3.4.2 Ground Reaction Forces (GRFs)

GRFs (**Figure 7**) provide insight on the amount of body support, the impacts of injury, and balance during ground contact in the stance phase of the gait cycle. They also identify where and when the rats absorb and generate propulsive force during heel strike and toe-off, as well as how stable the rats are during the contralateral swing phase as indicated by the lateral forces. GRFs for normal locomotion have been obtained for healthy rats, but previous studies collecting GRF data have varied in the velocity of their control animals (30–85 cm/s) (Allen et al., 2012; Muir & Whishaw, 1999a, 1999b) indicating that some of these animals were likely not walking. The data presented here was collected on animals with an average moving velocity of 30.3 cm/s, within the threshold for a lateral sequence walk (< 48 cm/s) as defined by Gillis and Biewener, thereby providing a basis for GRFs during normal walking. On average, the vertical GRFs in this study represent 67.5% of body weight and falls in the range of previously reported vertical GRF values (65–87% of BW) (Andrada et al., 2010, 2013; Howard et al., 2000; Muir & Whishaw, 1999a, 1999b; Roemhildt et al., 2010; Webb et al., 2011). These vertical forces are highest in early stance and then steadily decrease, which is different than what is typically seen in humans. The anterior–posterior GRFs represent braking/acceleration forces and pass just above and below the zero-level (braking 13.2% vs 4–15% of BW, acceleration 5.1% vs 2–16% of BW) (Howard et al., 2000; Muir & Whishaw, 1999a, 1999b; Roemhildt et al., 2010; Webb et al., 2011). Similar to humans, these forces show that the rats decelerate in early stance and accelerate in late stance. The medial–lateral GRFs pass below the zero-level as the rat lands on the outside of their foot at

heel strike and rolls off the second phalange at toe-off (medial 0.47% vs 0–3%, lateral 11.2% vs 5–8%) (Muir & Whishaw, 1999a, 1999b; Roemhildt et al., 2010; Webb et al., 2011). The fact that the medial–lateral GRF is always pushing back towards center is likely exaggerated by the wide step width of rats relative to what is typically seen in human subjects. The high number of foot strikes obtained in this study, low variance, and similarity to published data show the findings are representative of normal over ground walking at self-selected pace for healthy rats. However, as noted earlier, GRFs are a whole limb measurement. It is only when combined with kinematics that GRFs provide truly informative data through the calculation of joint-by-joint moments.

3.4.3 Kinematics

Joint kinematics have been examined extensively in rat models to evaluate changes in joint motion due to muscle, nerve, or joint injuries. 3-D kinematics, as shown by João et al. (2010), provide significant data for gait evaluation because they easily characterize classic compensation patterns (such as circumduction or vaulting) while also having enough precision to identify smaller changes in the motion of the hip, knee, or ankle that could have longer-term impacts such as osteoarthritis. Kinematics also provide the foundation for kinetic and energetic analysis by providing information on the angular acceleration and angular velocity of the limb segments. But as previously mentioned, there is a lack of congruence in the kinematic literature due to vast methodological differences. Previously reported values for sagittal plane kinematics vary significantly in their raw angles, primarily due to limitations in motion capture techniques. For example, some groups used permanent ink dots rather than reflective markers to track joint locations and/or only utilized 2-D motion capture to evaluate solely the sagittal plane.

Further, there are frequent differences in model definitions in the kinematic literature,

such as neutral joint angle definitions. Some groups define the neutral angle as 0° and others define neutral as 90°, leading to a disconnect in how data is reported. To address the latter point, neutral positions were defined to be consistent with existing protocols for human movement analysis (G. Wu & Cavanagh, 1995). Similarly, another limitation of kinematic analysis in rodents has been the inaccuracy of modeling the motion of the knee due to the extreme amount of skin artifact. Bauman & Chang, (2010) used 2-D X-ray fluoroscopy to show that there are broad differences in the kinematics of the knee when using skin-derived, triangulated, and bone-derived angle measurements. The data presented here compares favorably to the shape and motion of bone-derived knee kinematics reported by Bauman (2010) relative to their own skin-derived kinematics. There were only two differences observed when comparing the two datasets. The first difference was a slight offset in the hip flexion angle due to the aforementioned differences in neutral angle definition (the present study used the sacroiliac crest, while Bauman used the caudal ischium). Second, there is a discrepancy in the knee angle at mid-stance that could be attributed to the difference in collecting 3-D versus 2-D motion data. Significant out of plane movement of the knee joint center was observed in the present dataset, which would not be accounted for when using single plane fluoroscopy (**Figure 6**). A limitation of this study is the omission of the toe segment. However, even though rats use a digitigrade gait in mid to late stance, most other studies also exclude this segment in rat gait. The rationale for so doing is likely related to the small scale and independent motion of the toes—decreasing the feasibility of accurately tracking the segments. Current work is focused on including some motion of the toes.

3.4.4 Kinetics

As mentioned, joint kinetics are the gold standard for the evaluation of human biomechanics. They provide information on the internal forces being experienced on a joint-by-

joint basis that cannot be captured with any other evaluative method. This information is significant because the same angular joint motion can be produced using drastically different muscle activation patterns, and many times those alternative patterns are the driving cause of long-term comorbid joint conditions. Kinetics also reveal the working relationship between joints, as a deviation at one joint in a system nearly always results in a deviation at another joint, many times hidden in the contralateral limb. Further, the ability to do kinetic analysis of gait informs everything from the etiology of a disease to treatment decisions, treatment outcomes, and the ultimate health of the entire system. Recovery from a musculoskeletal or neural injury is more than just the local recovery from the immediate presenting issue, it is a systemic undertaking that requires a comprehensive evaluation to assess the true extent of recovery.

Three studies have previously attempted to characterize rat gait kinetics, and they were conducted by Bennett et al. (2012) and Andrada et al. (2010, 2013). These studies were performed on 5 animals and 2 animals, respectively, and calculated joint moments for the hip, knee, and ankle in only the sagittal plane. In addition, Wehner (2010) developed 3D joint moments, but because they did not measure GRFs they used measured kinematics combined with published GRF's to calculate joint loading. The curve shapes of the kinetic analysis presented here align well with the pre-surgery moments presented by Bennett and the shapes of the kinetic curves of the hip and ankle compare well to both sets of data presented by Andrada with peak values from this study falling within the range of their reported values. There is some disparity in the shape of the knee torque graphs, but because Andrada did not publish their kinematic curves it is also difficult to pinpoint the exact source of these differences. However, they did note that their imaging in 2-D would impact their sagittal plane angles. By design, imperfect knee angles would lead to incorrect knee moments. In the current study, the reported methods and data

permitted calculation of joint moments in all three planes at the hip (flexion/extension, ab/adduction, internal/external rotation). Because of the combination of consistent 3-D kinematic curves and low variance GRFs in this study, the calculated kinetic results in all three planes are reliable and provide a solid benchmark for 3-D rat gait analysis moving forward.

Joint power analysis is an under-researched area with respect to rodent gait studies, but the relative shapes of the sagittal plane power plots for the hip, knee, and ankle (**Figure 9**) compare favorably to the three other published datasets in Bennett et al. (2012) and Andrada et al. (2010, 2013). However, the values reported by Bennett for normalized power are extremely high (peaks greater than 60 W/kg). This may be due to a failure to convert from degrees/second to radians/second for angular momentum values, because both their kinematic and kinetic curves present reason- able data. For comparison, Bennett reports a peak hip power of ~ 60 W/kg, but this value is significantly higher than peak values reported for humans (~ 1.8 W/kg) (Farris & Sawicki, 2012), horses (~ 6 W/kg) (Dutto et al., 2006), or rats in the Andrada studies (0.08–1.2 W/kg). There is a clear discrepancy between Bennett's reported values and the field, but the values presented by Andrada fall far more within the reasonable expected range for peak joint power of walking rats. Based on that data, the power curves obtained in this experiment fall within the range presented by Andrada and are on the proper scale of the expected hip, knee, and ankle joint powers during healthy, normal walking for Lewis rats.

Because the rat hindlimb is utilized as a model system for the treatment and evaluation of so many pathologies, this method of comprehensive gait evaluation should be of broad utility to the field. The data presented in this paper is the first to characterize kinetics in all three planes, providing comprehensive insight into the biomechanics of rat walking on a joint-by-joint basis. In addition, kinematic analysis in this study was conducted on a larger cohort (24 vs. an average

of 11) (Allen et al., 2011; Alluin et al., 2011; Balbinot et al., 2018; Bauman & Chang, 2013; Bennett et al., 2012; Dienes et al., 2019; DiGiovanna et al., 2016; Filipe et al., 2006; Garnier et al., 2008, 2008; Gravel et al., 2010; João et al., 2010; Nakahata et al., 2018; Nica et al., 2017; Pereira et al., 2006; Perrot et al., 2011; Schmidt & Fischer, 2011; Thota et al., 2005) and included more kinetic data on both an animal basis and foot-strike basis than previous studies in the field. As such, this work extends the analytic methods available to investigators to study the rat hindlimb beyond more widely used measurements, such as muscle force production, to include insight into internal forces and movement compensation patterns. Furthermore, similarities of rat gait to the human crouch gait benchmark should provide additional translational value to these investigations for improved understanding, evaluation, and treatment in humans.

3.5 Outlook & Conclusion

We are particularly excited about the potential applications of this approach to provide improved understanding of the biomechanical mechanisms responsible for functional deficits caused by extremity trauma (e.g., VML injuries), and thus, to shed new insight on potential therapeutic solutions for improved treatment of limb trauma. High impact trauma such as VML and/or peripheral nerve injury to the extremities impacts thousands of wounded warriors and civilians each year. Frequently, especially in complex compartments with multiple muscles and innervation patterns, the biomechanical impact of these injuries and the route to recovery can be difficult to precisely identify. The addition of 3D kinetic analysis provides an important new tool to gain greater insight into the "black box" of potential mechanisms responsible for the functional deficits observed in these complex injuries, as well as any compensatory neuromuscular responses/adaptations. In theory, implementing this new evaluative tool into the

armamentarium of methods available should accelerate development of more effective treatments for functional restoration of extremity trauma, and ultimately significantly increase the quality of life for impacted individuals.

In this regard, a comprehensive method was developed to analyze the full 3D kinetics and 3D kinematics of the rat hindlimb during over ground walking to provide a clearer picture of the biomechanics required for normal movement function. This unique ability to measure gait parameters, as demonstrated in this study, facilitates a more thorough understanding of normal and healthy rodent gait. With this methodology and developed kinetic database in hand, it is possible to extend these protocols to quantify relevant functional deficits in rat models, as well as the functional effectiveness of therapeutic interventions on movement quality. Further, the normative database presented herein provides valuable data for comparison for any study making use of rat models for full biomechanical analysis (spatiotemporal parameters, GRFs, kinematics, kinetics, and energetics) of pathologies modeled in the hindlimb.

4. Characterizing Changes In Rat Gait Kinematics and Kinetics at Different Walking Speeds

4.1 Introduction

Rodent locomotion analyses are a robust method for quantifying functional outcomes and evaluating treatment efficacies in pre-clinical studies of musculoskeletal pathologies. Due to the parallels between human and animal gait, studies evaluating the spatiotemporal parameters, kinematics (joint angles), and kinetics (joint moments) of rat locomotion have become popular tools for analyzing a diverse set of conditions, such as volumetric muscle loss (Dienes et al., 2019), osteoarthritis (Allen et al., 2012), nerve injury (Bauman & Chang, 2013; Kemp et al., 2013), Parkinson's disease (Amende et al., 2005), and spinal cord injury (Hamers et al., 2001) in a pre-clinical setting. Typically, these studies aim to evaluate the impacts of a particular pathology by comparing pathologic animal groups to healthy control groups. However, several studies have demonstrated that the introduction of pathology can significantly decrease walking speed in both humans and rodents (Koopmans et al., 2005; Mountney et al., 2013). As a result, it can be difficult to discern which kinematic and kinetic adaptations are a direct result of pathology and which are more generally related to changes in walking speed. In other words, there is no way to separate the effects of changes in walking speed on gait from the effects of a pathology that simultaneously causes reduced locomotor function. The goal of this study is to provide deeper insight into normal rodent walking by examining the effects of walking speed on kinematics and kinetics, in order to provide context for evaluating pathologic rodent gait.

Speed has been shown to be a confounder for other spatiotemporal parameters in both normal and pathologic rodent gait (Herbin et al., 2007; Koopmans et al., 2007; Pereira et al., 2006). The relationships between speed and spatiotemporal parameters such as stride length,

stride time, cadence, and stance/swing have been well documented in the literature over a wide range of speeds. Specifically, it has been shown that faster speeds are driven by increased stride length and increased cadence (Batka et al., 2014; Clarke & Parker, 1986; Hruska et al., 1979). Stance time has also been shown to decrease as speed increases (Hruska et al., 1979). However, there is some debate in the literature about the dependence of swing time on speed. Some studies report that swing time decreases as speed increases, while other studies report no dependence on speed. A more detailed analysis of speed dependence on typically reported spatiotemporal parameters was presented in Batka et al. (2014). Prior research has also demonstrated large intra-animal and inter-animal speed variability in both normal and pathologic animals (Cendelín et al., 2010; Dienes & Hicks et al., 2022; Górska et al., 1999; Koopmans et al., 2007). In studies aiming to compare normal and pathologic gait, this variability can create significant challenges in standardizing data and comparing across experimental groups. In order to accurately compare healthy and pathologic data, it is necessary to separate gait changes due to pathology from gait changes induced by walking speed changes.

Although there is broad history of the relationships between speed and spatiotemporal parameters in rodent locomotion, there is still little understanding of how walking speed affects kinematic and kinetic gait parameters. In 2001, Gillis & Biewener studied rodent gait at self-selected speeds and reported that rats changed gaits from a lateral sequence walk (17-48 cm/s) to a trot (59-71 cm/s) to a transverse gallop (60-122 cm/s) with increasing speed. Their study demonstrated kinematic and spatiotemporal differences for each gait. However, their reported speed bin for walking encompassed a variable range of walking speeds, with the maximum speed for walking nearly 300% greater than the minimum speed. Furthermore, there was no discussion of kinematic variability within walking gait. Prior studies have reported kinematics and kinetics

for healthy control rodents walking (as defined by Gillis & Biewener) at their self-selected speed (Dienes & Hicks et al., 2022). However, this study reported high variability in kinematic and kinetics curves along with a wide range of walking speeds, prompting further investigation into kinematic and kinetic speed dependence within walking gait. Some studies that report kinematics or kinetics typically control for speed by employing the use of a treadmill (Bauman & Chang, 2010; Dienes et al., 2019; Pereira et al., 2006). While using a treadmill to standardize locomotion speed may remove variability in kinematics and kinetics, treadmill-based analyses have been shown to produce differences in gait patterns from over-ground walking, due to differences in proprioceptive and vestibular inputs from treadmill walking (Herbin et al., 2007; Pereira et al., 2006). Over-ground analyses are typically preferred, as they more closely approximate natural walking. Other studies reporting kinematics or kinetics do not consider speed variability in their analysis (Andrada et al., 2010, 2013; Bennett et al., 2012).

This study aims to quantitatively characterize the effects of speed on kinematic and kinetic gait variables during lateral sequence walking. This study also presents a normalization scheme to compare kinematics and kinetics between different speeds by utilizing the relationship between speed and the timing of gait events. This database will provide valuable data for comparison for studies utilizing biomechanical analyses of rodent walking. By using this framework to better understand normal rodent walking, these methodologies can be employed in future studies to quantify relevant pathologic gait adaptations, as well as to evaluate the efficacy of therapeutic interventions on functional recovery.

4.2 Methods

4.2.1 Data Acquisition

A total of 32 twelve-week-old male Lewis rats (297.2±19.6g) were tasked with walking

across a custom-built walkway and recorded with Vicon Nexus motion capture software. Ground reaction force data was acquired concurrently via four ATI 6-axis force transducers embedded in the walkway. Rats were anesthetized and shaved to allow for proper placement of the motion capture marker set. Body length, mass, pelvis width, and hindlimb segment lengths were also recorded for each animal. 4mm hemispherical reflective markers were placed on landmarks of the spine (L6 vertebra and 5^{th} caudal vertebra), pelvis (anterior superior iliac spinae), hips (superior to hip joint centers), knees (lateral femoral epicondyles), ankles (lateral malleoli), and toes (distal 5^{th} metatarsals). Once rats recovered from anesthesia, they were placed in the instrumented walkway. Rats were allowed to walk across the walkway at their self-selected walking speed. Marker data was collected at 200Hz in Vicon Nexus, and ground reaction force data was collected at 1000Hz. Rats were returned to the vivarium after data collection. Gait events and marker identification were completed in Vicon Nexus and exported to MATLAB for spatiotemporal calculations and use with OpenSim.

4.2.2 Animal Care

This study was conducted in compliance with the Animal Welfare Act, the Implementing Animal Welfare Regulations, and in accordance with the principles of the Guide for the Care and Use of Laboratory Animals. The University of Virginia Animal Care and Use Committee approved all animal procedures. Animals were pair housed in a vivarium accredited by the American Association for the Accreditation of Laboratory Animal Care, and they were provided with food and water *ad libitum*.

4.2.3 Musculoskeletal Model

Subject specific models were generated in OpenSim from a validated rat hindlimb model (Delp et al., 2007; Dienes & Hicks et al., 2022; Johnson et al., 2008), which has been augmented

to include the left hindlimb in order to model the hindlimbs bilaterally (Figure 10). There were no differences in kinematics, kinetics, or spatiotemporal parameters between the left and right hindlimbs for this study. Each hindlimb segment was modeled as a rigid body and scaled for each rat using the measurements described in the previous section. 3D scan data and cadaver measurements (Dienes & Hicks et al., 2022) were used to obtain accurate hindlimb segment mass and inertial parameters for each rat. These inertial parameters were applied to each scaled model before performing inverse dynamic simulations in OpenSim.

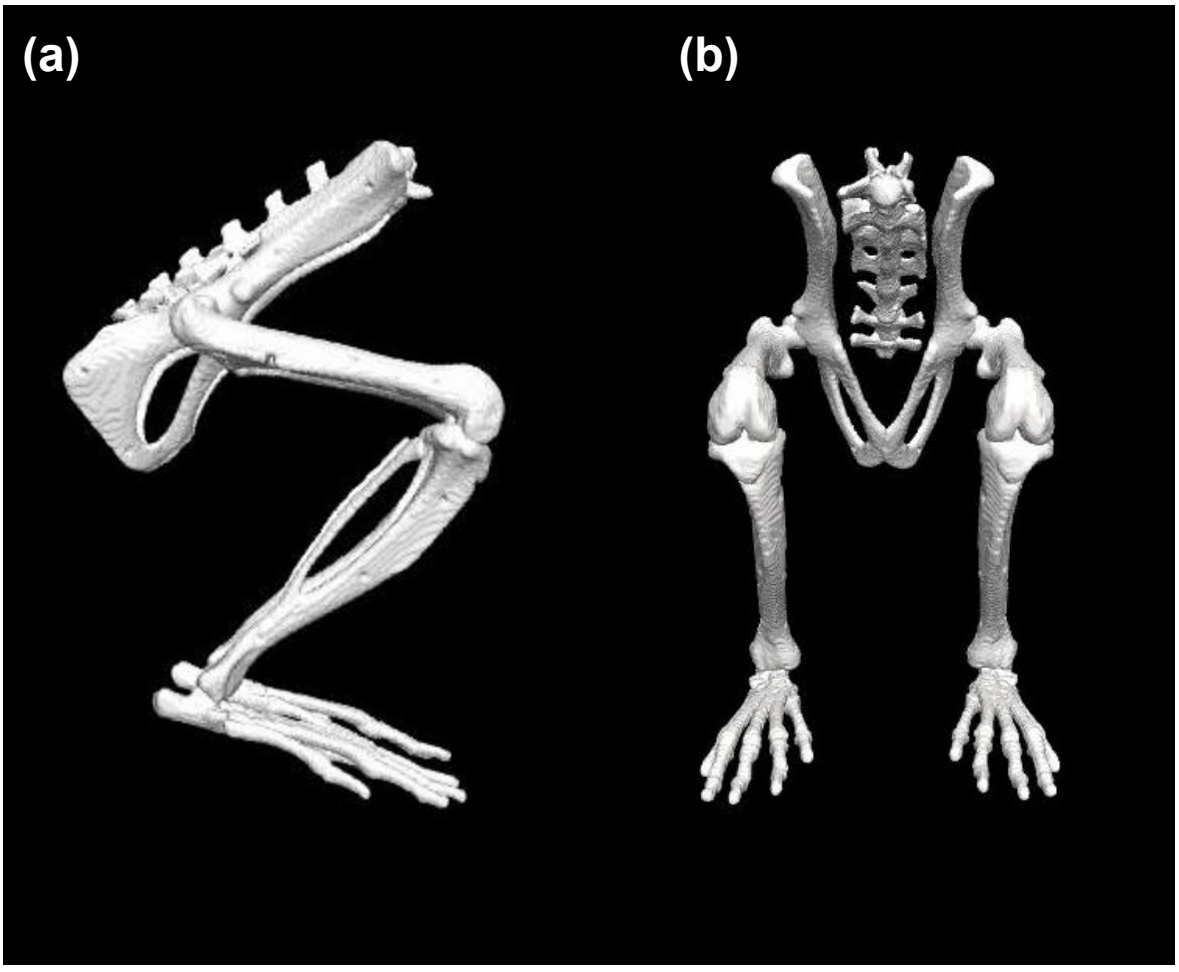

Figure 10: Sagittal plane (a) and frontal plane (b) views of the bilateral musculoskeletal model of the rodent hindlimbs.

4.2.4 Data Analysis

Each trial was visually screened to determine the rat's gait pattern (e.g. walking, trotting, and galloping) while moving across the load cells. Trials were only included in the analysis if the rat employed walking gait. Several trials were recorded in which rats employed trotting gait, but those trials were not included in this study. Trials were also excluded if the rat exhibited non-steady locomotion behavior, such as stopping, sniffing, jolting, rearing, or turning in the walkway, during a gait cycle in which the rat contacted one of the load cells. 6 trials meeting these criteria were analyzed for each rat, with the exception of two rats who only had 5 trials meet the exclusion criteria. Marker trajectories were filtered using a 4th order, low-pass, Butterworth filter with a cutoff frequency of 15 Hz. Ground reaction forces were filtered using a 4th order, low-pass, Butterworth filter with a cutoff frequency of 100 Hz. OpenSim's inverse kinematic and inverse dynamic solvers were used to compute hindlimb joint angles and joint moments for each analyzed gait cycle. Spatiotemporal parameters were acquired from marker positions. Walking speed and stride length were normalized by leg length, which was calculated from the sum of the animal's femur, tibia, and foot measurements. Relationships between speed and kinematic and kinetic points of interest were examined in MATLAB using regression analyses, and speed-dependence was evaluated with the coefficient of determination (R^2) and p-value. For each family of statistical inferences (kinematics, kinetics, and spatiotemporal parameters), Bonferroni corrections were used to reduce the probability of Type-I error. Corrected critical values were $\alpha = 0.005$, $\alpha = 0.0042$, $\alpha = 0.005$ for kinematics, kinetics, and spatiotemporal parameters, respectively.

4.3 Results

4.3.1 Speed distribution for all strides

Strides exhibiting walking gait were observed from 20.2-68.4 cm/s (2.05-7.05 leg lengths/s), with a mean value of 43.6 cm/s (4.57 leg lengths/s). At speeds faster than 68.4 cm/s, animals transitioned to trotting gait, characterized by a different limb-support sequence. The distribution for normalized walking speed, which approximated normal by an Anderson-Darling test (AD = 0.649, p = 0.090), is shown in **Figure 11**. Normalized speed was used in the following regression analyses in order to provide a standard comparison against datasets with rodents of different sizes.

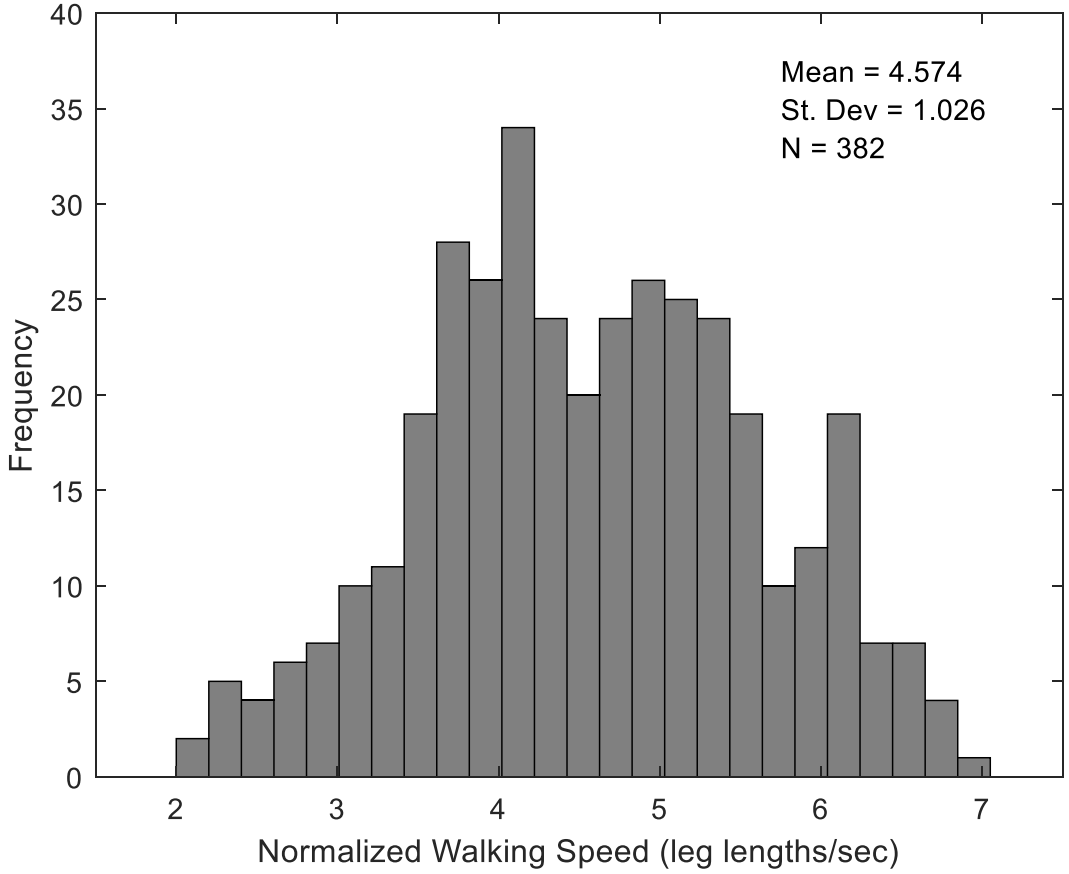

Figure 11: Distribution of normalized walking speed (mean = 4.574, SD = 1.026, n = 382 strides). The distribution approximated normal via the Anderson-Darling test (AD = 0.649, p = 0.090).

4.3.2 Spatiotemporal parameters as a function of normalized walking speed

Regression analyses were performed to characterize the relationship between normalized speed and normalized stride length, cadence, percent stance, percent double support, stride time, stance time, and swing time (**Table 2**). Each parameter showed significant dependence on speed ($p < 0.001$). Stride length and stride frequency increased with increasing speed, while percent stance, percent double support, stride time, stance time, and swing time each decreased with increasing speed. Stride length, cadence, percent stance, and percent double support were directly proportional to normalized walking speed (leg lengths/second). The best fit equations for stride time and stance time were of the form $\log(y) = a*\log(x) + b$, and the best fit equation for swing time was of the form $y = a*1/x + b$, which compares favorably with Hruska et al. (1979). However, linearly characterizing the relationships between stride, stance, and swing time and velocity results in a slight decrease in performance of the regression model and provides a simplified interpretation of the observed relationships. Furthermore, describing the stance and swing phases as a total percentage of the gait cycle demonstrated a linear dependence on walking speed (**Table 2**).

Parameter	Equation	SE	p-value	R^2
Stride Length (length/leg length)	$y = 0.122x + 1.037$	0.004, 0.018	$p < 0.001$	0.721
Cadence (steps/min)	$y = 49.747x + 113.114$	0.808, 3.786	$p < 0.001$	0.911
Double Support (% GC)	$y = -6.892x + 56.403$	0.260, 1.217	$p < 0.001$	0.654
Stride Time (s)	$y = -0.056x + 0.618$	0.001, 0.006	$p < 0.001$	0.845
Stride Time (s) – nonlinear	$\log(y) = -0.657\log(x) – 0.049$	0.011, 0.016	$p < 0.001$	0.911
Stance Time (s)	$y = -0.048x + 0.447$	0.001, 0.005	$p < 0.001$	0.826
Stance Time (s) – nonlinear	$\log(y) = -0.895\log(x) – 0.172$	0.016, 0.024	$p < 0.001$	0.892
Swing Time (s)	$y = -0.008x + 0.171$	0.001, 0.003	$p < 0.001$	0.280
Swing Time (s) – nonlinear	$y = 0.140(1/x) + 0.102$	0.011, 0.003	$p < 0.001$	0.299
Stance (% GC)	$y = -3.449x + 77.966$	0.159, 0.746	$p < 0.001$	0.558

Table 2: Summary of spatiotemporal regression equations analyzed as functions of normalized walking speed. Each spatiotemporal parameter (y) is expressed as a function of normalized walking speed (x). SE: standard error of the regression coefficients, in order. % GC: stance and double support were calculated as a percentage of the total gait cycle.

4.3.3 Kinematic and kinetic profiles as a function of normalized walking speed

Initially, trials were separated into five evenly spaced bins of equal size based on normalized walking speed to visualize speed-dependent effects on kinematics and kinetics. The normalized speed ranges for each bin were: [2.05-3.05], [3.05-4.05], [4.05-5.05], [5.05-6.05], and [6.05-7.05]. Average joint angles and joint moments for each speed bin are reported in **Figure 12** for the hip, knee, and ankle. The average curves across all speed bins are also reported. For each joint, points of interest corresponding to maximum and minimum curve values were detected and analyzed as a function of normalized walking speed. Regression analyses were performed to characterize the relationship between normalized speed and points of interest from joint angle/moment curves (**Table 3**).

For kinematic curves, minimum hip flexion, minimum hip abduction, maximum hip internal rotation, minimum late-stance knee flexion, and minimum ankle dorsiflexion angle values were analyzed with respect to speed. Linear regressions were performed with normalized walking speed as the independent variable, with each kinematic point of interest as the dependent variable in each test. Normalized walking speed had significant effects on the timing (location of kinematic points of interest relative to the gait cycle) and amplitude of kinematic extrema. Every analyzed point of interest occurred significantly earlier in the gait cycle with increasing speed ($p<0.001$). With respect to amplitude, the peak hip internal rotation angle increased with increasing speed ($p<0.001$), while the late-stance knee flexion minimum decreased with increasing speed ($p<0.001$). Minimum hip flexion angle also decreased with increasing speed ($p<0.01$). No other kinematic points of interest evaluated in this study displayed significant dependence on normalized walking speed.

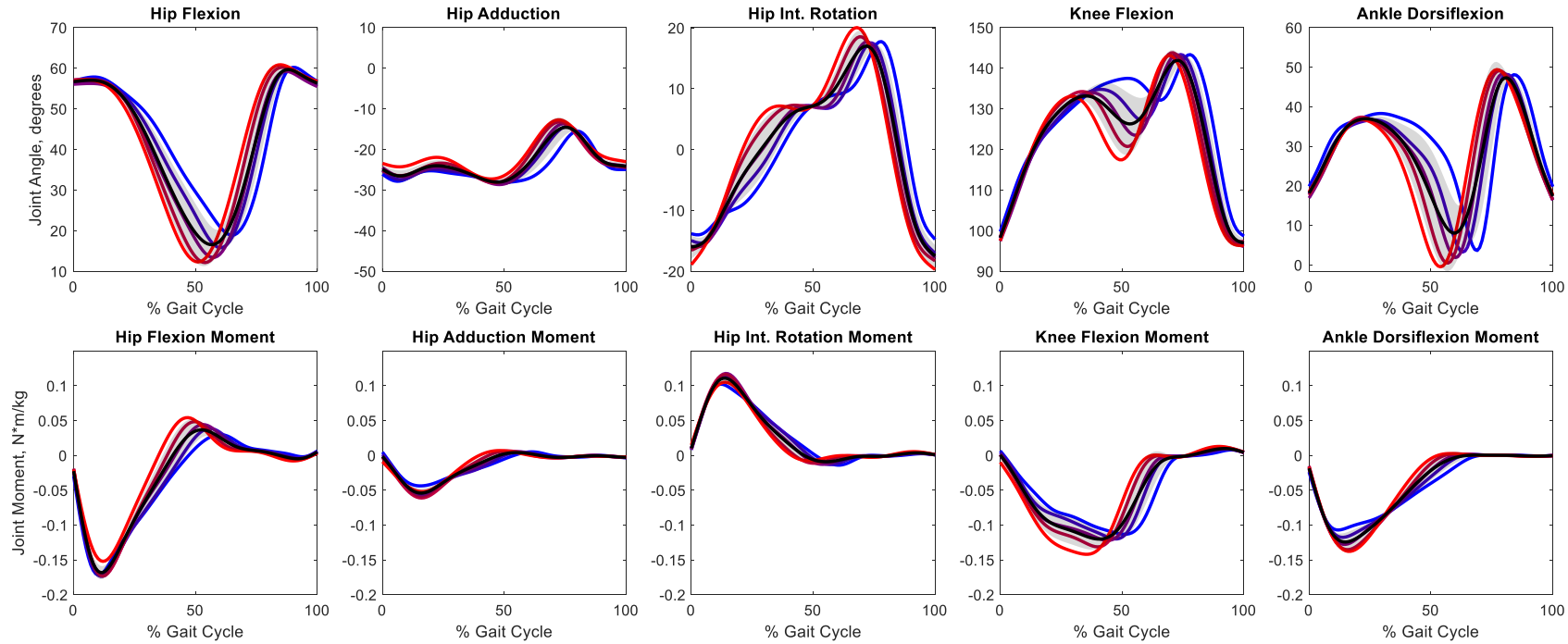

Figure 12: Average hindlimb kinematics and kinetics for each walking speed bin for the hip, knee, and ankle. Each curve is plotted over the entire gait cycle, foot strike to foot strike. The fastest bin is plotted in red, while the slowest bin is plotted in blue. Average +/- 1 S.D. of all bins shown with black line and light grey cloud.

Parameter	Equation	SE	p-value	R^2
	Hip			
Min Hip Flexion Angle	y = -1.67x + 20.583	0.332, 1.551	p < 0.001	0.064
Min Hip Flexion Angle (% GC)	y = -3.534x + 73.925	0.146, 0.682	p < 0.001	0.612
Min Hip Abduction Angle	y = 0.59x – 15.601	0.191, 0.894	p = 0.002	0.025
Min Hip Abduction Angle (% GC)	y = -1.9x + 83.492	0.157, 0.735	p < 0.001	0.282
Max Hip Int. Rot. Angle	y = 0.535x + 16.69	0.231, 1.081	p = 0.021	0.014
Max Hip Int. Rot. Angle (% GC)	y = -2.47x + 83.549	0.139, 0.651	p < 0.001	0.458
Max Hip Flexion Moment	y = 0.006x + 0.023	0.001, 0.003	p < 0.001	0.167
Max Hip Flexion Moment (% GC)	y = -3.651x + 70.09	0.216, 1.010	p < 0.001	0.435
Max Hip Extension Moment	y = 0.005x – 0.196	0.002, 0.009	p = 0.017	0.015
Max Hip Extension Moment (% GC)	y = 0.564x + 10.458	0.092, 0.429	p < 0.001	0.092
Max Hip Abduction Moment	y = -0.002x + -0.052	0.001, 0.006	p = 0.165	0.005
Max Hip Abduction Moment (% GC)	y = -0.541x + 20.366	0.267, 1.247	p = 0.043	0.011
Max Hip Int. Rot. Moment	y = -0.0005x + 0.119	0.002, 0.008	p = 0.768	0.000
Max Hip Int. Rot. Moment (% GC)	y = 0.213x + 14.314	0.118, 0.554	p = 0.074	0.009
	Knee			
Late-Stance Knee Flexion Angle	y = 3.63x + -138.924	0.411, 1.920	p < 0.001	0.174
Late-Stance Knee Flexion Angle (% GC)	y = -3.883x + 74.155	0.146, 0.683	p < 0.001	0.655
Max Knee Extension Moment	y = 0.008x + 0.095	0.001, 0.005	p < 0.001	0.156
Max Knee Extension Moment (% GC)	y = -3.987x + 60.681	0.420, 1.963	p < 0.001	0.195
	Ankle			
Min Ankle Dorsiflexion Angle	y = -0.637x + 1.886	0.404, 1.889	p = 0.116	0.007
Min Ankle Dorsiflexion Angle (% GC)	y = -3.649x + 77.511	0.138, 0.646	p < 0.001	0.652
Max Ankle Plantarflexion Moment	y = -0.008x – 0.092	0.0009, 0.004	p < 0.001	0.171
Max Ankle Plantarflexion Moment (% GC)	y = 0.484x + 14.356	0.180, 0.843	p = 0.008	0.019

Table 3: Summary of kinematic and kinetic regression equations analyzed as functions of normalized walking speed. Each kinematic and kinetic parameter (y) is expressed as a function of normalized walking speed (x). SE: standard error of the regression coefficients, in order. % GC: the timing of kinematic and kinetic extrema were identified by their location on the curve as a percentage of the total gait cycle.

Similarly, several kinetic points of interest also exhibited significant dependence on normalized speed. The maximum moments for hip extension ($p<0.001$) and ankle plantarflexion ($p<0.002$) each occur later in the gait cycle with increasing speed, while maximum hip flexion and knee extension moments occur earlier in the gait cycle with increasing speed ($p<0.001$). There was no significant relationship between speed and the timing of peak moments for hip abduction or hip internal rotation. Investigation of peak joint moment amplitudes also revealed significant differences with respect to speed. Namely, maximum hip flexion, hip abduction, knee flexion, and ankle plantarflexion moments all increased with increasing speed ($p<0.001$).

4.4 Discussion

The present study reiterated several effects of locomotion speed on spatiotemporal gait parameters previously discussed in other studies (Clarke & Parker, 1986; Herbin et al., 2007; Hruska et al., 1979). Consistent with findings in prior experiments, every spatiotemporal parameter examined in this study exhibited a significant linear relationship with walking speed, each with high correlations. Stance time sharply decreased, while swing time only minimally decreased with increasing speed. As a result, the portion of the gait cycle spent in stance was highly variable. The rats also increased their stride length and cadence with increasing speed. The portion of the gait cycle spent in hindlimb double support also decreased with increasing speed. In human studies, parameters such as double support percentage are often used as a metric to quantify stability, with less stable populations typically spending more time in double support. By characterizing the expected change in double support and other spatiotemporal values due to velocity, it is possible to understand how alternate changes in double support might point to changes in stability due to pathology. While these spatiotemporal findings are an important component of any gait analysis, there are an infinite number of movement patterns that can result

in a specific set of spatiotemporal parameters, and as such, it is necessary to examine kinematics and kinetics to gain a deeper understanding of the changes in joint mechanics that occur at different walking speeds.

Published values for normal rat walking speed vary widely, from 17-71 cm/s. However, discrepancies in rat size between experiments and lack of information about limb anthropometrics may exaggerate perceived variability. Rats with longer limbs have the capacity to achieve longer stride lengths, giving them the ability to cover more ground for the same stride frequency. In humans, walking speed is often normalized to account for size differences between non-similar populations. A similar method is proposed in the present study, normalizing walking speed by the total leg length of the rat in order to provide a standardized velocity metric that is applicable to rats of different sizes. When this method is applied to previously published values for walking speed and leg length in a study evaluating smaller, female rats (Dienes & Hicks et al., 2022), the range of normalized walking velocity is comparable to the normalized walking velocity range put forth in this study (**Figure 13**). It is important to note that while the average normalized walking speed differed between the male and female population, the range of walking speeds is similar between the two groups. Accounting for size discrepancies is particularly important in longitudinal studies where rat size may increase drastically over the course of the experiment, such as in studies where a treatment or therapy is analyzed at several post-operative time-points.

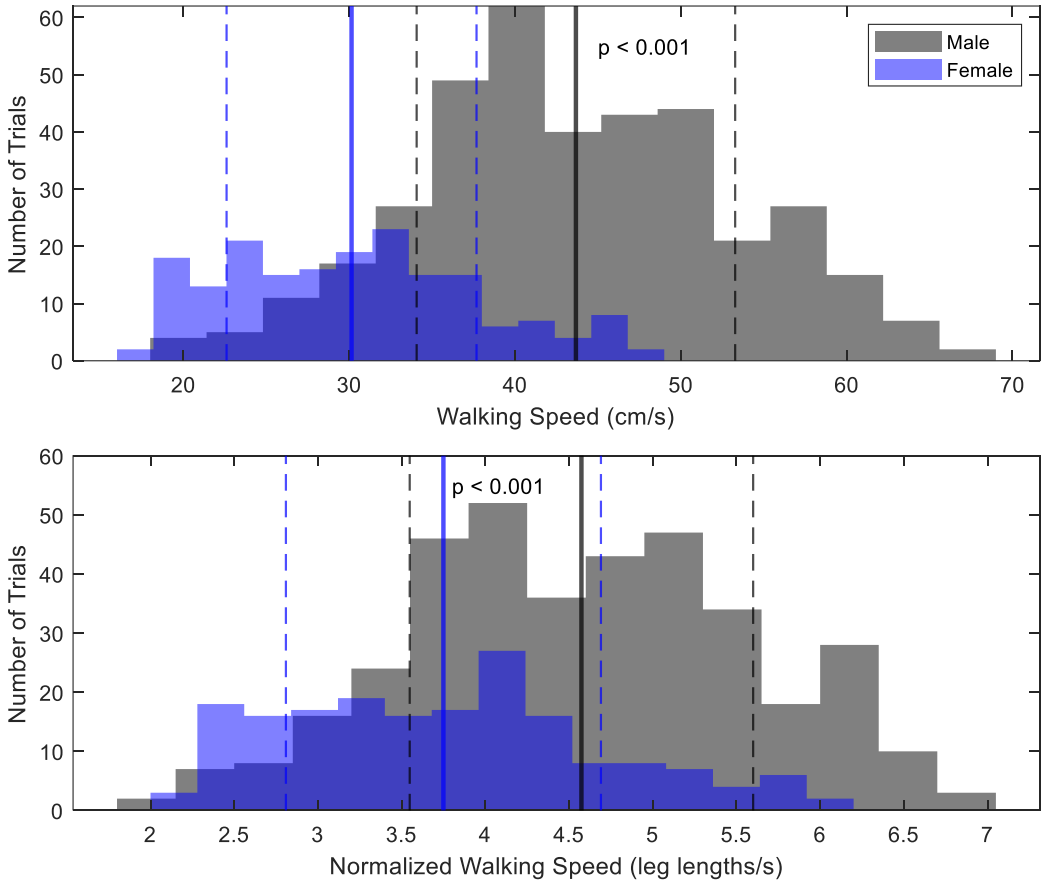

Figure 13: Comparison of the walking speed distribution during normal walking for male and female rats. (a) Non-normalized walking speed distribution. Male: [20.20 – 68.35 cm/s], Female: [17.31 – 48.82 cm/s] (b) Walking speed distribution when walking speed is normalized by hindlimb leg length. Male: [2.05 – 7.05 leg lengths/s], Female: [2.11 – 6.07 leg lengths/s].

This study also quantifies changes in rodent gait kinematics and kinetics that correlate to changes in walking speed. The peak values for several kinematic and kinetic points of interest were significantly linearly dependent on normalized walking speed (**Table 3**). Greater hip and knee extension angles occurred at faster speeds, while ankle dorsiflexion remained constant. The adjustments at the hip and knee are necessary in order to meet the increased spatiotemporal demands of faster speeds; namely, increasing stride length while maintaining swing time. Peak hip internal rotation angle also increased with increasing speed and occurred in early-swing. Increased hip internal rotation could be necessary for the rat to achieve foot clearance as it swings through to the following foot strike and recovers from increased hip and knee extension at faster speeds. Peak knee extension and peak ankle plantarflexion moments both increased with increasing speed, highlighting the increased propulsive demands that accompany faster walking. At the hip, peak extension moment showed no significant relationship with speed, while peak flexion moment was shown to increase with increasing speed. The peak hip flexion moment occurs just prior to foot-off, and is more prominent at faster speeds due to increased hip and knee extension putting more distance between the hip and the foot. Interestingly, peak extension moments at the knee and ankle both increase with increasing speed, while the hip does not. This could be due to the ankle and knee working to absorb energy in early stance and generate energy in late stance, while the hip works to generate energy in early stance and absorb energy in late stance (Bennett et al., 2012; Dienes & Hicks et al., 2022). While increased walking speed most significantly affected joint moment peaks in the direction of forward motion, peak hip abduction moment also increased with increasing speed. Typical gait involves subtle side-to-side oscillation during forward motion as support is transferred from one side to another. The hip abduction moment increase could be attributed to the significantly higher mediolateral forces occurring at

faster speeds, which are necessary to maintain balance during the increased frequency of side-to-side oscillation. It should be noted that the peak values for kinematics and kinetics are highly dependent on the joint coordinate being examined. For this reason, it is difficult to impose a uniform method for standardizing kinematic and kinetic curves for comparison between data of different speeds. However, the linear relationships reported in this work, which characterize each peak value individually, can be used to interpret magnitude changes in walking data.

Points of interest identified from kinematic curves unilaterally occurred earlier in the gait cycle with faster walking. This is indicative of a phase shift associated with the rodents spending a smaller percentage of the total gait cycle in stance with increasing speed. Gait analyses that report kinematics typically present curves that have been normalized to the gait cycle, from foot strike to the following foot strike. As a result, changes in walking speed can introduce phase changes in the curve, which lead to large variations in extrema timing and curve magnitude (**Figure 12**). These phase variations have been shown to significantly impact results from curve comparison techniques, such as statistical parametric mapping (Honert & Pataky, 2021). Furthermore, presenting kinematics that have been averaged from data containing phase discrepancies can misrepresent the amplitude of curve peaks. If these phase and amplitude variations are not properly accounted for, curve comparisons could misrepresent differences between experimental groups caused by pathology. However, the strong correlations between walking speed and kinematic/kinetic extrema (**Table 3**), combined with the strong correlation between walking speed and stance percent (**Table 2**), suggests an alternative method for presenting gait data that mitigates the phase shift caused by walking speed differences and preserves curve amplitudes. Namely, normalizing and presenting the stance and swing portions of gait curves independently, separated by toe-off, eliminates speed-dependent phase effects

caused by the variability in stance percent at different walking speeds (**Figure 14**). In addition, this presentation of gait curves minimizes the amplitude loss caused by averaging curves with phase differences and reduces the variance in both kinematic and kinetic curves (**Figure 15**). Analyzing the stance and swing phases of these curves independently is critical to minimizing the effects of walking speed on kinematics and kinetics.

It is clear that walking speed has significant effects on kinematic, kinetic, and spatiotemporal gait variables. However, it is evident that walking speed alone does not explain all of the variability in gait kinematics, kinetics, or spatiotemporal parameters. Other studies have previously discussed a number of other factors as sources of kinematic and spatiotemporal variability in analyses of rodent locomotion, including sex, age, weight, species, training history, and pathology (Dellon & Dellon, 1991; Koopmans et al., 2007; McIlwain et al., 2001; Wooley et al., 2009). While a specific investigation into each factor's contribution to kinematic and kinetic gait variability was outside the scope of this paper, the relationships developed in this experiment provide a method to normalize gait data and reduce the effects of velocity in order to better isolate and quantify the effects of pathology on gait.

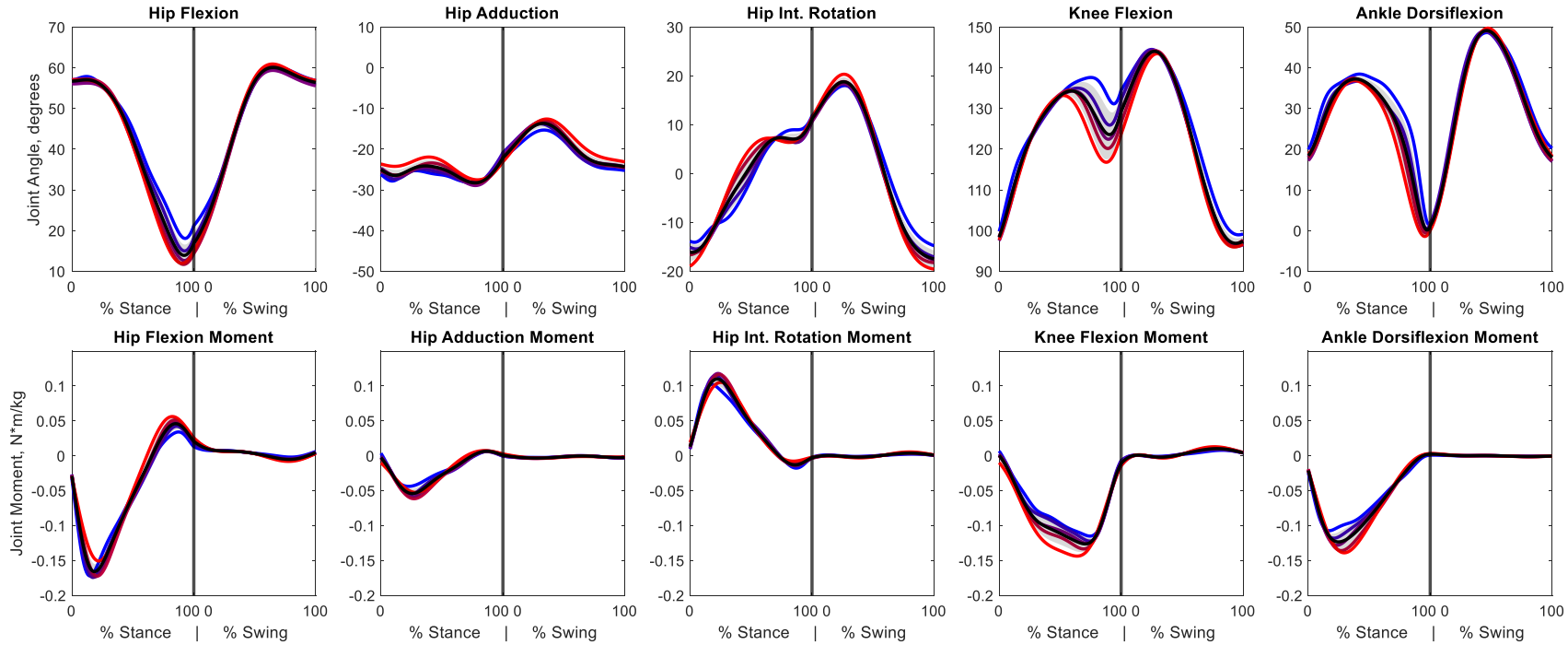

Figure 14: Average hindlimb kinematics and kinetics for each walking speed bin for the hip, knee, and ankle. The stance and swing portions of the gait cycle are plotted independently. The fastest bin is plotted in red, while the slowest bin is plotted in blue. Average +/- 1 S.D. of all bins shown with black line and light grey cloud.

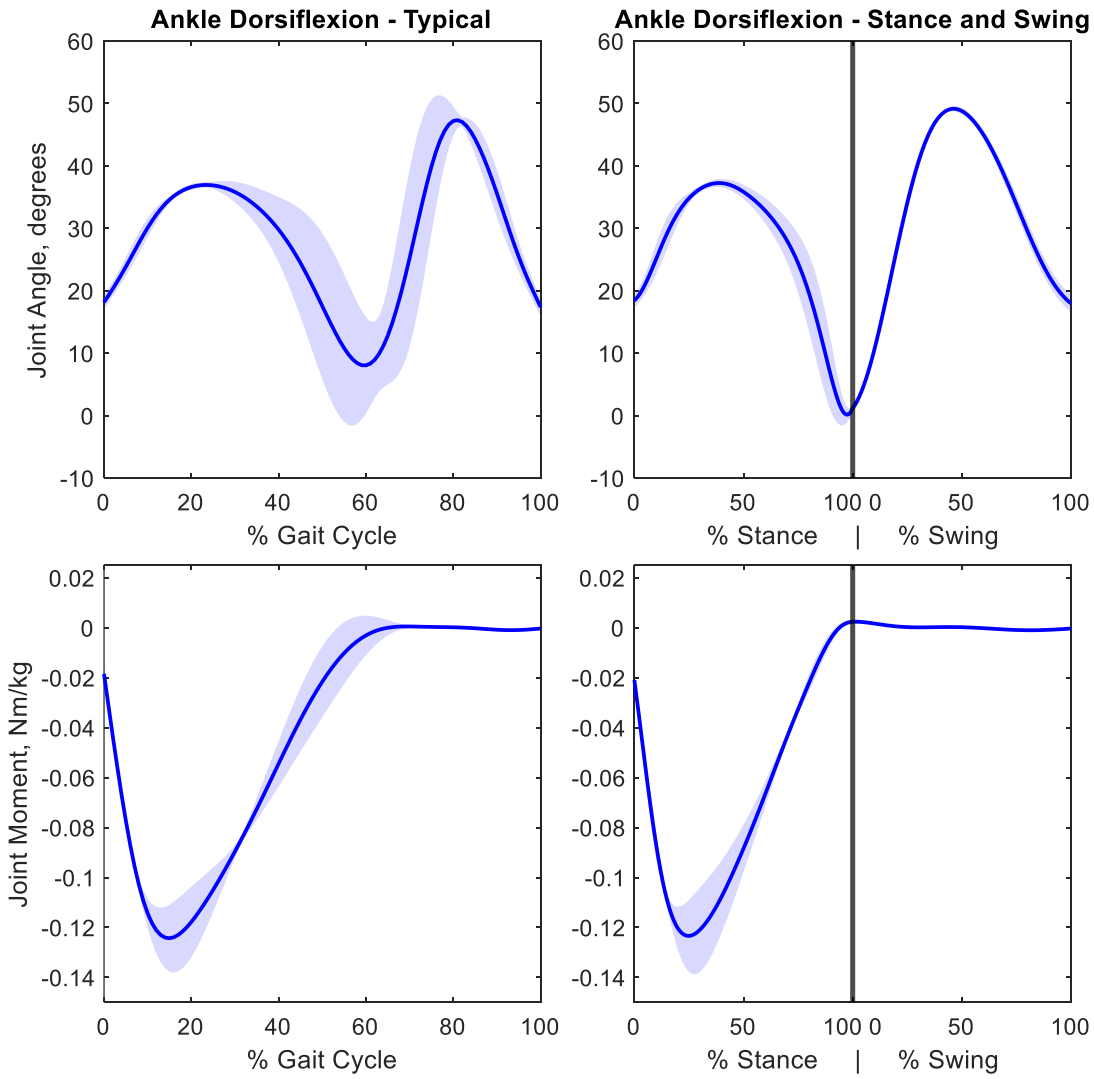

Figure 15: Average +/- 1 S.D. ankle dorsiflexion angle (top) and moment (bottom) of five speed bins for ankle dorsiflexion kinematics. Stance and swing normalization leads to reduced variance in joint kinematics and kinetics, and better represents total ankle joint angle excursion.

This study presents a method to normalize for the effects of walking speed on gait parameters in order to more accurately identify the effects of pathology on gait when the pathology also results in a change in walking speed. By characterizing the effects of walking speed on rodent gait kinematics and kinetics, this study has provided insights into the mechanisms rats use to modulate their walking speed. This study also presented a case for standardizing the reporting of walking speed data and joint angle/moment curves to enable comparison between different speeds and populations. In addition, this data provided a description of the speed variability present in normal rodent walking. Furthermore, walking speed data presented here was normalized by rat anthropometrics, providing the ability for comparison between different sized rats. Finally, normalizing kinematics and kinetics to swing and stance will minimize the impact of walking speed on both phasing and amplitude distortion when reporting gait curves. Understanding the effects of walking speed on gait kinematics and kinetics is a critical advancement in using rodent locomotion analyses to study movement pathologies and their treatments. Previously, spatiotemporal gait parameters have been shown to change significantly following the introduction of a variety of experimental injury models and treatment strategies (Dienes et al., 2019; Mountney et al., 2013; Vincelette et al., 2007; Vlamings et al., 2007). However, it has not been possible to identify the specific functional deficits that lead to these spatiotemporal adaptations. Prior studies characterizing functional deficits without considering walking speed have ignored the kinematic and kinetic variability that exists due to speed in normal rodent locomotion. Comparisons between experimental groups walking at different speeds can lead to the misinterpretation of observed differences in kinematic and kinetic trajectories. By quantifying the effects of normalized walking speed on gait variables, this information can be used in future studies to parse out gait adaptations occurring due to pathology

from adaptations occurring due to walking speed discrepancies.

5. A Biomechanical Analysis of Rat Gait to Quantify Functional Deficits in Response to Volumetric Muscle Loss Injury and Repair

This chapter illustrates the utility of the normative database developed in **Chapters 3 & 4**. In this chapter, deviations from typical kinematics and kinetics are used to elucidate specific pathologic gait compensation strategies and functional deficits arising from hindlimb volumetric muscle loss injuries.

5.1 Introduction

Volumetric muscle loss (VML) is defined as the traumatic or surgical loss of skeletal muscle which results in functional impairment (Grogan & Hsu, 2011). VML can be caused by a variety of circumstances, including combat injuries, surgical procedures, disease, sport injuries, and congenital abnormalities. In VML, the musculoskeletal damage and tissue loss exceeds the skeletal muscle's intrinsic capacity for regeneration, resulting in permanent functional deficits (Carnes & Pins, 2020; Dienes et al., 2019). Current clinical treatments for VML have demonstrated limited efficacy in restoring muscle function or improving muscle strength (Aurora et al., 2014; Garg et al., 2015). As a result, significant preclinical research is being done to develop treatment strategies for regeneration of lost muscle volume. These different treatment strategies have incorporated combinations of hydrogels, scaffolds, and exercise regimens to aid in recovery of muscle volume (Corona et al., 2013; Dziki et al., 2016; Grasman et al., 2015; Passipieri et al., 2019; X. Wu et al., 2012). Specifically, significant research has gone into the development of a tissue engineered muscle repair (TEMR) construct (Corona et al., 2012, 2013; Machingal et al., 2011). The goal of this study was to utilize a comprehensive kinematic and kinetic analysis of rodent gait to quantify gait adaptations in rats after VML injuries to the tibialis

anterior (TA) and lateral gastrocnemius (LG). In addition, this study evaluates the efficacy of a proposed therapy for VML (TEMR) by using kinematics and kinetics to quantify functional recovery after treatment.

Force-generating capacity is widely considered to be the most important and physiologically relevant metric for evaluating the efficacy of regenerative therapeutics as treatments VML (Dienes et al., 2019). However, examining force production in isolation fails to consider the resulting biomechanical function. Furthermore, several human studies have demonstrated that improved force-generation ability does not necessarily lead to increased movement function (Buchner et al., 1997; Damiano et al., 2010, 2013; Damiano & Abel, 1998; Topp et al., 1993). In order to comprehensively evaluate a treatment's effectiveness, it is necessary to consider the resultant adaptations that occur during functional movement, such as gait. Gait analyses have emerged as popular tools for the evaluation of a diverse set of movement pathologies in rodents, including VML (Dienes et al., 2019), arthritis (Allen et al., 2012; Hamilton et al., 2015; Vincelette et al., 2007), nerve injury (Bauman & Chang, 2013; Bennett et al., 2012; Kappos et al., 2017), and spinal cord injury (Beare et al., 2009; Bhimani et al., 2017; Hamers et al., 2001; Koopmans et al., 2005). While many of these studies provide valuable data on gait deviations via a spatiotemporal perspective, only one considers both kinematics and kinetics during locomotion (Bennett et al., 2012), which allow for deeper insight into the mechanisms behind specific compensation strategies.

Recent studies from the University of Virginia's Motion Analysis and Motor Performance Laboratory and Laboratory of Regenerative Therapeutics have contributed to a detailed understanding of both normal and pathologic rat gait. Dienes (2019) reported changes in gait kinematics in rats with VML injuries to the TA during treadmill walking. The function of

the TA during gait is to actuate ankle dorsiflexion during swing to allow for foot clearance (Thota et al, 2005). This study demonstrated the sensitivity of gait kinematics as an evaluative tool, even for a muscle that does not bear a significant burden throughout the gait cycle. Dienes and Hicks (2022) established a normative database for rat gait kinematics and kinetics during over-ground walking. These studies have established the necessary 3D motion capture and musculoskeletal modeling methodologies for evaluating the effectiveness of the TEMR construct as a VML treatment strategy. However, neither of these studies assessed gait in rats that had been given VML treatment.

This work examined changes in gait kinematics and kinetics of rats in response to VML injury and treatment with a TEMR construct. This study quantifies specific gait adaptations resulting from TA and LG VML injury and quantifies recovery of function exhibited in VML injuries treated with the TEMR construct. In addition to the TA, the LG was chosen as the muscle of interest for this study because it bears a significant responsibility during gait. The LG is a biarticular muscle, capable of actuating both knee flexion and ankle plantarflexion. By providing specific insights into the functional deficits caused by lower extremity VML injuries to the TA and LG, as well as assessing the efficacy of a particular treatment (TEMR), the findings presented in this study have major implications for the future development of regenerative and rehabilitative therapies to treat VML. This study presents a specific case for the use of rodent gait analysis to improve the understanding and treatment of VML injury, but also demonstrates the ability of rodent gait analysis to be used as a tool for evaluating and developing treatments for other forms of extremity injuries.

5.2 Methods

5.2.1 Animals

32 male Lewis rats were obtained from Charles River Laboratories, pair housed in a vivarium accredited by the American Association for the Accreditation of Laboratory Animal Care, and provided with food and water *ad libitum*. After an initial baseline gait collection, all animals were given VML injuries to the right LG (n = 16) or right TA (n = 16), and 8 from each injured group were treated with the TEMR construct. A schematic of TA and LG locations in the rat hindlimb is shown in **Figure 16**. Gait data was collected prior to surgery and again at 4-, 8-, and 12-weeks post-surgery. Prior to each data collection, rats were allowed an acclimation period on the walkway until they moved across the walkway without hesitation. All animal procedures were approved by the University of Virginia Animal Care and Use Committee.

5.2.2 Surgery and Repair – LG

The methodology of Merritt et al. (2010) was used as a guideline for creating the LG VML injuries. A longitudinal incision was made parallel to the tibia on the outside of the lower right leg. The skin was then cleared from the underlying fascia using blunt separation. A second incision was made through the biceps femoris to expose the lateral gastrocnemius. The muscles within the posterior compartment were also separated using blunt separation. Once exposed, the midpoint of the LG between the knee and ankle was identified. Preliminary evaluation of LG weights from sacrificed animals from other studies showed that the LG muscle corresponds to roughly 0.25% of the gross body weight of Lewis rats. A rectangular chunk of muscle was excised beginning at the lateral edge, which corresponded to approximately 20% of the total LG weight. In the repair group, a TEMR cell-seed porcine bladder construct was sutured into the injury site immediately after creation of the VML injury, following protocols outlined in the

literature (Corona et al., 2012, 2013; Machingal et al., 2011). No treatment was given to the no-repair (LGNR) group. The fascia was closed with 6-0 vicryl sutures and the skin was closed with 5-0 prolene using interrupted sutures. Skin glue was applied over the skin sutures to help prevent the incision from opening.

5.2.2 Surgery and Repair – TA

TA VML injuries were created as previously described (Corona et al., 2012; Passipieri et al., 2013; Wu et al., 2012). A longitudinal incision was made on the lateral portion of the lower right leg. The skin was then cleared from the underlying fascia using blunt separation, and the fascia covering the anterior crural muscles was separated using blunt dissection. The proximal and distal tendons of the extensor hallicus longus and extensor digitorum longus muscles were isolated and ablated. The TA corresponds to 0.17% gross body weight. A chunk of muscle was excised from the TA, corresponding to approximately 20% of the TA muscle weight from the middle third of the muscle belly. In the repair group, a TEMR cell-seed porcine bladder construct was sutured into the injury site immediately after creation of the VML injury, following protocols outlined in the literature (Corona et al., 2012, 2013; Machingal et al., 2011). The remaining animals (n = 8) with TA VML injuries were given no repair. The fascia was closed with 6-0 vicryl sutures and the skin was closed with 5-0 prolene using interrupted sutures. Skin glue was applied over the skin sutures to help prevent the incision from opening.

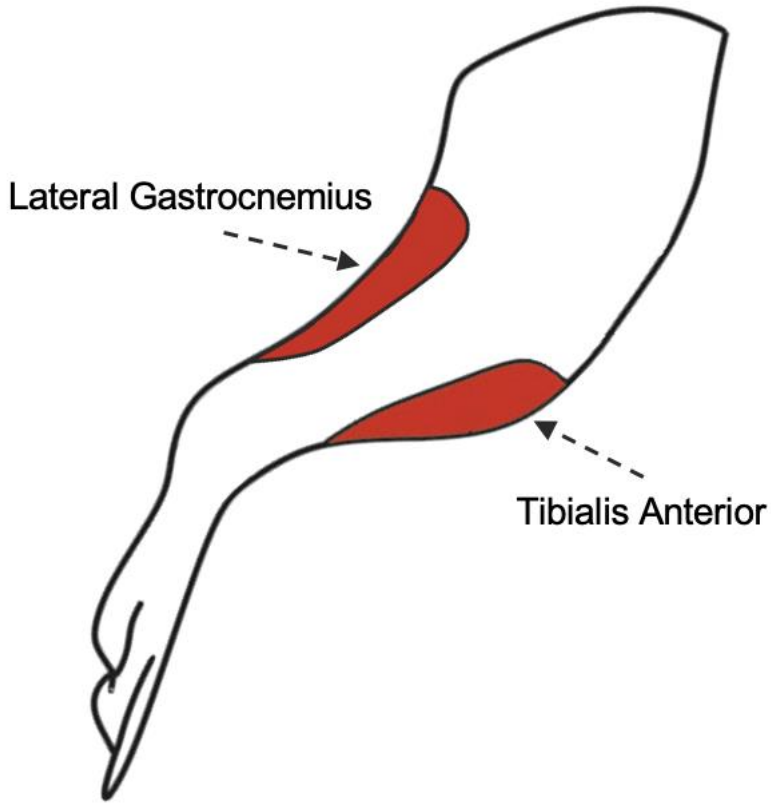

Figure 16: Simplified schematic of tibialis anterior and lateral gastrocnemius locations in the rat hindlimb.

5.2.4 Data Collection

Rats were tasked with walking freely across a custom-built instrumented walkway during each data collection. After a brief period of acclimation to the walkway, repeat walking trials were collected for each rat. During each trial, a 7-camera motion-capture system (Vicon, Oxford Metrics, Oxford, UK) was used to record 3D marker trajectories from 4mm hemispherical reflective markers placed over palpable landmarks on the rat spine, pelvis, and hindlimbs. Marker locations were: (1) L6 vertebra, (2) 5^{th} caudal vertebra, (3-4) left and right anterior iliac crests, (5-6) left and right greater trochanter of the femur, (7-8) left and right lateral femoral epicondyle, (9-10) left and right lateral malleolus, and (11-12) left and right lateral aspect of the distal end of the 5^{th} metatarsal. Marker data was collected at 200 Hz in Vicon Nexus. Ground reaction force (GRF) data was collected simultaneously at 1000 Hz via four ATI Nano43 6-axis force transducers (ATI Industrial Automation, NC) embedded in the walkway. Foot contact and foot off gait events for each trial were defined by a force of 0.07 N normal to the walkway surface. Rats were returned to the vivarium after each data collection period.

5.2.5 Data Analysis

Recorded trials were only included if the animal exhibited steady-state walking without deviations from normal locomotion behavior (e.g., stopping, sniffing, jolting, rearing, or turning around). Marker trajectories and ground reaction force data were filtered using a 4th order, low-pass, Butterworth filter (cutoff frequency of 15 Hz and 100 Hz, respectively). For each rat, a subject-specific OpenSim model of the hindlimbs was generated from limb measurements and previously acquired limb anthropometrics (Hicks and Dienes et al., 2022). OpenSim's inverse kinematic and inverse dynamic tools were used to compute hindlimb joint angles and joint moments. Reported data corresponds to one gait cycle, with the stance and swing phase of each

stride reported independently to minimize the effects of phasing caused by velocity differences. Each experimental group was independently analyzed and compared to its own baseline data. The two experimental groups examined were (1) *Tibialis Anterior* – no repair (TANR), (2) *Tibialis Anterior* – repair with TEMR construct (TAR), (3) *Lateral Gastrocnemius* – no repair (LGNR), and (4) *Lateral Gastrocnemius* – repair with TEMR construct (LGR), with each group containing 8 rats. Analysis of joint angle, joint moment, ground reaction force, and joint power curves was performed using Statistical Parametric Mapping (SPM) in MATLAB in accordance with procedures outlined by (Pataky (2012). Spatiotemporal parameters (STPs) were also evaluated using paired t-tests ($\alpha = 0.05$).

5.3 Results – TA VML Injury

A minimum of 2 (TANR group) or 4 (TAR group) gait cycles with concurrent 3-D motion capture and ground reaction force data were obtained for each rat during every data collection session (-1, 4, 8, and 12 weeks). Average STPs are a composite of all rats in each experimental group (n = 8) at each post-surgical time-point. Joint angles/moments, GRFs, and sagittal plane joint powers over the gait cycle are reported for the affected (right) and unaffected (left) hindlimb at each post-surgical time-point for the TAR group. In the TANR group, motion capture data was only collected on the right (affected) hindlimb. Hindlimb joint angles and moments, pelvis orientation, ground reaction forces, and joint power curves are shown in **Figure 17**-**Figure 26**. Shaded regions indicate locations of supra-threshold clusters (areas where the test statistic computed by SPM surpasses the critical value for that trajectory).

5.3.1 Spatiotemporal Parameters

The average values for walking velocity, stride length, stance time, swing time, cadence, and percent stance were calculated and compared across collection time-points. In the TAR

group, differences between affected and unaffected limb STP values were also examined at post-operative time-points (Week 4, Week 8, and Week 12). Velocity and stride length were normalized by each rat's leg length.

In the TANR group, there were no significant differences between baseline and post-surgical time-points for any of the parameters examined. Average STP values for affected limb gait cycles are shown in **Table 4**. In the TAR group, there were minimal significant differences detected between baseline data and later post-surgical time-points. Rats walked significantly faster at Week 8 ($p < 0.05$), which also significantly decreased time in stance ($p < 0.05$). At Week 12, stance time was still significantly decreased from baseline ($p < 0.05$). However, while an increase in velocity was observed, this change was not significant. Significant differences were also found between the affected and unaffected limb gait cycles at post-surgical time-points. Rats spent a smaller percent of affected limb gait cycles in stance at Week 4. In addition, velocity and cadence were significantly lower during affected limb gait cycles at Week 8. There were no significant differences detected between affected and unaffected hindlimbs during Week 12.

TANR Spatiotemporal Parameters	Baseline	Week04	Week08	Week12
Velocity (leg lengths/sec)	3.31±0.68	3.75±0.58	3.55±0.47	3.5±0.37
Stride Length (leg lengths)	1.51±0.12	1.61±0.12	1.64±0.07	1.62±0.11
Stance Time (sec)	0.32±0.06	0.29±0.06	0.32±0.08	0.31±0.04
Swing Time (sec)	0.15±0.02	0.16±0.01	0.17±0.02	0.17±0.02
Cadence (steps/min)	261.8±47.2	277.77±36.06	256.96±31.67	258.91±28.39
Stance (% GC)	67.89±3.46	63.7±5.02	63.54±3.07	64.65±2.91

Table 4: TANR spatiotemporal parameters at Baseline, Week 4, Week 8, and Week 12. No significant differences detected between baseline and post-surgical time-points ($p < 0.05$).

TAR	Baseline	Week4		Week8		Week12	
Spatiotemporal Parameters		Left	Right	Left	Right	Left	Right
Velocity (leg lengths/sec)	4.4±1.02	4.35±0.59	4.34±0.54	**5.12±0.83***	**4.93±0.9^**	4.77±0.81	4.73±0.8
Stride Length (length/leg length)	1.56±0.13	1.56±0.09	1.57±0.09	1.63±0.1	1.61±0.14	1.63±0.06	1.64±0.07
Stance Time (sec)	0.24±0.05	0.23±0.02	0.22±0.03	**0.19±0.03***	**0.2±0.03***	**0.21±0.04***	**0.21±0.04***
Swing Time (sec)	0.13±0.01	0.14±0.01	**0.15±0.01***	0.13±0.01	0.14±0.01	0.14±0.02	**0.15±0.01***
Cadence (steps/min)	332.48±52.27	331.9±29.39	330.8±28.88	**375.14±39.13**	**364.95±40.3^**	348.62±50.52	343.7±47
Stance (% GC)	63.36±3.2	**61.72±2.04**	**59.23±2.91^**	58.41±3.03	57.71±3.5	59.9±1.67	57.98±3.32

Table 5: TAR spatiotemporal parameters at Baseline, Week 4, Week 8, and Week 12. *significantly different than baseline ($p < 0.05$) ^significant difference between affected and unaffected limb STPs at that time-point ($p < 0.05$).

5.3.2 TANR Kinematics and Kinetics

In the TANR group, there were several significant differences in kinematics and kinetics between baseline and Week 4 (**Figure 17**). The pelvis tilt angle was flatter at Week 4 in both stance and swing. In addition, the hip was less abducted during the swing phase for affected limb gait cycles. The knee was less flexed during stance, while the ankle was less dorsiflexed during swing. There were no significant differences found between baseline and Week 4 joint moments, other than a slightly increased hip internal rotation moment in late-stance during Week 4. Minimal changes were also observed in hip adduction and knee flexion moments during swing. A full list of SPM supra-threshold cluster locations and p-values can be found in **Table 6**.

At Week 8, kinematics were similar to those seen at Week 4 (**Figure 18**). Again, the pelvis tilt angle was flatter, while the hip was less abducted and the knee was less flexed. Similar to Week 4, the ankle was less dorsiflexed during swing, but this trend was not significant. Unlike Week 4, the hip was significantly less flexed during early stance and late swing. In addition to changes seen in kinematics, rats also produced a greater hip extension moment at push off and a greater knee extension moment during stance. Supra-threshold cluster locations and p-values computed from SPM are shown in **Table 7**.

Minimal differences were found at Week 12 for the TANR group (**Figure 19**). Similar to prior weeks, the pelvis tilt angle was flatter, and the knee was less flexed in both stance and swing. No significant differences were found in stance phase joint moments at Week 12. Supra-threshold cluster locations and p-values computed from SPM are shown in **Table 8**.

GRF curves were also examined for the TANR group (**Figure 20**). There were no significant differences detected between baseline and post-surgical time-point GRFs. However, TANR animals did show trends of reduced peak medial GRFs, particularly at Week 8. Similarly,

there were no significant differences in sagittal plane joint powers calculated at the hip, knee, or ankle during stance (**Figure 21**). At Week 4, the affected hip generated significantly more power in late swing, just before foot contact.

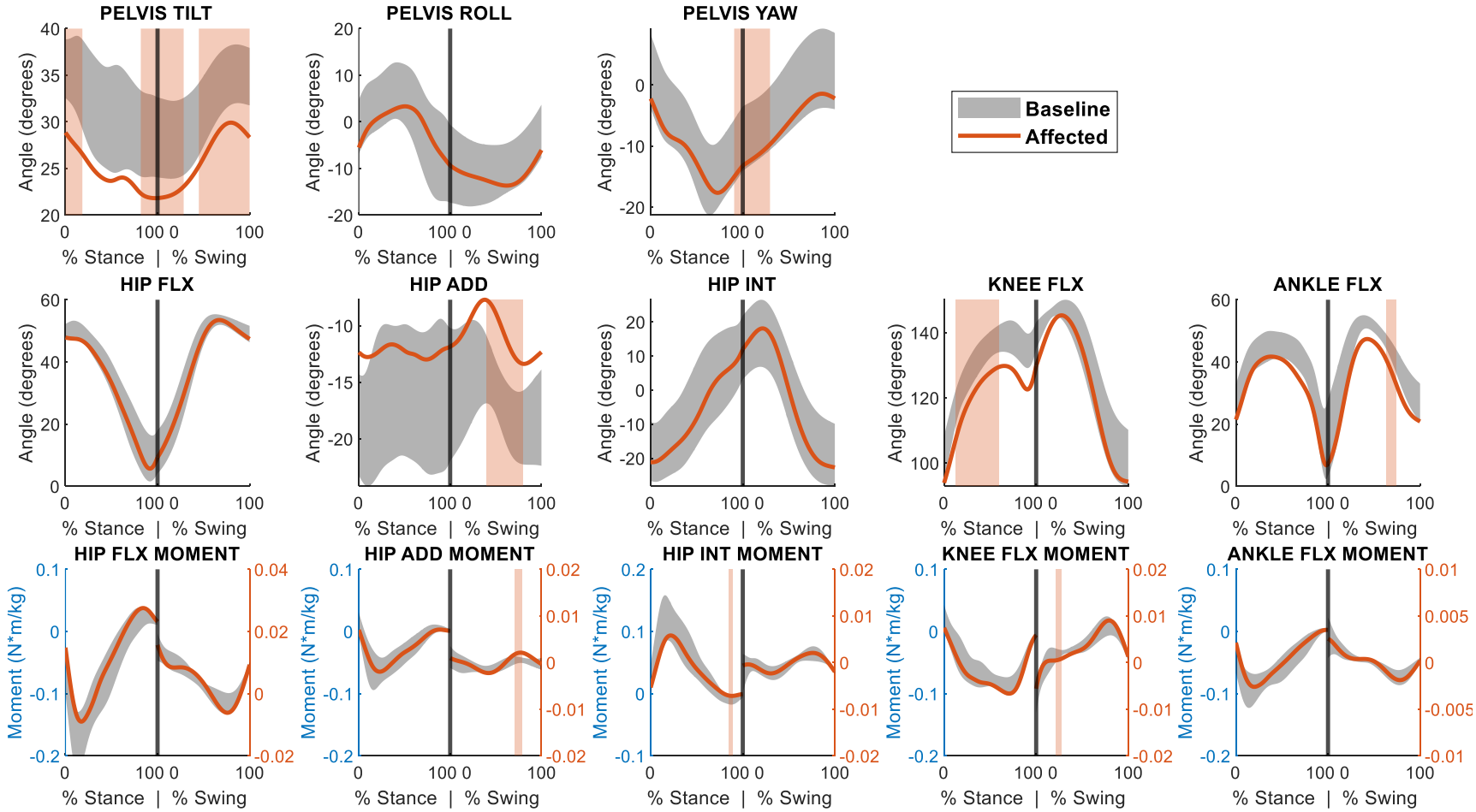

Figure 17: Mean trajectories for joint kinematics and joint kinetics during stance and swing for the TANR group at 4 weeks post-surgery. Curves compare baseline (shaded grey) to Week 4 for the affected hindlimb (orange) hindlimb. Vertical shaded regions represent supra-threshold clusters determined from SPM paired t-tests with a significance level of $\alpha = 0.05$, indicating a significant deviation from the baseline trajectory. The supra-threshold cluster probability for each cluster is given in **Table 6**.

	Affected (Right)	
Coordinate	**Stance**	**Swing**
Pelvis Tilt	0-18.4% (p = 0.033)	0-28.4% (p = 0.028)
Pelvis Roll		
Pelvis Yaw	90.7-100% (p = 0.044)	0-29.6% (p = 0.028)
Hip Flexion		
Hip Adduction		39.7-79.4% (p = 0.024)
Hip Internal Rot.		
Knee Flexion	12.2-59.4% (p < 0.001)	
Ankle Flexion		63.1-73.8% (p = 0.032)
Hip Flexion Moment		
Hip Adduction Moment		70.7-78.3% (p = 0.007)
Hip Internal Rot. Moment	84.7-88.5% (p = 0.039)	
Knee Flexion Moment		21.2-27.7% (p = 0.015)
Ankle Dorsiflexion Moment		

Table 6: Locations of supra-threshold clusters exceeding the critical value for each joint coordinate for the TANR group at 4 weeks post-surgery. Supra-threshold cluster locations pertain to the shaded regions identified in **Figure 17**, presented here as a percentage of the stance or swing phase. The associated p-value designates the precise probability that a given supra-threshold cluster of that size would be observed in random samplings. The null hypothesis is rejected for each curve containing a supra-threshold cluster.

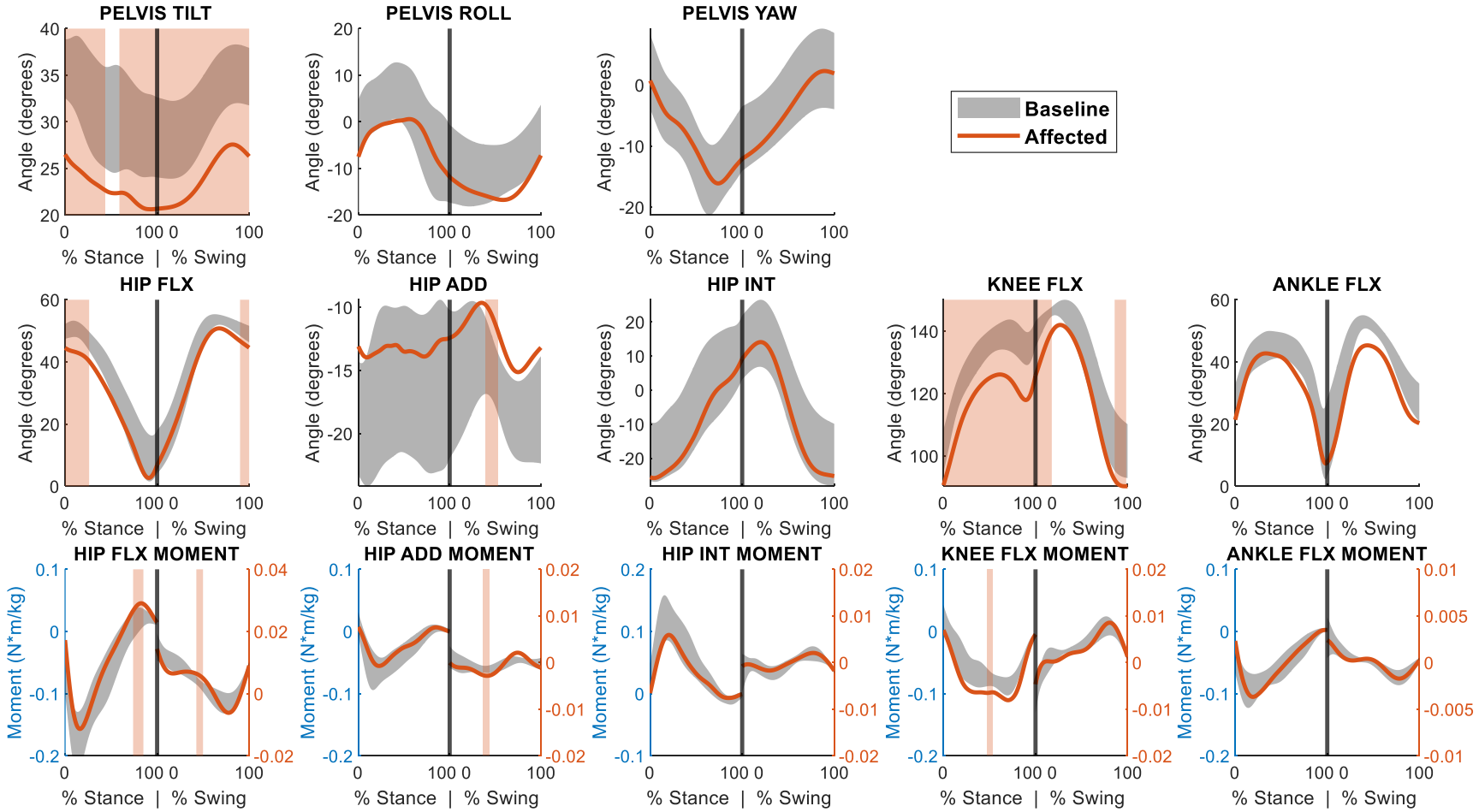

Figure 18: Mean trajectories for joint kinematics and joint kinetics during stance and swing for the TANR group at 8 weeks post-surgery. Curves compare baseline (shaded grey) to Week 8 for the affected hindlimb (orange) hindlimb. Vertical shaded regions represent supra-threshold clusters determined from SPM paired t-tests with a significance level of $\alpha = 0.05$, indicating a significant deviation from the baseline trajectory. The supra-threshold cluster probability for each cluster is given in **Table 7**.

	Affected (Right)	
Coordinate	**Stance**	**Swing**
Pelvis Tilt	0-43.7% (p = 0.006) 59-100% (p = 0.008)	0-100% (p < 0.001)
Pelvis Roll		
Pelvis Yaw		
Hip Flexion	0-26.2% (p = 0.011)	90.1-100% (p = 0.04)
Hip Adduction		39.7-53.2% (p = 0.039)
Hip Internal Rot.		
Knee Flexion	0.4-100% (p < 0.001)	0-17.7% (p = 0.018) 86-98.5% (p = 0.03)
Ankle Flexion		
Hip Flexion Moment	73.9-85.1% (p = 0.01)	42.6-49.9% (p = 0.012)
Hip Adduction Moment		36.4-43% (p = 0.019)
Hip Internal Rot. Moment		
Knee Flexion Moment	47.2-53.3% (p = 0.025)	
Ankle Dorsiflexion Moment		

Table 7: Locations of supra-threshold clusters exceeding the critical value for each joint coordinate for the TANR group at 8 weeks post-surgery. Supra-threshold cluster locations pertain to the shaded regions identified in **Figure 18**, presented here as a percentage of the stance or swing phase. The associated p-value designates the precise probability that a given supra-threshold cluster of that size would be observed in random samplings. The null hypothesis is rejected for each curve containing a supra-threshold cluster.

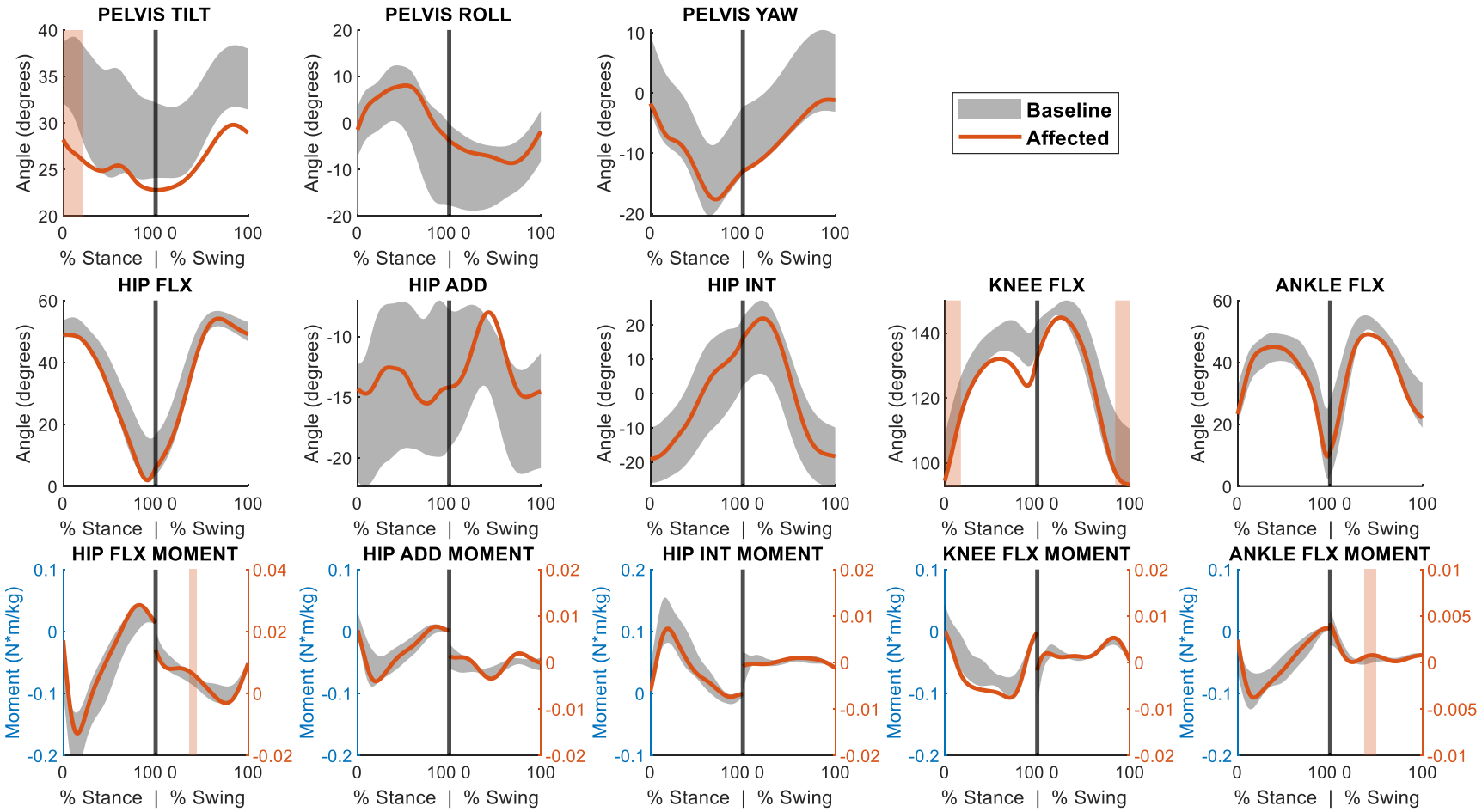

Figure 19: Mean trajectories for joint kinematics and joint kinetics during stance and swing for the TANR group at 12 weeks post-surgery. Curves compare baseline (shaded grey) to Week 12 for the affected hindlimb (orange) hindlimb. Vertical shaded regions represent supra-threshold clusters determined from SPM paired t-tests with a significance level of $\alpha = 0.05$, indicating a significant deviation from the baseline trajectory. The supra-threshold cluster probability for each cluster is given in **Table 8**.

	Affected (Right)	
Coordinate	**Stance**	**Swing**
Pelvis Tilt	0-23.3% (p = 0.033)	
Pelvis Roll		
Pelvis Yaw		
Hip Flexion		
Hip Adduction		
Hip Internal Rot.		
Knee Flexion	0.6-14.8% (p = 0.034)	83.1-100% (p = 0.028)
Ankle Flexion		
Hip Flexion Moment		
Hip Adduction Moment		40.9-51.1% (p = 0.007)
Hip Internal Rot. Moment		
Knee Flexion Moment		
Ankle Dorsiflexion Moment		

Table 8: Locations of supra-threshold clusters exceeding the critical value for each joint coordinate for the TANR group at 12 weeks post-surgery. Supra-threshold cluster locations pertain to the shaded regions identified in **Figure 19**, presented here as a percentage of the stance or swing phase. The associated p-value designates the precise probability that a given supra-threshold cluster of that size would be observed in random samplings. The null hypothesis is rejected for each curve containing a supra-threshold cluster.

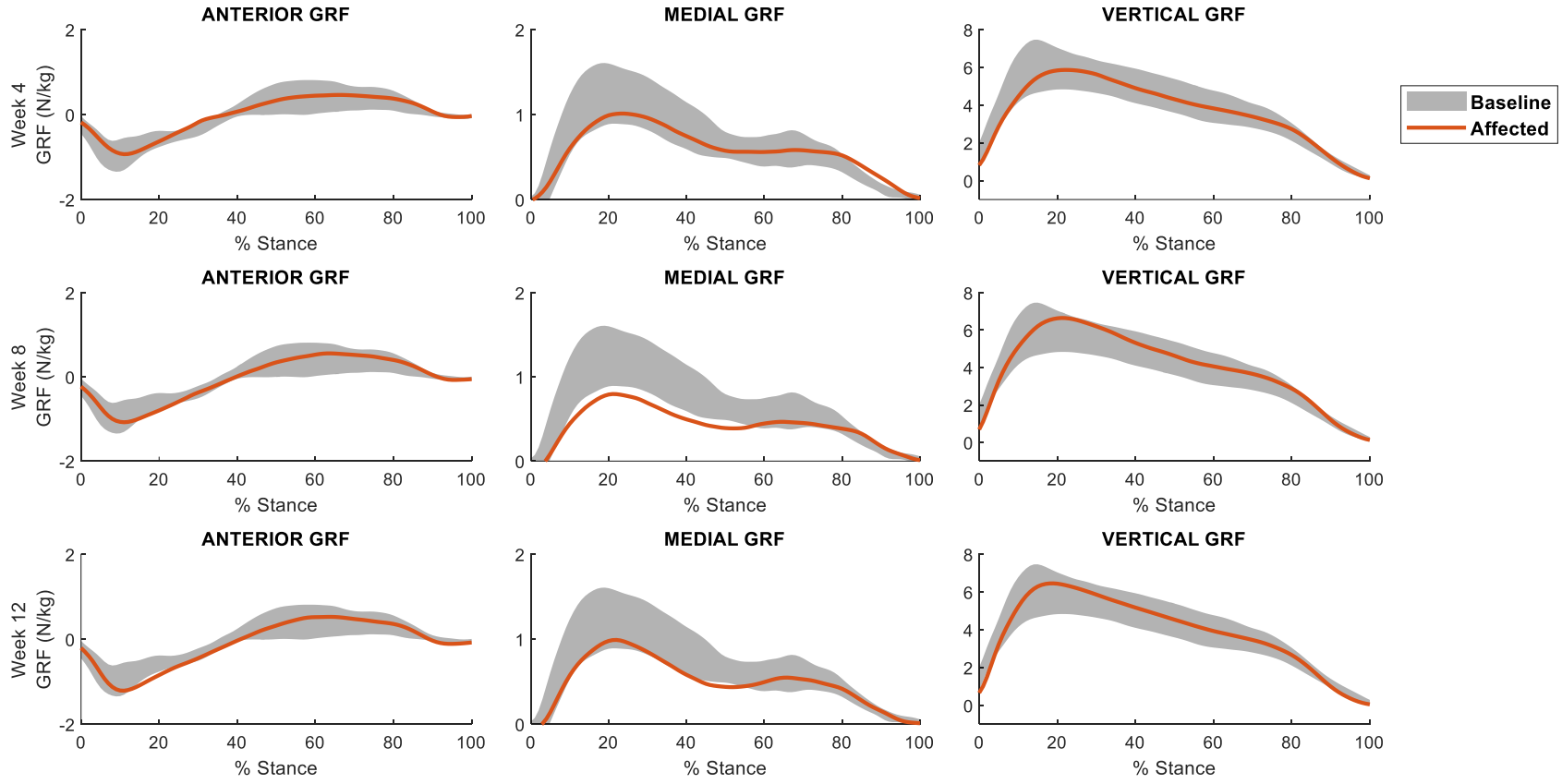

Figure 20: Ground reaction force (GRF) curves for TANR rats. Curves compare baseline (shaded grey) to affected limb (orange) GRFs during stance. GRFs were normalized by body mass. There were no significant differences between baseline and post-operation GRFs.

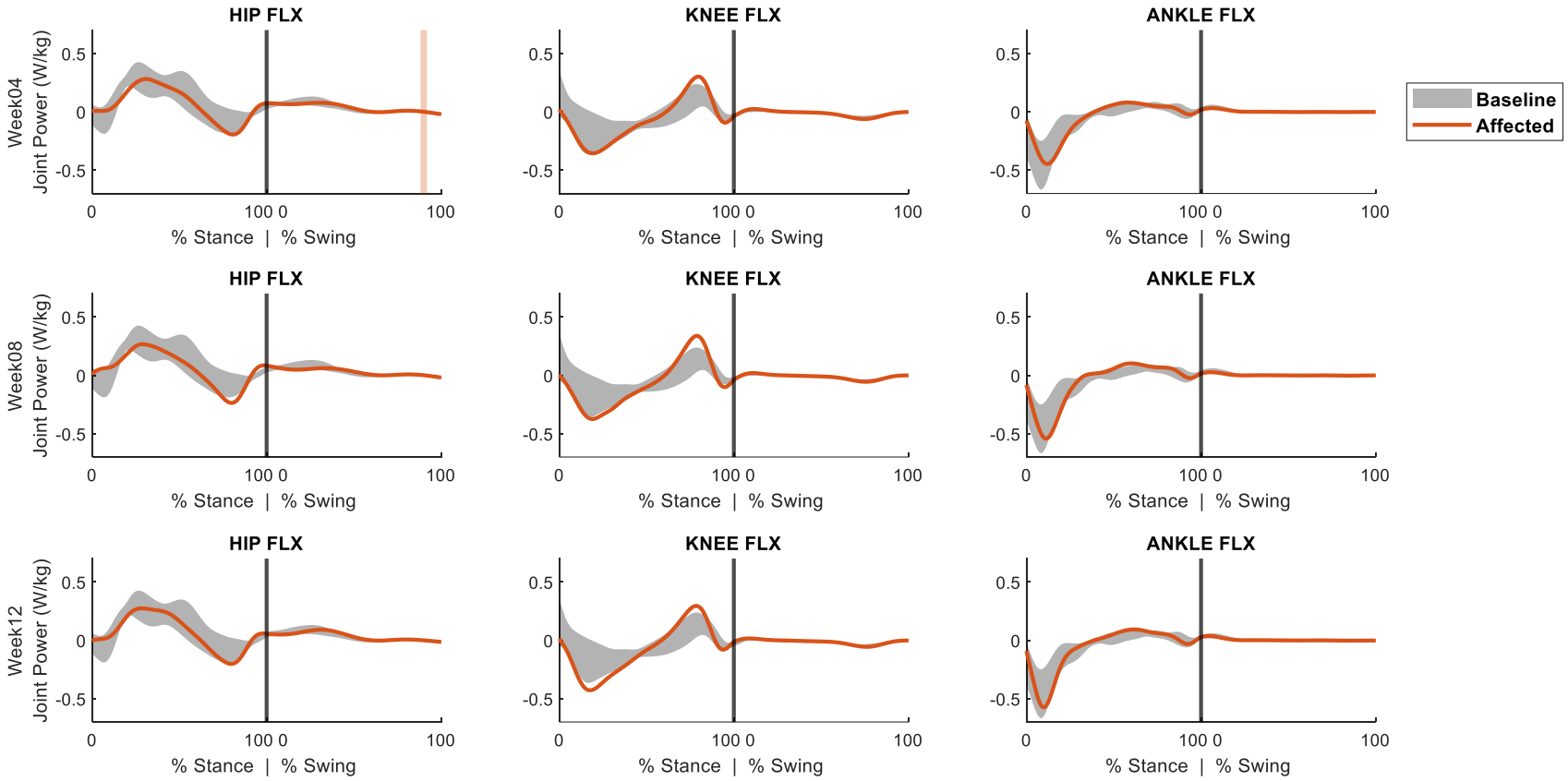

Figure 21: Sagittal plane joint power curves for TANR rats. Curves compare baseline (shaded grey) to affected limb (orange) joint power in stance and swing. Vertical shaded regions represent supra-threshold clusters determined from SPM paired t-tests with a significance level of $\alpha = 0.05$, indicating a significant deviation from the baseline trajectory. The supra-threshold cluster probability for each cluster is given in **Table 9**.

		Affected (Right)	
		Stance	**Swing**
Week 4	Hip Flexion		88.2-91.8% (p = 0.019)
	Knee Flexion		
	Ankle Dorsiflexion		
Week 8	Hip Flexion		
	Knee Flexion		
	Ankle Dorsiflexion		
Week 12	Hip Flexion		
	Knee Flexion		
	Ankle Dorsiflexion		

Table 9: Locations of supra-threshold clusters exceeding the critical value for TANR sagittal plane joint power curves at Weeks 4, 8, and 12. Supra-threshold cluster locations pertain to the shaded regions identified in **Figure 21**, presented here as a percentage of the stance phase. The associated p-value designates the precise probability that a given supra-threshold cluster of that size would be observed in random samplings. The null hypothesis is rejected for each curve containing a supra-threshold cluster.

5.3.3 TAR Kinematics and Kinetics

There were several significant differences between baseline and Week 4 kinematics and kinetics for the TAR rats (**Figure 22**). The pelvis was significantly more rolled toward the unaffected limb side during both affected and unaffected limb gait cycles, indicating that rats were favoring their unaffected leg. Both the affected and unaffected hips were less flexed, more abducted, and more externally rotated during both stance and swing. Moreover, the left knee was less flexed during stance. Interestingly, there were no significant differences found at the ankle joint for either hindlimb. Joint moments also exhibited significant differences from baseline. There were significant increases in unaffected limb hip moments across the board. In addition, both limbs produced greater hip extension moments during stance. No differences were found in ankle joint moments between Week 4 and baseline. **Table 10** contains a full list of SPM supra-threshold cluster locations and corresponding p-values.

At Week 8, rats still exhibited significant differences from baseline kinematics and kinetics (**Figure 23**). Both the affected and unaffected hips were significantly more abducted and externally rotated during both stance and swing when compared to baseline. In addition, both knees were less flexed during stance. Ankle dorsiflexion was also significantly decreased at push-off during unaffected limb gait cycles. Kinetic changes at Week 8 were largely similar to those seen at Week 4. Namely, the unaffected limb produced greater hip extension, hip abduction, and hip internal rotation moments during stance, while both knees produced greater extension moments. A full list of supra-threshold cluster locations and p-values computed from SPM paired t-tests are shown in **Table 11**.

Week 12 kinematics and kinetics were similar to those demonstrated at prior post-surgical time-points (**Figure 24**). Each hip was less flexed during stance and swing. In addition,

the affected hip was more abducted and more externally rotated, while the unaffected hip was slightly externally rotated. Both knees were significantly less flexed, while ankle kinematics were comparable to baseline for both hindlimbs. Joint moments at the hip and knee were also similar to those produced at Week 8. In addition, both ankles produced a significantly greater plantarflexion moments during stance at Week 12. Exact supra-threshold cluster locations and corresponding p-values for Week 12 kinematics and kinetics are shown in **Table 12**.

GRF curves were also examined for TAR rats (**Figure 25**). At Week 4, GRFs exhibited no significant differences from baseline data. At Week 8 and Week 12, rats generated a significantly greater vertical ground reaction force with both the affected and unaffected hindlimbs. In addition, Week 8 medial GRFs were significantly lower in late stance. A full list of SPM supra-threshold cluster locations and p-values is given in **Table 13**.

Sagittal plane joint powers were calculated for TAR rats (**Figure 26**). Over the recovery period, joint power curves were increasingly more deviant from baseline data. At Week 4, TAR rats generated more power with the hip than at baseline during stance. Simultaneously, the affected limb knee absorbed more power during stance. At Week 8, rats generated more power with the hip in the unaffected limb during early stance, while absorbing significantly more power in each knee in early stance. In late stance, rats generated significantly more power with both knees. Similarly, each ankle absorbed significantly more power during early stance, while producing more power in late stance. At Week 12, rats produced more power with each hip and absorbed more power with each knee during early stance. Rats also absorbed more power with their affected ankle in early stance, and generated more power with both ankles in late stance. Minimal significant differences were observed in joint power curves during swing. **Table 14** shows exact supra-threshold cluster locations and p-values computed with SPM.

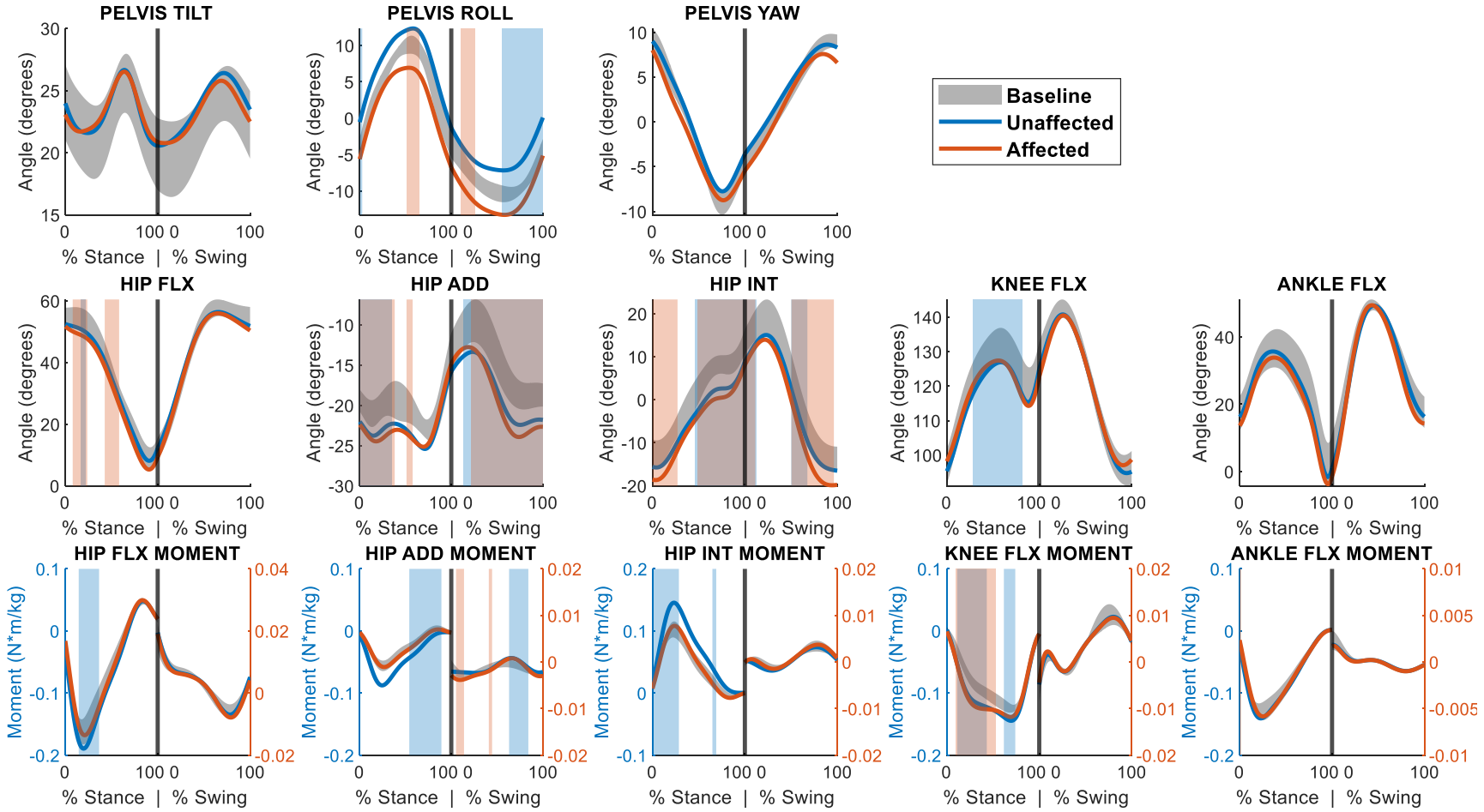

Figure 22: Mean trajectories for joint kinematics and joint kinetics during stance and swing for the TAR group at 4 weeks post-surgery. Curves compare baseline (shaded grey) to Week 4 for the left (blue, unaffected) and right (orange, affected) hindlimbs. Vertical shaded regions represent supra-threshold clusters determined from SPM paired t-tests with a significance level of $\alpha = 0.05$, indicating a significant deviation from the baseline trajectory. The supra-threshold cluster probability for each cluster is given in **Table 10.**

	Left		Right	
Coordinate	**Stance**	**Swing**	**Stance**	**Swing**
Pelvis Tilt				
Pelvis Roll	0-2.8% (p = 0.05)	55.5-100% (p = 0.008)	51.5-65% (p = 0.035)	10.2-26% (p = 0.041)
Pelvis Yaw				
Hip Flexion	16.7-21.7% (p = 0.047)		8-23.8% (p = 0.029) 42.7-58.3% (p = 0.029)	
Hip Adduction	0-35.3% (p < 0.001)	13-100% (p < 0.001)	0-38.2% (p = 0.003) 51.1-57.8% (p = 0.046)	21.5-100% (p < 0.001)
Hip Internal Rot.	45.8-100% (p < 0.001)	0-12.6% (p = 0.042) 50.1-67.7% (p = 0.035)	0-27.1% (p = 0.019) 48.6-100% (p = 0.002)	0-11.3% (p = 0.042) 50.4-96.4% (p = 0.003)
Knee Flexion	28.5-81.7% (p < 0.001)			
Ankle Flexion				
Hip Flexion Moment	14.5-36.6% (p < 0.001)			
Hip Adduction Moment	54.1-89.2% (p < 0.001)	63.1-84.1% (p < 0.001)		5.2-13.9% (p = 0.002) 41-44.5% (p = 0.028)
Hip Internal Rot. Moment	0-28.6% (p < 0.001) 64.9-69% (p = 0.039)			
Knee Flexion Moment	11.2-43.2% (p < 0.001) 61.7-74.1% (p = 0.011)		9.7-53.3% (p < 0.001)	
Ankle Dorsiflexion Moment			0-1.2% (p = 0.049)	

Table 10: Locations of supra-threshold clusters exceeding the critical value for each coordinate for the TAR group at 4 weeks post-surgery. Supra-threshold cluster locations pertain to the shaded regions identified in **Figure 22**, presented here as a percentage of the stance or swing phase. The associated p-value designates the precise probability that a given supra-threshold cluster of that size would be observed in random samplings. The null hypothesis is rejected for each curve containing a supra-threshold cluster.

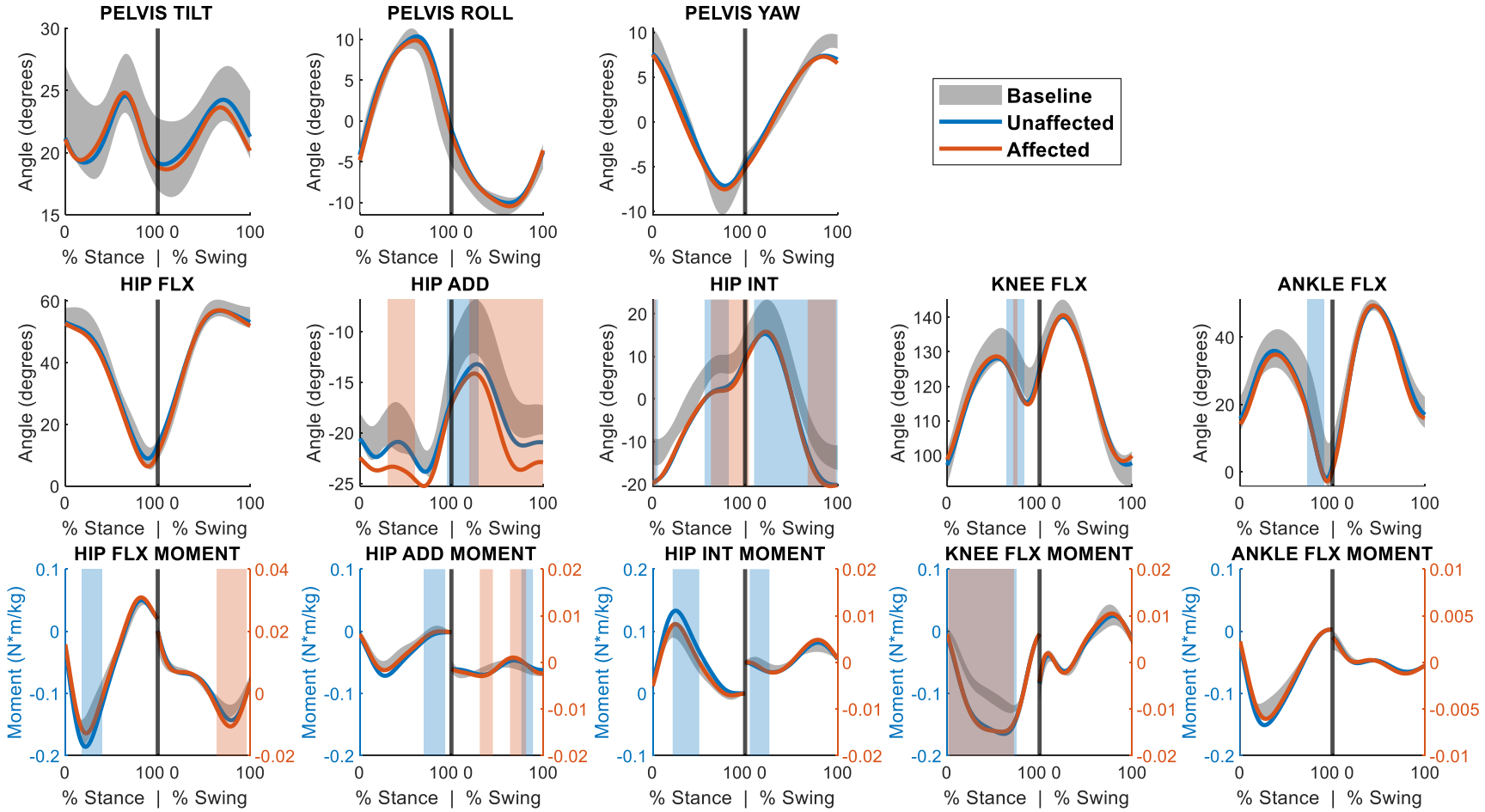

Figure 23: Mean trajectories for joint kinematics and joint kinetics during stance and swing for the TAR group at 8 weeks post-surgery. Curves compare baseline (shaded grey) to Week 8 for the left (blue, unaffected) and right (orange, affected) hindlimbs. Vertical shaded regions represent supra-threshold clusters determined from SPM paired t-tests with a significance level of $\alpha = 0.05$, indicating a significant deviation from the baseline trajectory. The supra-threshold cluster probability for each cluster is given in **Table 11**.

	Left		Right	
Coordinate	**Stance**	**Swing**	**Stance**	**Swing**
Pelvis Tilt				
Pelvis Roll				
Pelvis Yaw				
Hip Flexion				
Hip Adduction	95.4-100% (p = 0.047)	0-29.7% (p = 0.014)	30.6-60.3% (p = 0.012)	19.9-100% (p < 0.001)
Hip Internal Rot.	0-5.7% (p = 0.048) 56.1-82.3% (p = 0.02) 99.7-100% (p = 0.05)	0-0.6% (p = 0.05) 9.7-100% (p < 0.001)	0-3.5% (p = 0.049) 62.9-100% (p = 0.01)	0-4.2% (p = 0.049) 67.7-98.4% (p = 0.016)
Knee Flexion	64.2-83% (p = 0.027)		72.1-76% (p = 0.049)	
Ankle Flexion	72.5-90.3% (p = 0.014)			
Hip Flexion Moment	17.4-39.5% (p < 0.001)			64.1-96.4% (p < 0.001)
Hip Adduction Moment	69.7-93.3% (p < 0.001)	76.3-89% (p = 0.005)		30.9-45.2% (p = 0.002) 64-81.5% (p < 0.001)
Hip Internal Rot. Moment	21.6-50.4% (p < 0.001)	5-26.3% (p < 0.001)		
Knee Flexion Moment	1.9-74.7% (p < 0.001)		1-72.4% (p < 0.001)	
Ankle Dorsiflexion Moment			0-0.7% (p = 0.05)	

Table 11: Locations of supra-threshold clusters exceeding the critical value for each coordinate for the TAR group at 8 weeks post-surgery. Supra-threshold cluster locations pertain to the shaded regions identified in **Figure 23**, presented here as a percentage of the stance or swing phase. The associated p-value designates the precise probability that a given supra-threshold cluster of that size would be observed in random samplings. The null hypothesis is rejected for each curve containing a supra-threshold cluster.

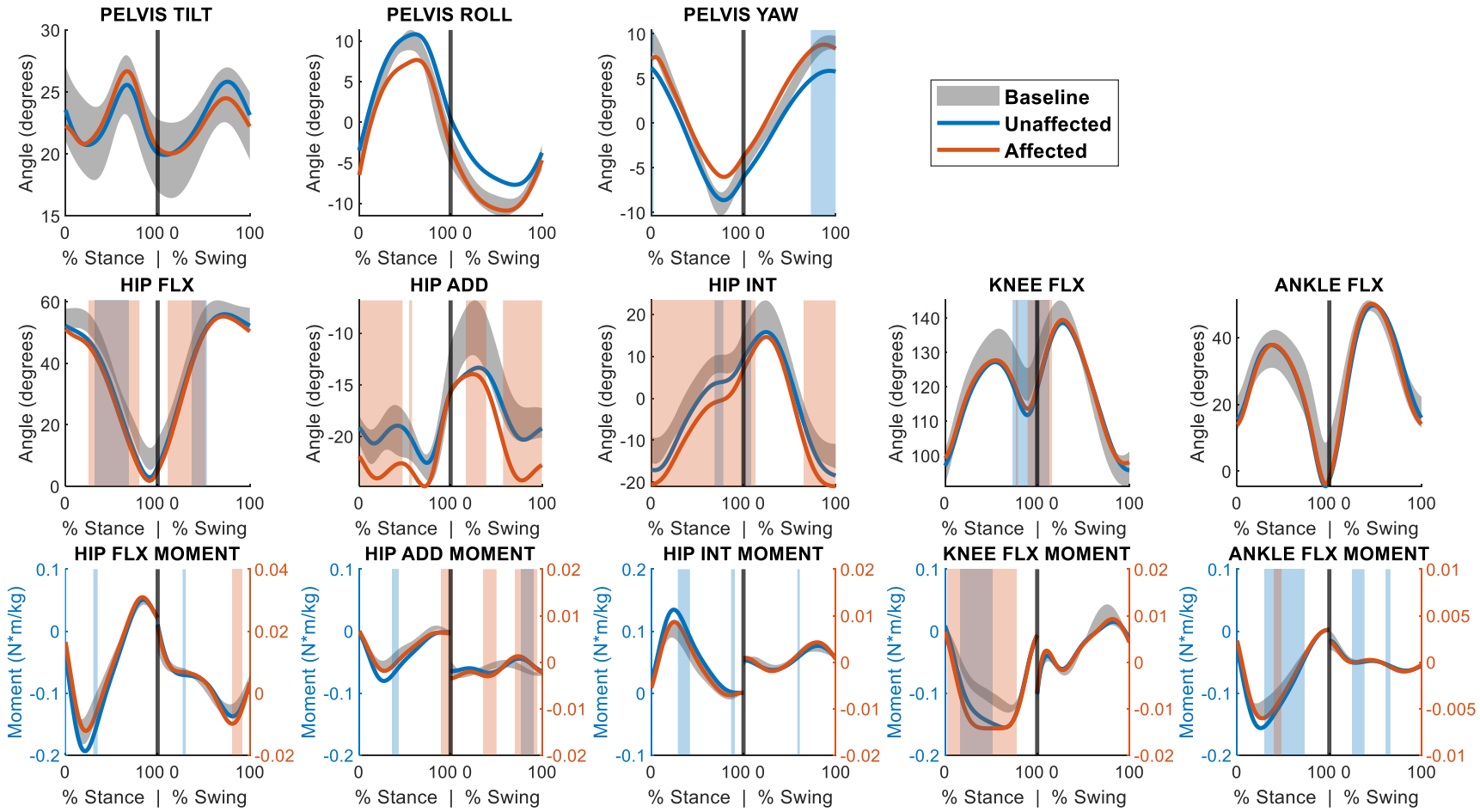

Figure 24: Mean trajectories for joint kinematics and joint kinetics during stance and swing for the TAR group at 12 weeks post-surgery. Curves compare baseline (shaded grey) to Week 12 for the left (blue, unaffected) and right (orange, affected) hindlimbs. Vertical shaded regions represent supra-threshold clusters determined from SPM paired t-tests with a significance level of $\alpha = 0.05$, indicating a significant deviation from the baseline trajectory. The supra-threshold cluster probability for each cluster is given in **Table 12**.

	Left		Right	
Coordinate	**Stance**	**Swing**	**Stance**	**Swing**
Pelvis Tilt				
Pelvis Roll				
Pelvis Yaw	0-2.5% (p = 0.049)	73.1-100% (p = 0.029)		
Hip Flexion	31.8-68.5% (p = 0.001)	36.8-53.4% (p = 0.033)	24.8-80.2% (p < 0.001)	10.8-52% (p < 0.001)
Hip Adduction			1.2-47.5% (p < 0.001) 54.6-57.9% (p = 0.046)	16.7-39.1% (p = 0.008) 57.4-100% (p < 0.001)
Hip Internal Rot.	68.5-78.2% (p = 0.044) 99.9-100% (p = 0.05)	0-7.5% (p = 0.047)	0-100% (p < 0.001)	0-13.1% (p = 0.035) 65.2-100% (p = 0.004)
Knee Flexion	73-100% (p = 0.024)	0-13.3% (p = 0.042)	76.8-79% (p = 0.05) 89.6-100% (p = 0.043)	0-15.4% (p = 0.041)
Ankle Flexion				
Hip Flexion Moment	30.2-34.9% (p = 0.041)	27-30.5% (p = 0.04)		81.2-91.6% (p = 0.011)
Hip Adduction Moment	36.3-43.3% (p = 0.027)	77.1-90.4% (p = 0.003)	89.7-100% (p = 0.005)	0-2.1% (p = 0.046) 35.5-50.2% (p = 0.001) 70.3-94.9% (p < 0.001)
Hip Internal Rot. Moment	28.8-41.9% (p = 0.004) 86.6-90.7% (p = 0.039)	58.5-61.1% (p = 0.038)		
Knee Flexion Moment	16.2-50.9% (p < 0.001)		2.4-77.1% (p < 0.001)	
Ankle Dorsiflexion Moment	29.2-73% (p < 0.001)	24.5-38.2% (p < 0.001) 61-66.4% (p = 0.014)	39.7-47.4% (p = 0.02)	

Table 12: Locations of supra-threshold clusters exceeding the critical value for each coordinate for the TAR group at 12 weeks post-surgery. Supra-threshold cluster locations pertain to the shaded regions identified in **Figure 24**, presented here as a percentage of the stance or swing phase. The associated p-value designates the precise probability that a given supra-threshold cluster of that size would be observed in random samplings. The null hypothesis is rejected for each curve containing a supra-threshold cluster.

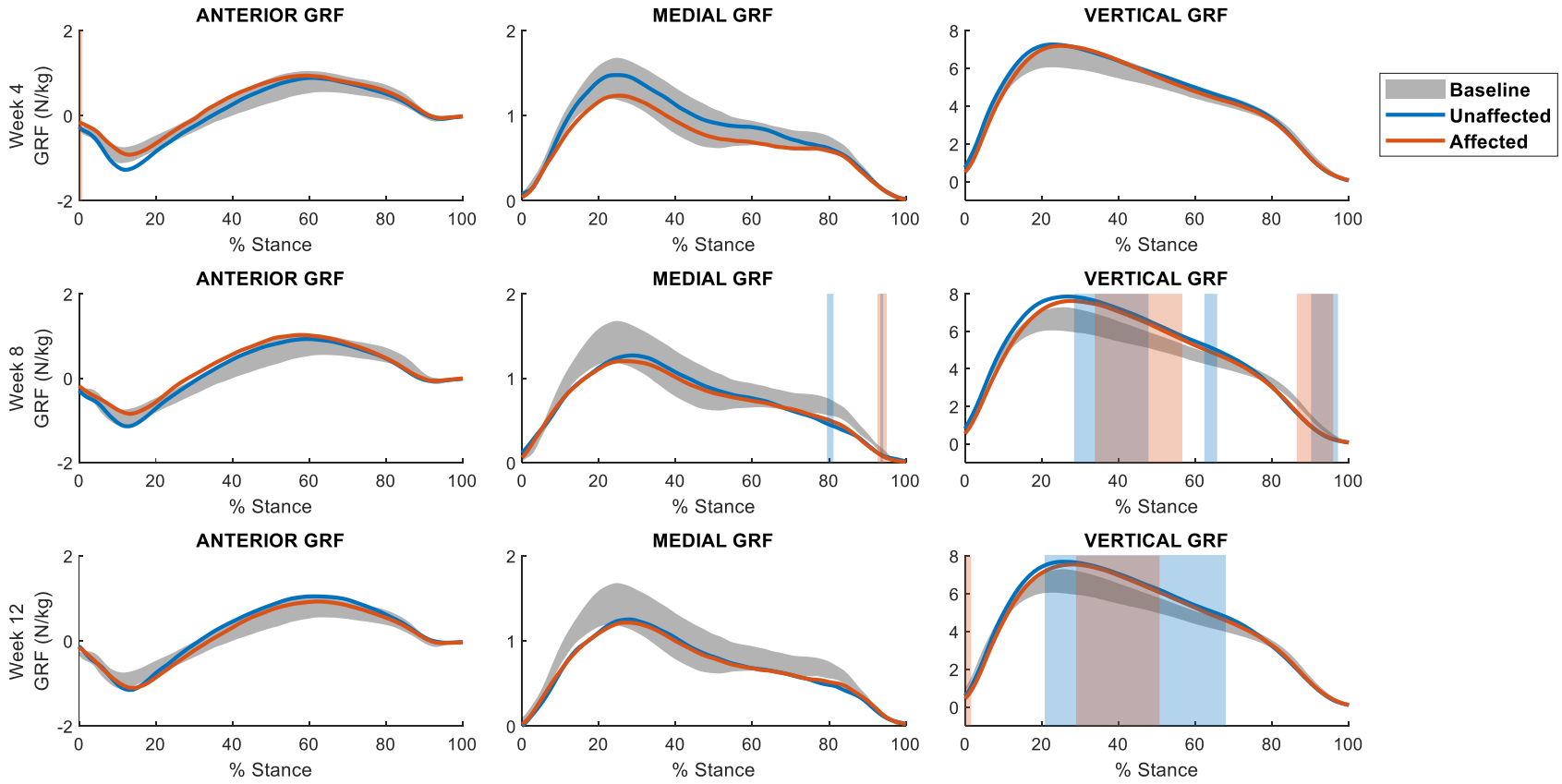

Figure 25: Ground reaction force (GRF) curves for TAR rats. Curves compare baseline (shaded grey) to affected (orange) and unaffected (blue) hindlimb GRFs. GRFs were normalized by body mass. Vertical shaded regions represent supra-threshold clusters determined from SPM paired t-tests with a significance level of $\alpha = 0.05$, indicating a significant deviation from the baseline trajectory. The supra-threshold cluster probability for each cluster is given in **Table 13.**

		Left	Right
Week 4	Anterior GRF		0-0.8% (p = 0.047)
	Vertical GRF		
	Medial GRF		
Week 8	Anterior GRF		
	Vertical GRF	28.4-47.8% (p < 0.001) 62.4-65.7% (p = 0.034) 90.2-97.2% (p = 0.009)	33.8-56.6% (p < 0.001) 86.4-95.9% (p = 0.002)
	Medial GRF	79.5-81.2% (p = 0.041) 93.3-94.1% (p = 0.048)	92.8-95.1% (p = 0.039)
Week 12	Anterior GRF		
	Vertical GRF	20.9-67.8% (p < 0.001)	0-1.6% (p = 0.046) 28.9-50.7% (p < 0.001)
	Medial GRF		

Table 13: Locations of supra-threshold clusters exceeding the critical value for TAR GRFs at Weeks 4, 8, and 12. Supra-threshold cluster locations pertain to the shaded regions identified in **Figure 25**, presented here as a percentage of the stance phase. The associated p-value designates the precise probability that a given supra-threshold cluster of that size would be observed in random samplings. The null hypothesis is rejected for each curve containing a supra-threshold cluster.

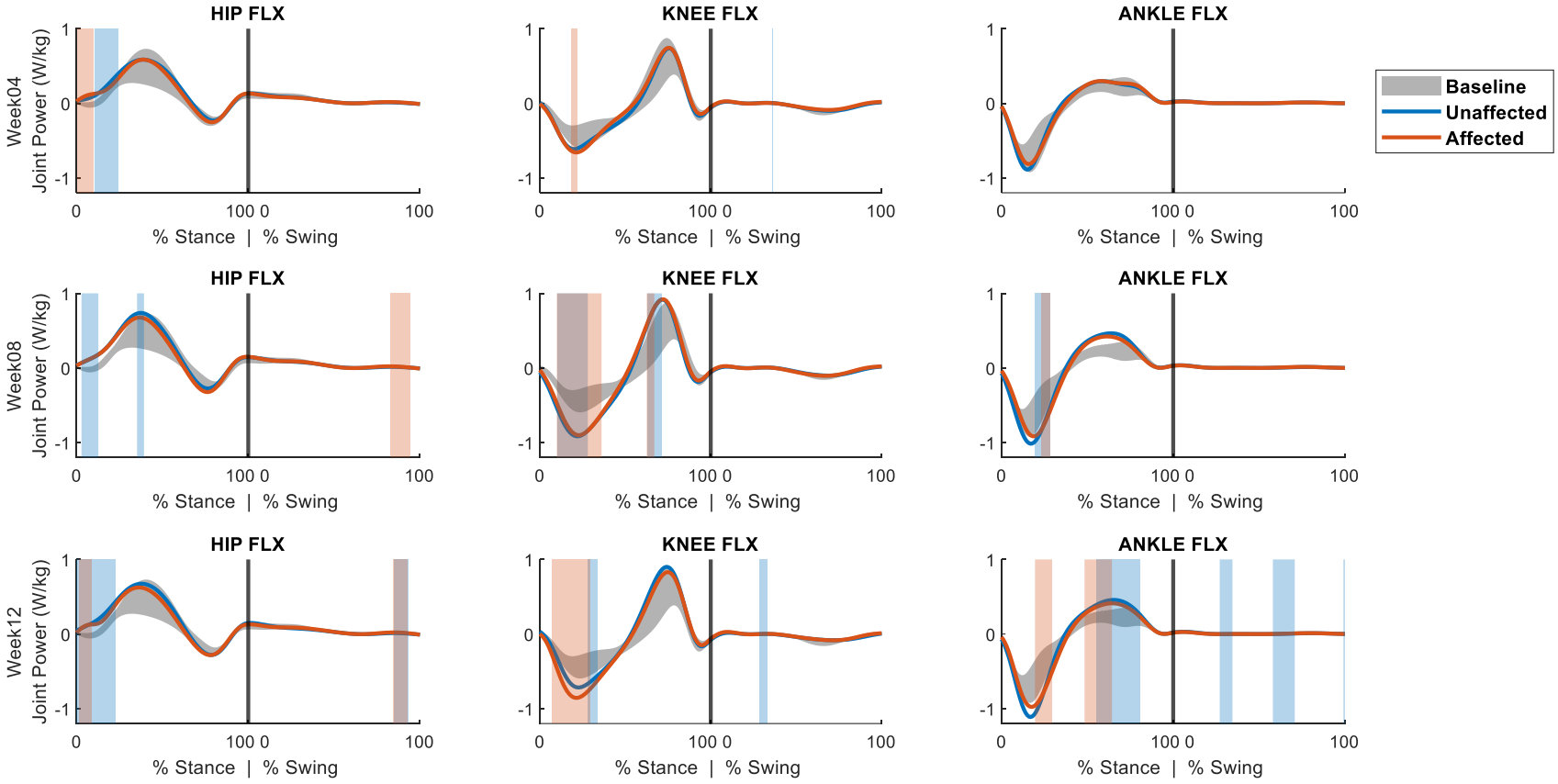

Figure 26: Sagittal plane joint power curves for TAR rats. Curves compare baseline (shaded grey) to affected limb (orange) and unaffected limb (blue) joint power in stance and swing. Vertical shaded regions represent supra-threshold clusters determined from SPM paired t-tests with a significance level of $\alpha = 0.05$, indicating a significant deviation from the baseline trajectory. The supra-threshold cluster probability for each cluster is given in **Table 14**.

		Unaffected (Left)		Affected (Right)	
		Stance	**Swing**	**Stance**	**Swing**
Week 4	Hip Flexion	10.5-23.9% ($p < 0.001$)		0.6-9.9% ($p = 0.002$)	
	Knee Flexion		36-36.5% ($p = 0.049$)	18.3-21.8% ($p = 0.031$)	
	Ankle Dorsiflexion				
Week 8	Hip Flexion	2.9-12.7% ($p = 0.002$) 35.2-39.3% ($p = 0.03$)			83-94.4% ($p < 0.001$)
	Knee Flexion	10.2-28.1% ($p < 0.001$) 62.9-71.5% ($p < 0.001$)		9.9-36.1% ($p < 0.001$) 62.5-67% ($p = 0.009$)	
	Ankle Dorsiflexion	19.5-28.3% ($p < 0.001$)		22.9-28.2% ($p = 0.005$)	
Week 12	Hip Flexion	0-22.6% ($p < 0.001$)	85.1-93.2% ($p = 0.006$)	1.5-8.6% ($p = 0.001$)	84.4-92.5% ($p = 0.006$)
	Knee Flexion	28.3-33.7% ($p = 0.013$)	28.8-33.3% ($p = 0.015$)	7.2-29.2% ($p < 0.001$)	
	Ankle Dorsiflexion	55.1-80.5% ($p < 0.001$)	27.1-34.5% ($p = 0.002$) 58.1-70.8% ($p < 0.001$) 99.1-100% ($p = 0.048$)	19.5-29.5% ($p < 0.001$) 48.3-64.3% ($p < 0.001$)	

Table 14: Locations of supra-threshold clusters exceeding the critical value for TAR sagittal plane joint power curves at Weeks 4, 8, and 12. Supra-threshold cluster locations pertain to the shaded regions identified in **Figure 26**, presented as a percentage of stance or swing phase. The associated p-value designates the precise probability that a given supra-threshold cluster of that size would be observed in random samplings. The null hypothesis is rejected for each curve containing a supra-threshold cluster.

5.4 Results – LG VML Injury

A minimum of 4 gait cycles with concurrent 3-D motion capture and ground reaction force data were obtained for each rat during every data collection session (-1, 4, 8, and 12 weeks). Average STPs are a composite of all rats in each experimental group (n = 8) at each post-surgical time-point. Joint angles/moments, GRFs, and sagittal plane joint powers over the gait cycle are reported for the affected (right) and unaffected (left) hindlimb at each post-surgical time-point. Hindlimb joint angles/moments, pelvis orientation, ground reaction forces, and joint power curves are shown in **Figure 27**-**Figure 36**. Shaded regions indicate locations of supra-threshold clusters (areas where the test statistic computed by SPM surpasses the critical value for that trajectory).

5.4.1 Spatiotemporal Parameters

The average values for walking velocity, stride length, stance time, swing time, cadence, and percent stance were calculated and compared across collection time-points. Differences between affected and unaffected limb STP values were also examined at post-operative time-points (Week 4, Week 8, and Week 12). Velocity and stride length were normalized by each rat's leg length.

In the LGNR group, several significant differences were observed throughout the study and across the hindlimbs (**Table 15**). At Week 4, rats demonstrated spatiotemporal changes consistent with significantly faster walking ($p < 0.05$), including significantly longer strides ($p < 0.005$) and a smaller percentage of the gait cycle in stance ($p < 0.05$). Additionally, rats significantly increased time in swing ($p < 0.05$), while time in stance did not significantly change. LGNR rats showed no significant changes between affected and unaffected hindlimbs for any of the evaluated parameters at Week 4. At Week 8, stride length was still significantly

greater than baseline ($p < 0.05$). Again, rats spent a smaller percentage of the gait cycle in stance ($p < 0.001$). Stance time decreased ($p < 0.05$) and swing time increased ($p < 0.01$). At Week 12, stride length and velocity were comparable to baseline values. Furthermore, time in swing was still significantly greater than baseline ($p < 0.001$). Cadence was significantly faster in the affected limb compared to the unaffected limb ($p < 0.05$). In addition, percent stance during unaffected limb steps ($p < 0.05$) was significantly decreased from baseline.

In the LGR group, STPs proved to be highly consistent over the duration of the study and between the hindlimbs (**Table 16**). At Week 4 and Week 8, no significant changes were observed from baseline. At Week 12, percent stance during affected limb steps showed a significant decrease from baseline ($p < 0.05$). Percent stance in the unaffected limb also decreased, but this relationship was not significant. There were no significant differences observed between affected and unaffected limb spatiotemporal values at any of the post-surgical time-points.

LGNR	Baseline	Week4		Week8		Week12	
Spatiotemporal Parameters		Left	Right	Left	Right	Left	Right
Velocity (leg lengths/sec)	4.43±0.7	**5.08±0.8***	**5.00±0.94***	4.93±0.81	4.93±0.73	4.33±0.4	4.34±0.44
Stride Length (leg lengths)	1.51±0.1	**1.68±0.08***	**1.64±0.12***	**1.61±0.13***	**1.61±0.12***	1.58±0.06	1.55±0.07
Stance Time (sec)	0.23±0.03	0.21±0.04	0.21±0.03	**0.2±0.03***	**0.2±0.02***	0.23±0.02	0.23±0.02
Swing Time (sec)	0.12±0.00	**0.14±0.01***	**0.13±0.01***	**0.13±0.01***	**0.13±0.01***	**0.14±0.01***	**0.13±0.00***
Cadence (steps/min)	349.48±34.1	360.31±42.06	361.35±45.74	364.37±35.5	365.63±33.33	328.13±22.03	**334.83±22.78^**
Stance (% GC)	64.41±2.95	**59.73±4.2***	**59.97±3.6***	**59.64±3.4***	**59.99±2.78***	**61.48±2.06***	62.56±2.56

Table 15: LGNR spatiotemporal parameters at Baseline, Week 4, Week 8, and Week 12. *significantly different than baseline ($p < 0.05$) ^significant difference between affected and unaffected limb STPs at that time-point ($p < 0.05$).

LGR	Baseline	Week4		Week8		Week12	
Spatiotemporal Parameters		Left	Right	Left	Right	Left	Right
Velocity (leg lengths/sec)	4.76±0.88	5.02±0.87	5.11±0.87	4.76±0.74	4.78±0.77	4.99±0.66	4.95±0.67
Stride Length (leg lengths)	1.61±0.12	1.65±0.1	1.65±0.09	1.63±0.08	1.63±0.07	1.64±0.07	1.62±0.06
Stance Time (sec)	0.22±0.05	0.2±0.03	0.2±0.04	0.21±0.04	0.21±0.04	0.2±0.02	0.2±0.03
Swing Time (sec)	0.13±0.01	0.14±0.01	0.14±0.01	0.14±0.01	0.14±0.01	0.14±0.01	0.13±0.01
Cadence (steps/min)	350.81±43.89	361.62±48.44	368.74±54.18	348.93±44.49	350.37±46.57	363.73±33.36	363.86±37.31
Stance (% GC)	61.48±3.78	58.45±2.48	58.97±2.5	60.25±3.29	60.08±3.47	**58.99±2.58***	59.66±2.29

Table 16: LGR spatiotemporal parameters at Baseline, Week 4, Week 8, and Week 12. *significantly different than baseline ($p < 0.05$) ^significant difference between affected and unaffected limb STPs at that time-point ($p < 0.05$).

5.4.2 LGNR Kinematics and Kinetics

SPM paired t-tests showed that LGNR Week 4 kinematics exhibited significant differences when compared to baseline data for several examined trajectories (**Figure 27**). The specific location and p-value associated with each supra-threshold cluster is reported in **Table 17**. In the pelvis, SPM results indicate that the pelvis tilt angle was significantly lower in stance at Week 4 than baseline. Changes observed in the affected limb were consistent with those observed in a circumduction gait compensation strategy. The right hip was more abducted during the swing portion of the gait cycle. Both the affect and unaffected hips were more externally rotated at Week 4, with the unaffected hip more externally rotated in stance and swing and the affected hip more externally rotated during swing. SPM analysis also indicated a decrease in affected limb knee flexion during stance at Week 4. Surprisingly, mean trajectories for ankle kinematics at Week 4 were highly similar to baseline data in the affected and unaffected limbs. However, one supra-threshold cluster in the unaffected ankle flexion trajectory indicated that the unaffected ankle was more plantarflexed during stance. Comparison of joint moment data between baseline and Week 4 also revealed significant differences in both the affected and unaffected hindlimbs (**Figure 27**, **Table 17**). In the affected limb, there was a significant increase in the hip abduction moment during stance. Interestingly, rats produced greater knee extension moments in both hindlimbs at Week 4 post-surgery. Furthermore, rats at Week 4 produced a smaller ankle plantarflexion moment in the affected hindlimb during stance. There were minimal changes seen in joint moments during swing for the knee and ankle, which are detailed in **Table 17**.

Similar to Week 4, SPM paired t-tests were used to compare Week 8 data to baseline (**Figure 28**, **Table 18**). At Week 8, pelvis kinematics were similar to baseline kinematics for

most of the gait cycle. However, the pelvis tilt angle was lower than baseline during the swing portion of the gait cycle for the unaffected limb. Meanwhile, the affected hip was significantly more flexed and abducted during swing, and more externally rotated in both stance and swing. The unaffected limb was more abducted during swing, as well as more externally rotated during both stance and swing. No significant differences were observed in knee or ankle kinematics for either hindlimb. Net joint moments at Week 8 also exhibited significant deviations from baseline across the board (**Figure 28**, **Table 18**). In stance, the unaffected hip produced a greater extension moment. Similar to Week 4, the knees produced greater extension moments at Week 8, while the right ankle produced a smaller ankle plantarflexion moment during stance. SPM also revealed minor deviations from baseline moments in the swing phase at the hip and ankle (**Table 18**). There was a significantly greater hip external rotation moment in early stance for both hindlimbs.

Week 12 kinematics and kinetics were also compared to baseline (**Figure 29**), with the p-value and location for each supra-threshold cluster reported in **Table 19**. Again, the pelvis tilt angle was significantly lower than during both stance and swing. In contrast to Week 8 data, both the affected and unaffected hips were less flexed than baseline in both stance and swing. The affected limb was also more abducted during swing, and both hindlimbs were more externally rotated in both stance and swing. In addition, both knees were less flexed during stance and swing. Ankle kinematics did not significantly differ between baseline and Week 12 data in either stance or swing. Surprisingly, no significant differences were found between Week 12 and baseline hip joint moments during stance. Similar to Week 4 and Week 8 data, animals produced a larger knee extension moment in both hindlimbs during stance. There were no significant changes in ankle joint moments during stance. During swing, the hip, knee, and ankle each

exhibited small changes from baseline swing moments (**Table 19**).

GRFs for LGNR rats are shown in **Figure 30**. At Week 4, rats produced a significantly greater posterior force in early stance with both hindlimbs. At Week 8, the affected hindlimb produced a significantly greater posterior force in early stance, while the unaffected limb produced a smaller medial force and a greater vertical force. The affected hindlimb showed similar trends to the unaffected hindlimb, but these changes were not significant. No significant differences were found between baseline and Week 12 GRFs for either hindlimb. Supra-threshold cluster locations and p-values is shown in **Table 20**.

Joint power curves were also calculated for LGNR rats. At Week 4, rats generated more power in early stance with their unaffected limb hip, while simulataneously absorbing more power with their affected limb knee. Similar changes were observed at Week 8 and Week 12, with increased power generation in the hip and increased power absorption in the knee. Minimal changes were observed in ankle power generation/absorption, with the only significant difference being a minimal decrease in power production at Week 4 in late stance. Minimal significant differences were observed during swing at all time-points. A full list of SPM supra-threshold cluster locations and p-values is shown in **Table 21**.

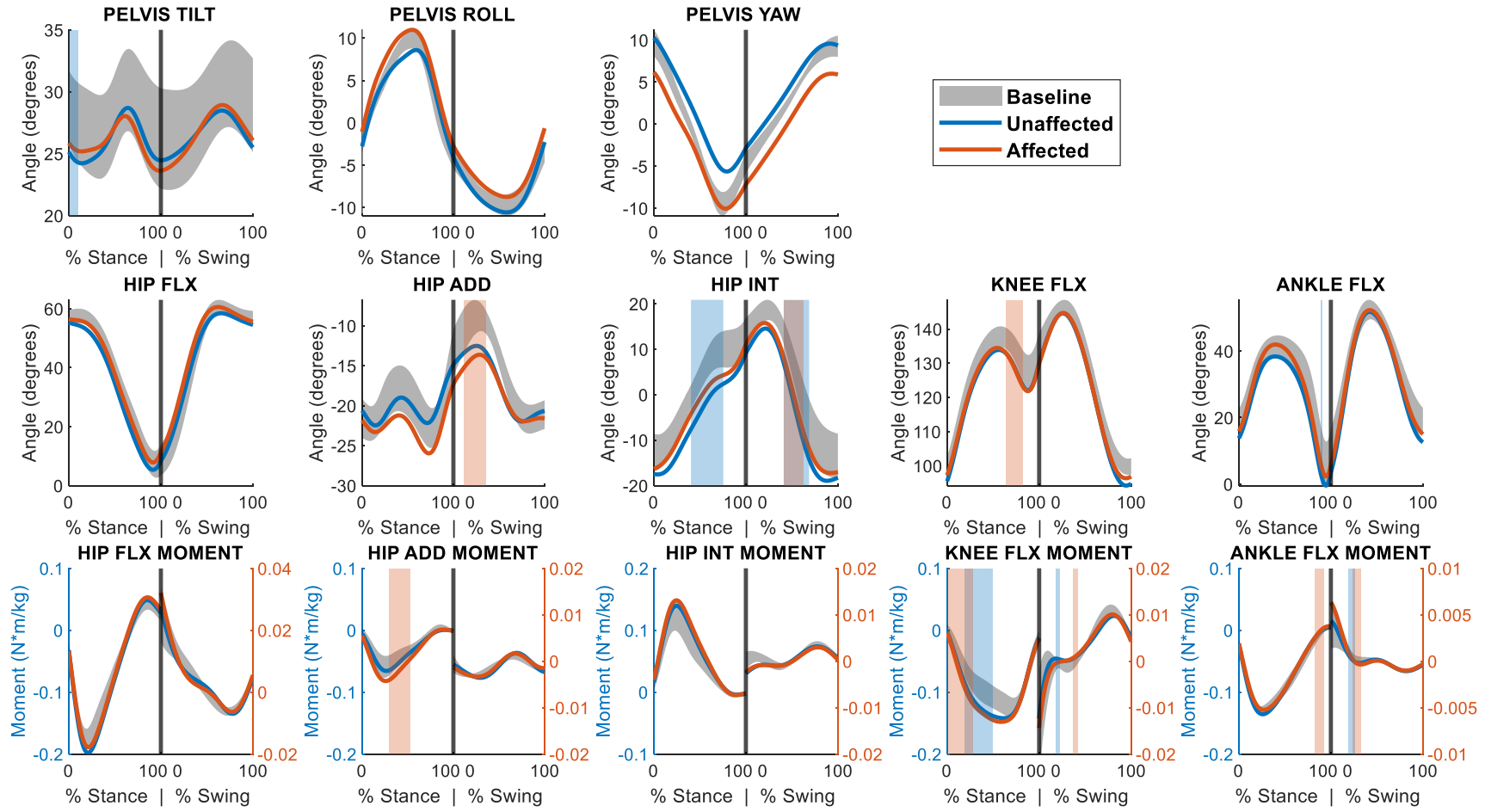

Figure 27: Mean trajectories for joint kinematics and joint kinetics during stance and swing for the LGNR group at 4 weeks post-surgery. Curves compare baseline (shaded grey) to Week 4 for the left (blue, unaffected) and right (orange, affected) hindlimbs. Vertical shaded regions represent supra-threshold clusters determined from SPM paired t-tests with a significance level of $\alpha = 0.05$, indicating a significant deviation from the baseline trajectory. The supra-threshold cluster probability for each cluster is given in **Table 17**.

	Unaffected (Left)		Affected (Right)	
Coordinate	**Stance**	**Swing**	**Stance**	**Swing**
Pelvis Tilt	0-9.5% (p = 0.042)			
Pelvis Roll				
Pelvis Yaw				
Hip Flexion				
Hip Adduction				11.4-35.7% (p = 0.018)
Hip Internal Rot.	40.3-75.5% (p = 0.026)	41-68.7% (p = 0.022)		41.4-62.6% (p = 0.03)
Knee Flexion			64.6-82.4% (p = 0.021)	
Ankle Flexion	89.3-90.9% (p = 0.05)			
Hip Flexion Moment				
Hip Adduction Moment			29.7-52.7% (p < 0.001)	
Hip Internal Rot. Moment				
Knee Flexion Moment	19.4-49.7% (p < 0.001)	18.6-22.4% (p = 0.033)	0-27.5% (p < 0.001)	37.2-42.5% (p = 0.023)
Ankle Dorsiflexion Moment		18.7-25.4% (p = 0.007)	82.7-92.3% (p = 0.012)	24-32.9% (p = 0.01)

Table 17: Locations of supra-threshold clusters exceeding the critical value for each coordinate for the LGNR group at 4 weeks post-surgery. Supra-threshold cluster locations pertain to the shaded regions identified in **Figure 27**, presented here as a percentage of the stance or swing phase. The associated p-value designates the precise probability that a given supra-threshold cluster of that size would be observed in random samplings. The null hypothesis is rejected for each curve containing a supra-threshold cluster.

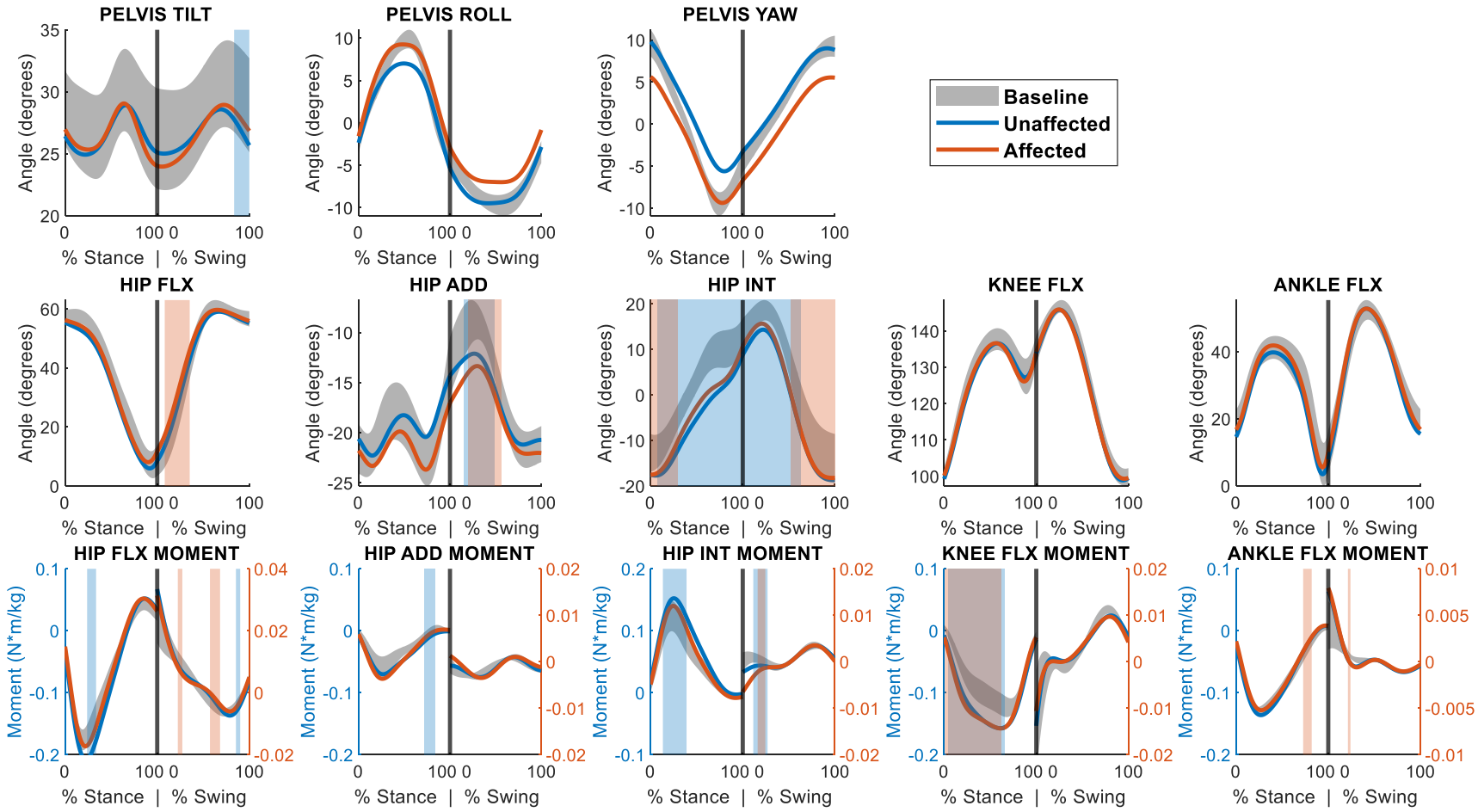

Figure 28: Mean trajectories for joint kinematics and joint kinetics during stance and swing for the LGNR group at 8 weeks post-surgery. Curves compare baseline (shaded grey) to Week 8 for the left (blue, unaffected) and right (orange, affected) hindlimbs. Vertical shaded regions represent supra-threshold clusters determined from SPM paired t-tests with a significance level of $\alpha = 0.05$, indicating a significant deviation from the baseline trajectory. The supra-threshold cluster probability for each cluster is given in **Table 18**.

	Unaffected (Left)		Affected (Right)	
Coordinate	**Stance**	**Swing**	**Stance**	**Swing**
Pelvis Tilt		9.3-100% (p = 0.009)	17.6-70.7% (p = 0.001) 81.9-100% (p = 0.03)	0-16.6% (p = 0.049)
Pelvis Roll				
Pelvis Yaw				
Hip Flexion	3.2-94.2% (p < 0.001)	32.1-68.7% (p = 0.001)	11.4-100% (p < 0.001)	0-0.9% (p = 0.05) 33.5-71.9% (p = 0.003)
Hip Adduction				16.7-41.6% (p = 0.004)
Hip Internal Rot.	36.6-100% (p = 0.001)	0-19.8% (p = 0.03)	41.1-94.1% (p = 0.001)	
Knee Flexion	84.9-100% (p = 0.039)	0-8.3% (p = 0.047)	35.4-100% (p < 0.001)	0-27.6% (p = 0.011)
Ankle Flexion				
Hip Flexion Moment		46.5-63.6% (p < 0.001) 84.8-95.6% (p = 0.001)		
Hip Adduction Moment				
Hip Internal Rot. Moment				17.9-22.4% (p = 0.01)
Knee Flexion Moment	2.2-54.5% (p < 0.001)	59.4-83% (p < 0.001)	11-34.4% (p = 0.006) 59.3-73.8% (p = 0.022)	
Ankle Dorsiflexion Moment		20.6-23.1% (p = 0.028)		21-23.3% (p = 0.033) 71.8-77.2% (p = 0.005)

Table 18: Locations of supra-threshold clusters exceeding the critical value for each coordinate for the LGNR group at 12 weeks post-surgery. Supra-threshold cluster locations pertain to the shaded regions identified in **Figure 28**, presented here as a percentage of the stance or swing phase. The associated p-value designates the precise probability that a given supra-threshold cluster of that size would be observed in random samplings. The null hypothesis is rejected for each curve containing a supra-threshold cluster.

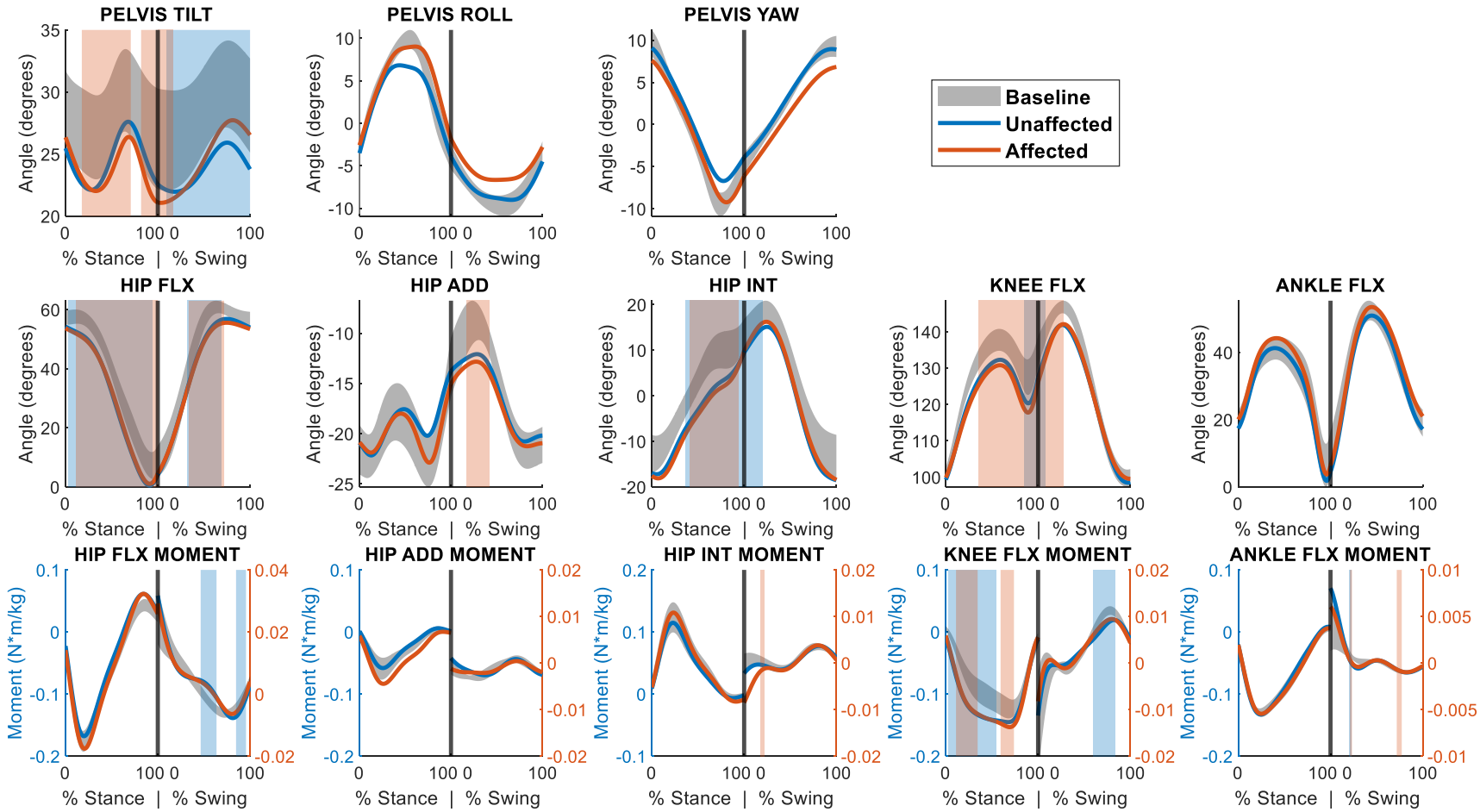

Figure 29: Mean trajectories for joint kinematics and joint kinetics during stance and swing for the LGNR group at 12 weeks post-surgery. Curves compare baseline (shaded grey) to Week 12 for the left (blue, unaffected) and right (orange, affected) hindlimbs. Vertical shaded regions represent supra-threshold clusters determined from SPM paired t-tests with a significance level of $\alpha = 0.05$, indicating a significant deviation from the baseline trajectory. The supra-threshold cluster probability for each cluster is given in **Table 19**.

	Unaffected (Left)		Affected (Right)	
Coordinate	**Stance**	**Swing**	**Stance**	**Swing**
Pelvis Tilt				
Pelvis Roll	0-20.2% ($p = 0.025$)	90.3-100% ($p = 0.048$)		
Pelvis Yaw				
Hip Flexion			0-53.3% ($p = 0.002$)	58.8-100% ($p = 0.018$)
Hip Adduction		21.7-57.9% ($p < 0.001$)	77.7-96.4% ($p = 0.022$)	
Hip Internal Rot.			0-100% ($p < 0.001$)	0-75.2% ($p < 0.001$)
Knee Flexion	6.3-66.1% ($p < 0.001$)	22.1-63.7% ($p < 0.001$)	0-90.4% ($p < 0.001$)	10.1-73.4% ($p < 0.001$)
Ankle Flexion	52-100% ($p < 0.001$)	0-14.5% ($p = 0.03$)	35.6-95.4% ($p < 0.001$)	94.2-100% ($p = 0.045$)
Hip Flexion Moment				
Hip Adduction Moment				
Hip Internal Rot. Moment				8.1-20.8% ($p = 0.001$)
Knee Flexion Moment	3.3-56.3% ($p < 0.001$)		4.7-43.3% ($p < 0.001$)	
Ankle Dorsiflexion Moment	15.5-29% ($p = 0.004$)	21-25.2% ($p = 0.025$) 42.3-55.6% ($p < 0.001$)		41.2-54.1% ($p < 0.001$)

Table 19: Locations of supra-threshold clusters exceeding the critical value for each coordinate for the LGNR group at 12 weeks post-surgery. Supra-threshold cluster locations pertain to the shaded regions identified in **Figure 29**, presented here as a percentage of the stance or swing phase. The associated p-value designates the precise probability that a given supra-threshold cluster of that size would be observed in random samplings. The null hypothesis is rejected for each curve containing a supra-threshold cluster.

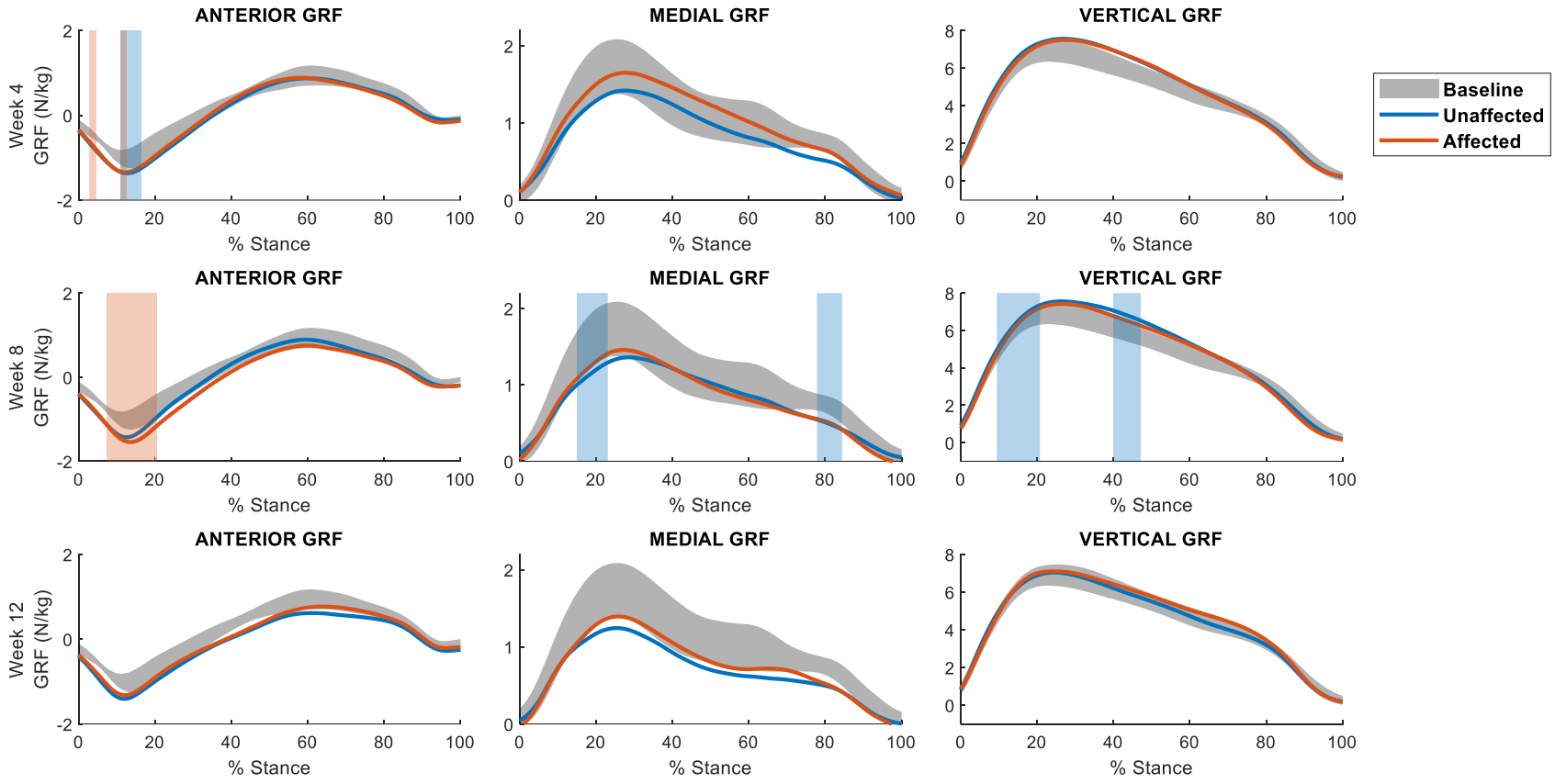

Figure 30: Ground reaction force (GRF) curves for LGNR rats. Curves compare baseline (shaded grey) to affected (orange) and unaffected (blue) hindlimb GRFs. GRFs were normalized by body mass. Vertical shaded regions represent supra-threshold clusters determined from SPM paired t-tests with a significance level of $\alpha = 0.05$, indicating a significant deviation from the baseline trajectory. The supra-threshold cluster probability for each cluster is given in **Table 20**.

		Left	Right
Week 4	Anterior GRF	11-16.4% (p = 0.018)	2.8-4.7% (p = 0.042) 11-12.6% (p = 0.043)
	Vertical GRF		
	Medial GRF		
Week 8	Anterior GRF		7.3-20.5% (p = 0.005)
	Vertical GRF	9.5-20.8% (p = 0.003) 39.9-47.2% (p = 0.015)	
	Medial GRF	15-23.1% (p = 0.015) 77.8-84.4% (p = 0.022)	
Week 12	Anterior GRF		
	Vertical GRF		
	Medial GRF		

Table 20: Locations of supra-threshold clusters exceeding the critical value for LGNR GRFs at Weeks 4, 8, and 12. Supra-threshold cluster locations pertain to the shaded regions identified in **Figure 30**, presented here as a percentage of the stance phase. The associated p-value designates the precise probability that a given supra-threshold cluster of that size would be observed in random samplings. The null hypothesis is rejected for each curve containing a supra-threshold cluster.

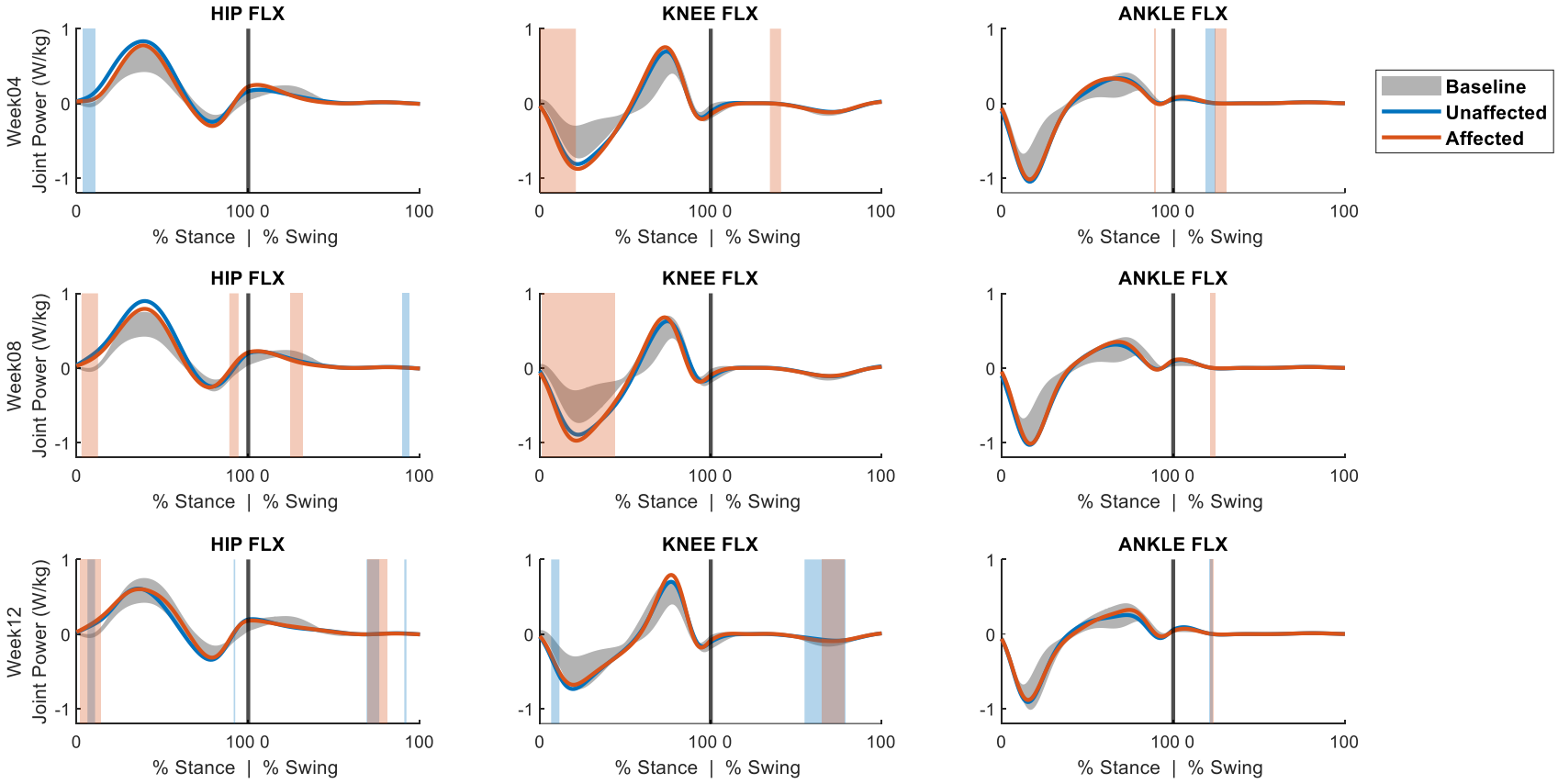

Figure 31: Sagittal plane joint power curves for LGNR rats. Curves compare baseline (shaded grey) to affected limb (orange) and unaffected limb (blue) joint power in stance and swing. Vertical shaded regions represent supra-threshold clusters determined from SPM paired t-tests with a significance level of $\alpha = 0.05$, indicating a significant deviation from the baseline trajectory. The supra-threshold cluster probability for each cluster is given in **Table 21**.

		Unaffected (Left)		Affected (Right)	
		Stance	**Swing**	**Stance**	**Swing**
Week 4	Hip Flexion	3.8-11.1% (p = 0.01)			
	Knee Flexion			0-21.1% (p < 0.001)	34.6-41.1% (p = 0.002)
	Ankle Dorsiflexion		19.2-24.8% (p = 0.001)	89-90.1% (p = 0.045)	23.9-30.8% (p = 0.003)
Week 8	Hip Flexion		89.6-93.7% (p = 0.019)	2.9-12.5% (p = 0.001) 89-94.4% (p = 0.016)	24.7-32.1% (p = 0.001)
	Knee Flexion			0.9-43.7% (p < 0.001)	
	Ankle Dorsiflexion				21.6-24.6% (p = 0.016)
Week 12	Hip Flexion	6.3-10.8% (p = 0.029) 91.5-92.4% (p = 0.049)	68.9-76.3% (p = 0.002) 90.9-92.2% (p = 0.046)	1.9-14.1% (p < 0.001)	69.6-81.2% (p < 0.001)
	Knee Flexion	6.6-11.5% (p = 0.015)	54.9-78.9% (p < 0.001)		64.9-78.2% (p < 0.001)
	Ankle Dorsiflexion		21.1-23% (p = 0.034)		21.4-23.2% (p = 0.035)

Table 21: Locations of supra-threshold clusters exceeding the critical value for LGNR sagittal plane joint power curves at Weeks 4, 8, and 12. Supra-threshold cluster locations pertain to the shaded regions identified in **Figure 31**, presented as a percentage of stance or swing phase. The associated p-value designates the precise probability that a given supra-threshold cluster of that size would be observed in random samplings. The null hypothesis is rejected for each curve containing a supra-threshold cluster.

5.4.3 LGR Kinematics and Kinetics

LGR kinematics and kinetics showed several significant differences from baseline at Week 4 (**Figure 32**, **Table 22**). In the pelvis, Week 4 rats were rolled farther onto their unaffected side during both stance and swing. SPM highlighted significant changes in hip flexion, adduction, and internal rotation during the right gait cycle. The affected hip was less flexed during stance and swing, less abducted during stance, and more externally rotated in both stance and swing. Additionally, the unaffected limb was more abducted during swing. Both knees were significantly less flexed during stance and swing. In addition, each ankle was less dorsiflexed during both stance and swing. There were no significant differences in hip moments during stance for either the affected or unaffected hindlimb. Consistent with the LGNR group, the LGR rats produced greater knee extension moments during stance at Week 4. In swing, the affected knee produced a smaller knee flexion moment while the unaffected knee produced a greater knee flexion moment. Additionally, the left ankle produced a greater ankle plantarflexion moment during stance. There were minimal changes in swing joint moments for hip internal rotation and ankle plantarflexion moments in each limb.

Week 8 kinematics and kinetics for the LGR group displayed similar trends to Week 4 data (**Figure 33**, **Table 23**). Again, the rats were rolled more in favor of their unaffected side. The affected limb was less flexed in stance and swing, less abducted in stance and more abducted in swing, and more externally rotated throughout the gait cycle. Unaffected limb kinematics were more similar to baseline, but the hip was significantly more abducted during stance. Each knee was significantly less flexed than baseline, with the affected knee less flexed in both stance and swing and the unaffected knee less flexed during swing. Unaffected ankle kinematics compared well to baseline, but the affected ankle was less dorsiflexed throughout the

gait cycle. Once again, there were no significant differences in hip moments during stance for either hindlimb. Knee joint moments were similar to those seen in Week 4, with greater extension moments during stance for each hindlimb. No differences were observed in ankle moments during stance at Week 8. Changes in joint moments during swing were comparable to those seen in Week 4.

At Week 12 post-surgery, rats still exhibited significant deviations from baseline kinematics and kinetics (**Figure 34**, **Table 24**). Hip kinematics were similar to data from previous weeks. Both hips were more adducted during swing. In addition, the affected hip was more externally rotated over the whole gait cycle. The knees maintained a less flexed position throughout swing. A similar phenomenon was observed during stance, but this effect was not significant. Both ankles were also less dorsiflexed in late stance, just before push off. Week 12 joint moments compared well to joint moments from Week 4 and Week 8. At the hip, no significant differences were observed in stance, except for a small increase in the hip abduction moment produced by the affected hip at push off. Knee joint moments were significantly greater in stance, consistent with the previous post-surgery time-points. Joint moments during swing were also comparable to Week 4 and Week 8 trajectories, with small changes observed in swing moments at the hip, knee, and ankle.

GRFs for LGR rats are shown in **Figure 35**. At Week 4, rats produced a significantly greater vertical GRF with the unaffected hindlimb. At Week 8, rats produced significantly greater posterior GRFs in early stance, and significantly smaller anterior GRFs just before push off. In addition, rats produced a smaller vertical GRF in late stance at Week 8. At Week 12, mean GRF trajectories closely resembled those seen at Week 8. Similar deviations from baseline were observed, in addition to an increased vertical GRF with the affected limb in mid-stance. At

all post-surgical time-points, rats produced greater medial ground reaction forces with the affected limb than with the unaffected limb. However, these trajectories were typically not significantly different than baseline data. All supra-threshold cluster locations and p-values are shown in **Table 25**

Sagittal plane joint power curves were also calculated for LGR rats at the hip, knee, and ankle (**Figure 36**). LGR rats generated significantly more power with the hip and absorbed more power with the knee during early stance. Rats also generated more power with the ankle during mid-stance after surgery. Similar trends persisted throughout the recovery period at Week 8 and Week 12 (**Figure 35**, **Table 26**).

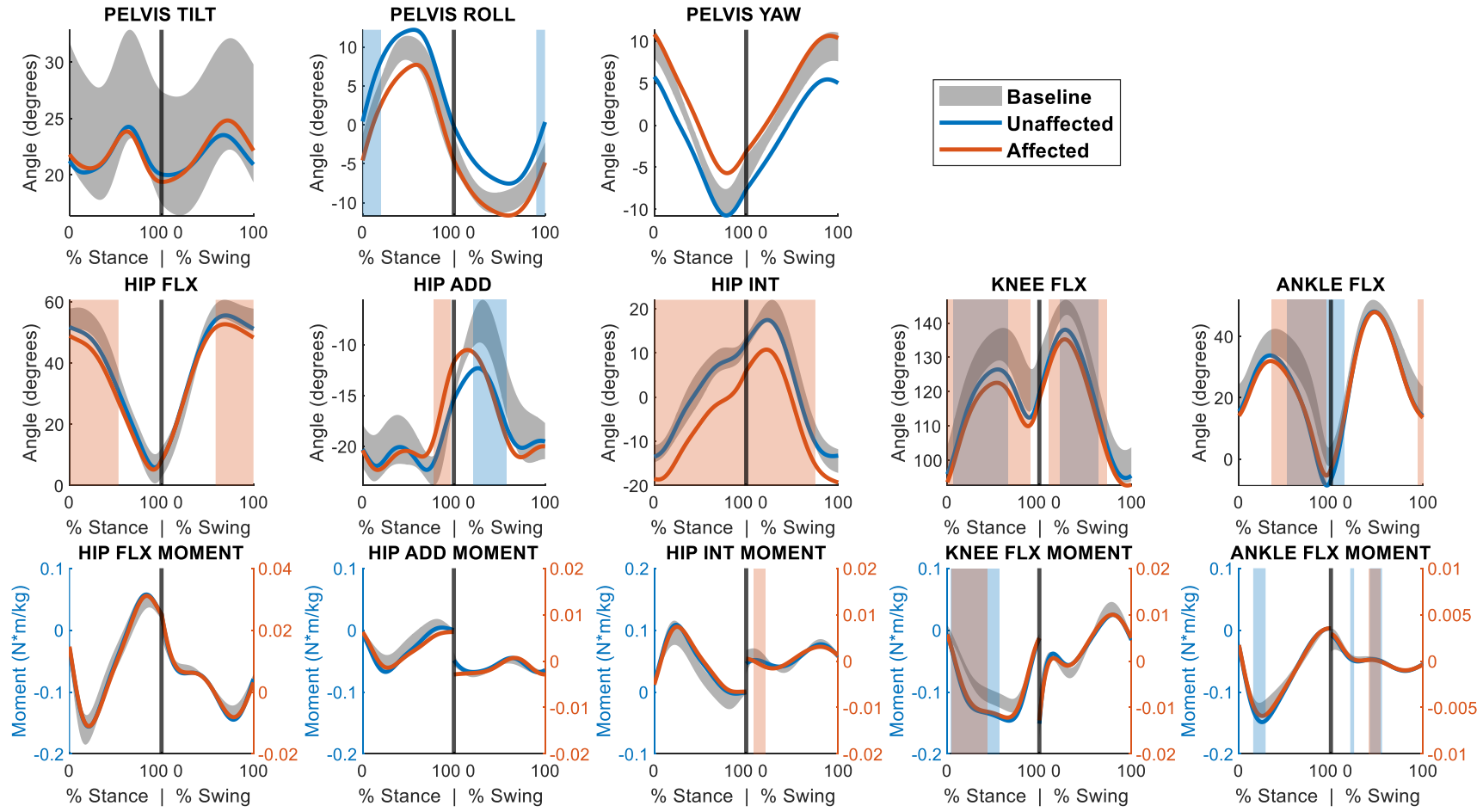

Figure 32: Mean trajectories for joint kinematics and joint kinetics during stance and swing for the LGR group at 4 weeks post-surgery. Curves compare baseline (shaded grey) to Week 4 for the left (blue, unaffected) and right (orange, affected) hindlimbs. Vertical shaded regions represent supra-threshold clusters determined from SPM paired t-tests with a significance level of $\alpha = 0.05$, indicating a significant deviation from the baseline trajectory. The supra-threshold cluster probability for each cluster is given in **Table 22**.

	Unaffected (Left)		Affected (Right)	
Coordinate	**Stance**	**Swing**	**Stance**	**Swing**
Pelvis Tilt				
Pelvis Roll	0-20.2% (p = 0.025)	90.3-100% (p = 0.048)		
Pelvis Yaw				
Hip Flexion			0-53.3% (p = 0.002)	58.8-100% (p = 0.018)
Hip Adduction		21.7-57.9% (p < 0.001)	77.7-96.4% (p = 0.022)	
Hip Internal Rot.			0-100% (p < 0.001)	0-75.2% (p < 0.001)
Knee Flexion	6.3-66.1% (p < 0.001)	22.1-63.7% (p < 0.001)	0-90.4% (p < 0.001)	10.1-73.4% (p < 0.001)
Ankle Flexion	52-100% (p < 0.001)	0-14.5% (p = 0.03)	35.6-95.4% (p < 0.001)	94.2-100% (p = 0.045)
Hip Flexion Moment				
Hip Adduction Moment				
Hip Internal Rot. Moment				8.1-20.8% (p = 0.001)
Knee Flexion Moment	3.3-56.3% (p < 0.001)		4.7-43.3% (p < 0.001)	
Ankle Dorsiflexion Moment	15.5-29% (p = 0.004)	21-25.2% (p = 0.025) 42.3-55.6% (p < 0.001)		41.2-54.1% (p < 0.001)

Table 22: Locations of supra-threshold clusters exceeding the critical value for each coordinate for the LGR group at 4 weeks post-surgery. Supra-threshold cluster locations pertain to the shaded regions identified in **Figure 32**, presented here as a percentage of the stance or swing phase. The associated p-value designates the precise probability that a given supra-threshold cluster of that size would be observed in random samplings. The null hypothesis is rejected for each curve containing a supra-threshold cluster.

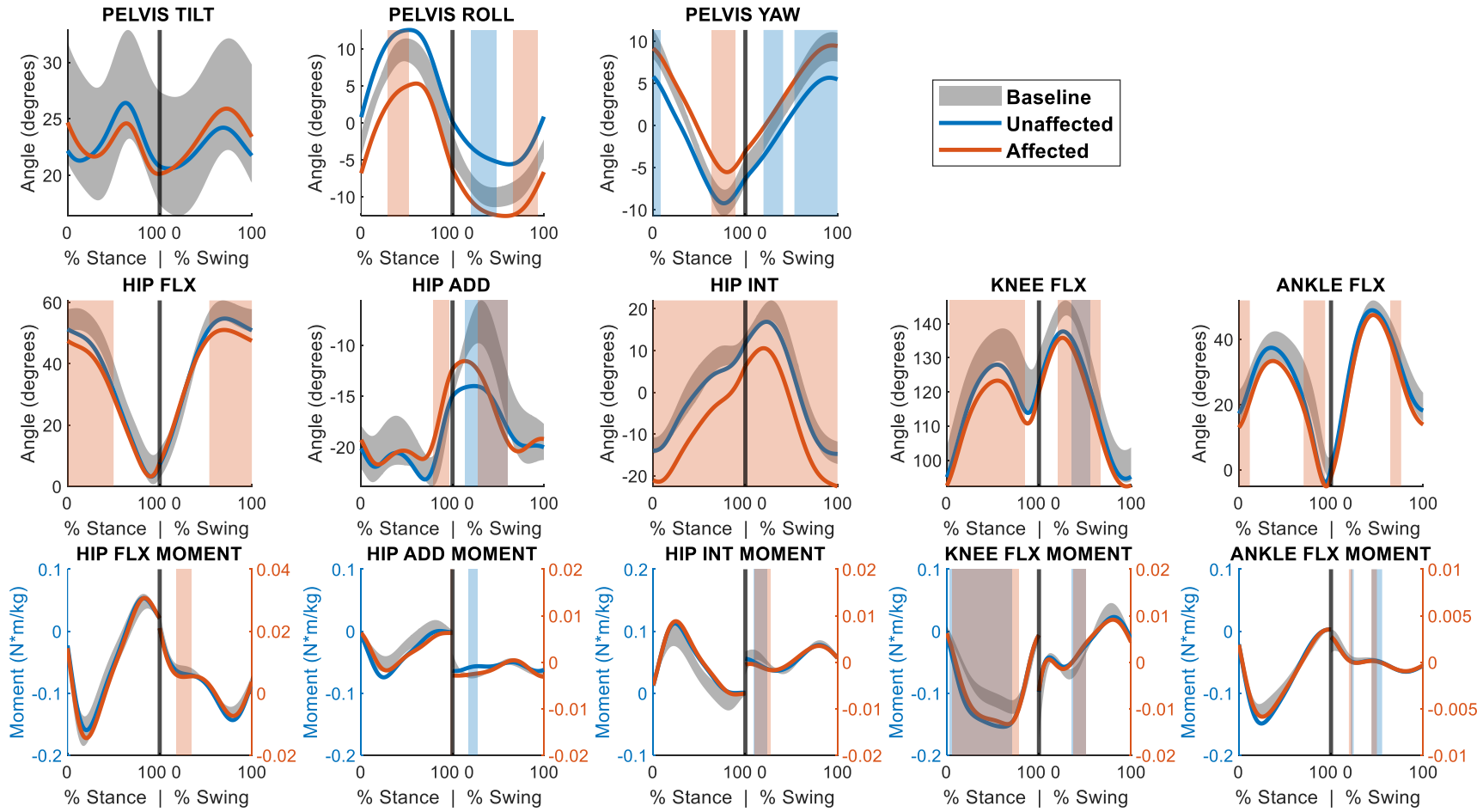

Figure 33: Mean trajectories for joint kinematics and joint kinetics during stance and swing for the LGR group at 8 weeks post-surgery. Curves compare baseline (shaded grey) to Week 8 for the left (blue, unaffected) and right (orange, affected) hindlimbs. Vertical shaded regions represent supra-threshold clusters determined from SPM paired t-tests with a significance level of $\alpha = 0.05$, indicating a significant deviation from the baseline trajectory. The supra-threshold cluster probability for each cluster is given in **Table 23**.

	Unaffected (Left)		Affected (Right)	
Coordinate	**Stance**	**Swing**	**Stance**	**Swing**
Pelvis Tilt				
Pelvis Roll		19.7-47.8% (p = 0.033)	28.7-52.1% (p = 0.025)	66.1-92.6% (p = 0.032)
Pelvis Yaw	0-8.1% (p = 0.043)	19.7-41% (p = 0.035) 53.2-100% (p = 0.009)	63.8-89.5% (p = 0.012)	
Hip Flexion			0-50% (p = 0.003)	53.8-100% (p = 0.021)
Hip Adduction		13.8-60.1% (p < 0.001)	78.7-96% (p = 0.02)	27.8-60.5% (p = 0.005)
Hip Internal Rot.			0-100% (p < 0.001)	0-100% (p < 0.001)
Knee Flexion		35.1-55.2% (p = 0.034)	3.3-85.3% (p = 0.003)	20.6-66.7% (p = 0.015)
Ankle Flexion			0-11.9% (p = 0.042) 70.3-93.6% (p = 0.025)	64.3-76.2% (p = 0.031)
Hip Flexion Moment				17.5-34.1% (p < 0.001)
Hip Adduction Moment		17.7-28% (p = 0.002)	97.7-100% (p = 0.047)	
Hip Internal Rot. Moment		9.7-23.8% (p = 0.002)		10.2-27.6% (p < 0.001)
Knee Flexion Moment	2.9-70.4% (p < 0.001)	35.8-51% (p < 0.001)	5.6-78.2% (p < 0.001)	37.8-50.9% (p < 0.001)
Ankle Dorsiflexion Moment		21.4-24.7% (p = 0.035) 44-55.5% (p = 0.001)		19.4-23% (p = 0.033) 43.8-49.8% (p = 0.016)

Table 23: Locations of supra-threshold clusters exceeding the critical value for each coordinate for the LGR group at 8 weeks post-surgery. Supra-threshold cluster locations pertain to the shaded regions identified in **Figure 33**, presented here as a percentage of the stance or swing phase. The associated p-value designates the precise probability that a given supra-threshold cluster of that size would be observed in random samplings. The null hypothesis is rejected for each curve containing a supra-threshold cluster.

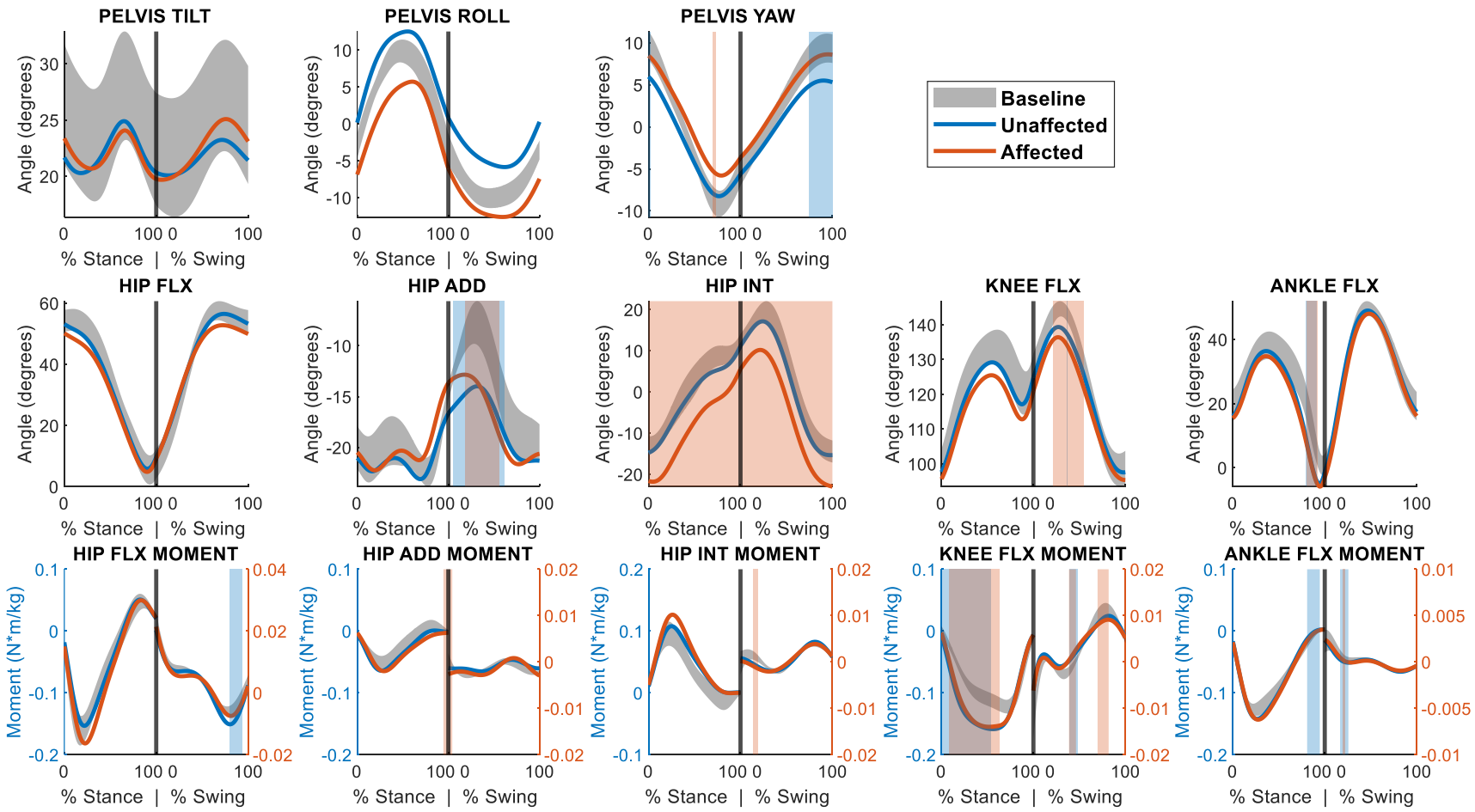

Figure 34: Mean trajectories for joint kinematics and joint kinetics during stance and swing for the LGR group at 12 weeks post-surgery. Curves compare baseline (shaded grey) to Week 12 for the left (blue, unaffected) and right (orange, affected) hindlimbs. Vertical shaded regions represent supra-threshold clusters determined from SPM paired t-tests with a significance level of $\alpha = 0.05$, indicating a significant deviation from the baseline trajectory. The supra-threshold cluster probability for each cluster is given in **Table 24**.

	Unaffected (Left)		Affected (Right)	
Coordinate	**Stance**	**Swing**	**Stance**	**Swing**
Pelvis Tilt				
Pelvis Roll				
Pelvis Yaw	0-2.6% ($p = 0.049$)	74-100% ($p = 0.034$)	69.7-73.2% ($p = 0.049$)	
Hip Flexion				
Hip Adduction		5.8-61.7% ($p < 0.001$)		18.9-55.9% ($p = 0.005$)
Hip Internal Rot.			0-100% ($p < 0.001$)	0-100% ($p < 0.001$)
Knee Flexion		36.7-37.5% ($p = 0.05$)		21.4-54.5% ($p = 0.023$)
Ankle Flexion	79.5-90.8% ($p = 0.041$)		79.9-91.7% ($p = 0.043$)	
Hip Flexion Moment		79.6-93.5% ($p = 0.002$)		
Hip Adduction Moment			94.5-100% ($p = 0.036$)	0-4.3% ($p = 0.034$)
Hip Internal Rot. Moment				13.6-18.8% ($p = 0.017$)
Knee Flexion Moment	1.3-53.7% ($p < 0.001$)	39.3-48.2% ($p = 0.005$)	8.3-62.7% ($p < 0.001$)	38.7-46.3% ($p = 0.007$) 69.8-81.9% ($p < 0.001$)
Ankle Dorsiflexion Moment	80.8-94.6% ($p = 0.004$)	16.7-25.7% ($p = 0.005$)		19.1-21.7% ($p = 0.043$)

Table 24: Locations of supra-threshold clusters exceeding the critical value for each coordinate for the LGR group at 12 weeks post-surgery. Supra-threshold cluster locations pertain to the shaded regions identified in **Figure 34**, presented here as a percentage of the stance or swing phase. The associated p-value designates the precise probability that a given supra-threshold cluster of that size would be observed in random samplings. The null hypothesis is rejected for each curve containing a supra-threshold cluster.

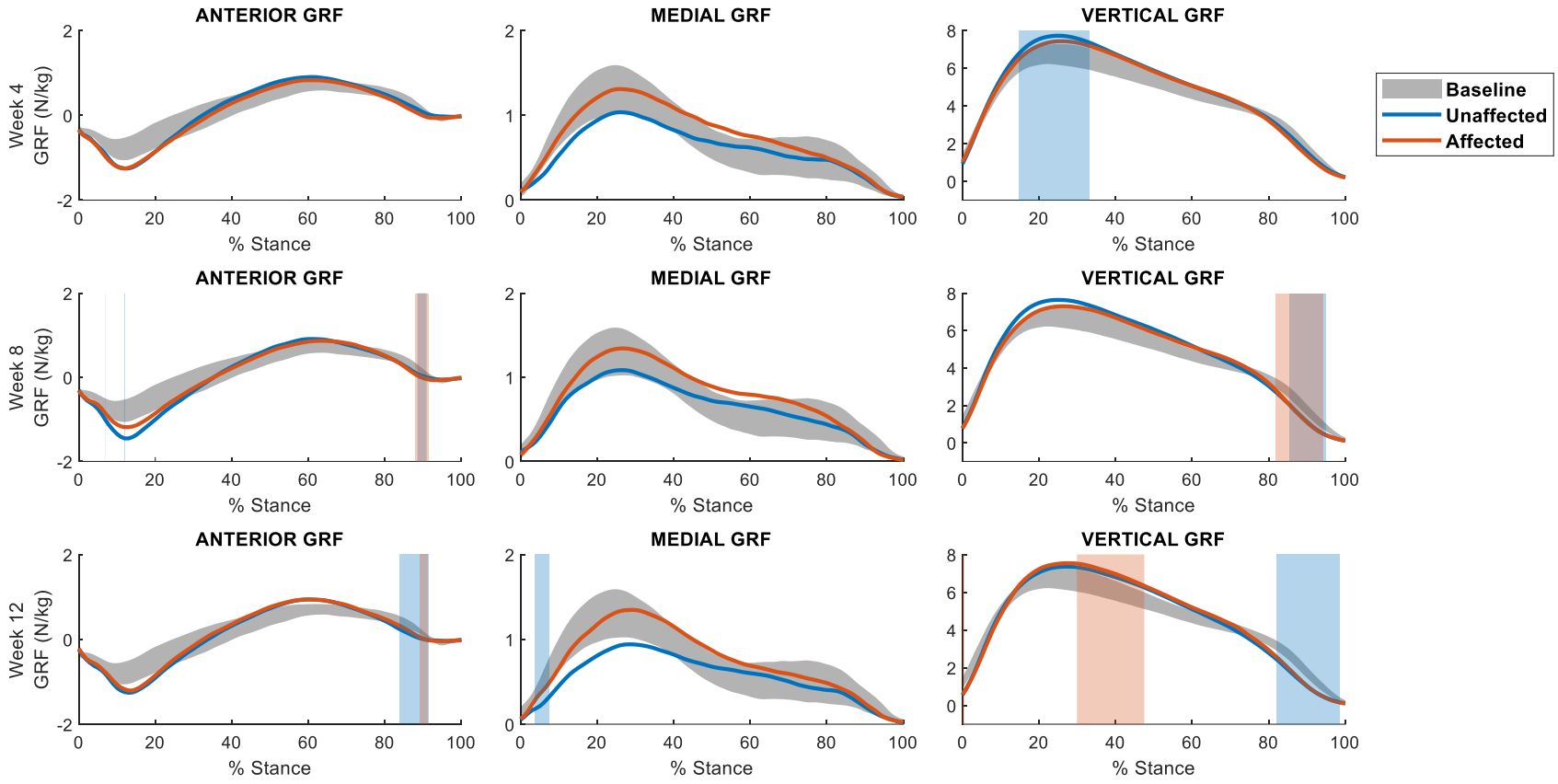

Figure 35: Ground reaction force (GRF) curves for LGR rats. Curves compare baseline (shaded grey) to affected (orange) and unaffected (blue) hindlimb GRFs. GRFs were normalized by body mass. Vertical shaded regions represent supra-threshold clusters determined from SPM paired t-tests with a significance level of $\alpha = 0.05$, indicating a significant deviation from the baseline trajectory. The supra-threshold cluster probability for each cluster is given in **Table 25**.

		Left	Right
Week 4	Anterior GRF		
	Vertical GRF	14.7-33.2% ($p < 0.001$)	
	Medial GRF		
Week 8	Anterior GRF	7-7% ($p < 0.05$) 11.9-12.1% ($p < 0.05$) 88.5-90.9% ($p = 0.037$)	87.9-91.5% ($p = 0.019$)
	Vertical GRF	85.5-95% ($p = 0.017$)	81.9-94.3% ($p = 0.002$)
	Medial GRF		
Week 12	Anterior GRF	83.9-91.5% ($p = 0.003$)	89-91.2% ($p = 0.038$)
	Vertical GRF	82.2-98.6% ($p = 0.002$)	0-0.5% ($p = 0.05$) 29.9-47.5% ($p < 0.001$)
	Medial GRF	3.7-7.4% ($p = 0.037$)	

Table 25: Locations of supra-threshold clusters exceeding the critical value for LGR GRFs at Weeks 4, 8, and 12. Supra-threshold cluster locations pertain to the shaded regions identified in **Figure 35**, presented here as a percentage of the stance phase. The associated p-value designates the precise probability that a given supra-threshold cluster of that size would be observed in random samplings. The null hypothesis is rejected for each curve containing a supra-threshold cluster.

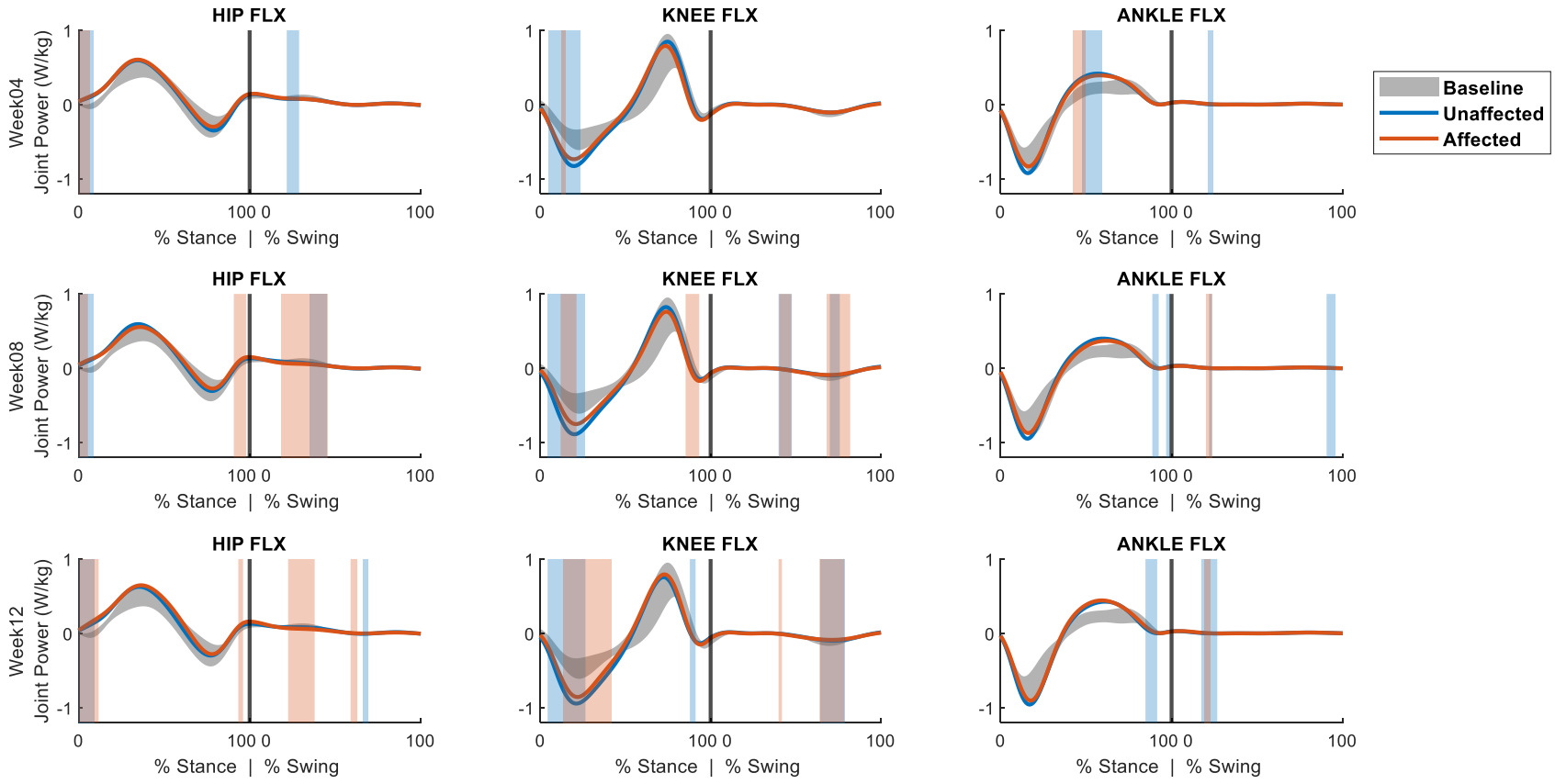

Figure 36: Sagittal plane joint power curves for LGR rats. Curves compare baseline (shaded grey) to affected limb (orange) and unaffected limb (blue) joint power in stance and swing. Vertical shaded regions represent supra-threshold clusters determined from SPM paired t-tests with a significance level of $\alpha = 0.05$, indicating a significant deviation from the baseline trajectory. The supra-threshold cluster probability for each cluster is given in **Table 26**.

		Unaffected (Left)		Affected (Right)	
		Stance	**Swing**	**Stance**	**Swing**
Week 4	Hip Flexion	0-8.8% ($p = 0.006$)	21.7-28.9% ($p = 0.002$)	0-6.7% ($p = 0.012$)	
	Knee Flexion	5.1-23.5% ($p < 0.001$)		12.7-15.1% ($p = 0.04$)	
	Ankle Dorsiflexion	47.7-59.3% ($p < 0.001$)	21.5-24.5% ($p = 0.027$)	42.7-49.8% ($p = 0.002$)	
Week 8	Hip Flexion	0-9% ($p = 0.005$)	35.1-45.1% ($p < 0.001$)	0-5.5% ($p = 0.022$) 90.7-98% ($p = 0.012$)	18.3-45.6% ($p < 0.001$)
	Knee Flexion	4.5-26.3% ($p < 0.001$)	39.9-47.7% ($p < 0.001$) 69.9-75.8% ($p = 0.003$)	11.9-21.3% ($p < 0.001$) 85.3-93.3% ($p = 0.001$)	40.3-47.4% ($p = 0.001$) 68.1-81.9% ($p < 0.001$)
	Ankle Dorsiflexion	88.7-92.5% ($p = 0.022$) 96.8-99.2% ($p = 0.036$)	21.9-23.5% ($p = 0.041$) 90.6-95.8% ($p = 0.005$)		19.9-23.6% ($p = 0.021$)
Week 12	Hip Flexion	0.1-9.4% ($p = 0.01$)	66.3-69.3% ($p = 0.034$)	0-11.7% ($p = 0.001$) 93.4-96.2% ($p = 0.039$)	22.5-38% ($p < 0.001$) 59-62.9% ($p = 0.027$)
	Knee Flexion	4.3-26.5% ($p < 0.001$) 87.8-91.2% ($p = 0.025$)	64.4-78.5% ($p < 0.001$)	13.6-41.7% ($p < 0.001$)	39.9-41.9% ($p = 0.037$) 63.9-78.4% ($p < 0.001$)
	Ankle Dorsiflexion	84.7-91.6% ($p = 0.004$)	17.3-26.7% ($p = 0.001$)		19.3-22.9% ($p = 0.026$)

Table 26: Locations of supra-threshold clusters exceeding the critical value for LGR sagittal plane joint power curves at Weeks 4, 8, and 12. Supra-threshold cluster locations pertain to the shaded regions identified in **Figure 36**, presented as a percentage of stance or swing phase. The associated p-value designates the precise probability that a given supra-threshold cluster of that size would be observed in random samplings. The null hypothesis is rejected for each curve containing a supra-threshold cluster.

5.5 Discussion

This study aimed to provide a more comprehensive evaluation of the effects of VML injury and recovery in rats by analyzing changes in gait biomechanics. The ability to utilize a combined spatiotemporal, kinematic, and kinetic analysis provides a robust methodology for detecting and quantifying gait adaptations. With this in mind, 3-D motion capture and concurrent GRF data was collected for both sham (TANR and LGNR) and treated (TAR and LGR) groups in order to evaluate the effects of TA and LG VML injuries and assess recovery at multiple points throughout the recovery period. The TA is a uniarticular muscle responsible for ankle dorsiflexion, and its sole function during gait is to provide foot clearance during the swing phase. In contrast, the LG is a complex muscle which acts on both the ankle and the knee and is of critical importance during gait. The contributions of these muscles toward normal gait function make them ideal injury sites for evaluating recovery of movement function with gait analyses. Additionally, analysis of the unaffected (left) hindlimb was included in order to provide insight into systemic compensation strategies spanning both hindlimbs. Ultimately, this work can be used to advance the development of VML treatments and therapies by highlighting the necessary functional deficits to overcome and quantifying return to normal function.

3-D motion capture, GRFs, and an associated musculoskeletal model are the gold standard techniques for obtaining joint kinematics and kinetics during gait in humans. Prior work has demonstrated the applications of these methods for quantifying rodent gait (Dienes & Hicks et al., 2022). Furthermore, the baseline data obtained in this study compare favorably with joint angles, moments, power, and GRF values obtained for normal rat walking throughout the literature (Bauman & Chang, 2010; Bennett et al., 2012; Dienes & Hicks et al., 2022; Gillis & Biewener, 2001; Pereira et al., 2006). Age-matched control animals were not included in this

study, as other experiments have reported no changes in gait kinematics with animal growth over the course of an experiment (Dienes et al., 2019). Instead, kinematic and kinetic data at post-surgical time-points were compared to baseline data to identify changes in gait patterns throughout recovery.

5.5.1 TA VML Injury

Differences in data collection protocols between the TANR and TAR groups presented several challenges for analyzing and comparing gait data across groups. First and foremost, motion capture data was only collected on the affected hindlimb for the TANR group. For the TAR group, collection protocols were expanded to include the unaffected hindlimb. As a result, the TAR results can provide insight into contralateral hindlimb gait adaptations that the TANR results cannot address. In addition, the expanded motion capture marker set utilized during bilateral collection allowed for better tracking of the pelvis, which significantly improved the ability to model pelvis rotations during gait (**Figure 37**). Rats were also more willing to walk across the walkway at all time-points during bilateral data collections, largely due to the use of augmented training protocols and extended acclimation periods in the motion capture arena. The utility of these advancements is evidenced by an increased number of gait cycles collected for the TAR group (n = 4+ vs. n = 2+ per rat at each time-point), along with much faster walking observed in the TAR group, even during baseline walking (**Table 4**, **Table 5**). Thus, while unilateral kinematics and kinetics can still offer useful insights into gait adaptations for the TANR group, caution should be taken when comparing these results to bilateral data. In the future, the developed data collection and modeling approach should be utilized to quantify bilateral gait adaptations for rats with untreated TA VML injuries.

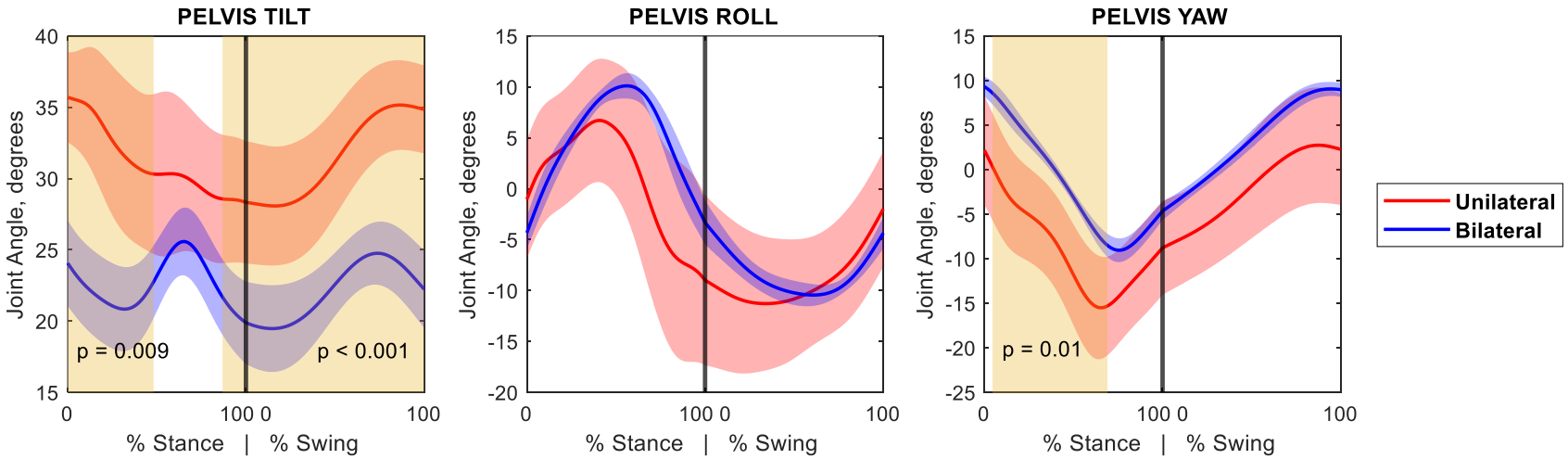

Figure 37: Comparison of healthy baseline pelvis kinematics between unilateral and bilateral motion capture and modeling. Shaded regions and corresponding p-values indicate areas of statistically significant difference detected by SPM t-tests.

In the TANR group, deviations from baseline kinematics and kinetics in the affected limb were relatively minor, especially by Week 12. As previously stated, the function of the TA during gait is to provide foot clearance during swing. In the literature, TA VML injuries have been shown to lead to gait compensation strategies similar to those employed by humans with foot drop, such as vaulting and circumduction (Dienes et al, 2019). While TANR kinematics did show evidence of foot drop during swing **(Figure 17**), there was no evidence of rats employing circumduction or vaulting in order to compensate for ankle dorsiflexor impairment. Instead, many of the significant kinematic changes observed in the TANR group do not provide advantages in compensating for foot drop. Namely, the hip and knee were each more extended during stance, and the hip was less abducted during swing. Affected limb joint moments were highly similar to healthy baseline data at all post-surgical time-points. As a result, injured animals were still able to produce joint moments sufficient to generate the propulsive power necessary for forward locomotion (**Figure 21**). This is consistent with expectations following an injury to the TA, as an ankle dorsiflexor impairment would not be expected to greatly impact extension moments during stance.

It is interesting that the hip and knee experienced several significant kinematic changes during stance, since neither joint is directly connected to the TA. Kinematic adaptations at the hip (more extended and less abducted) and knee (more extended) are consistent with the rats straightening their injured leg and bringing it more under their body during stance. This adaptation could be an alternative method to allow foot clearance in response to lack of TA function. Rats lengthened their affected limb during stance, effectively raising the height of their pelvis, but maintained similar values for hip and knee flexion during swing. If the unaffected limb was also more extended during its respective stance phase, this would provide more room

for the affected limb to swing forward into the next gait cycle. However, more data is needed to determine if the unaffected limb employs similar gait adaptations to the affected limb. Future work should investigate compensatory mechanisms in both hindlimbs following TA VML injury.

Similar to the TANR group, gait adaptations in the TAR group primarily occurred at the hip and knee, while there were very minimal changes seen at the ankle. However, TAR animals showed no evidence of the foot drop pathology exhibited by TANR animals and discussed in other studies of TA VML injury (Dienes et. al, 2019). This is a promising result, as it is evidence that the TEMR treatment sufficiently restored TA function during locomotion to the point of no significant functional deficits in the ankle dorsiflexors. However, the presence of significant kinematic/kinetic deviations from baseline at the hip and knee suggests that animals are still negatively compensating for the impacts of the TA injury or TEMR implantation. More work is needed to investigate whether these changes are due to pain response, some change in proprioception after injury, or some other unknown cause.

Throughout the recovery period, rats appeared to be compensating for their injury by favoring their unaffected limb. This was demonstrated by increased pelvic roll onto the unaffected side, as well as increased hip extension, hip abduction, and hip internal rotation, and ankle plantarflexion moments in the unaffected hindlimb. Favoritism of the unaffected hindlimb persisted throughout the study, with significantly increased joint moments seen during stance at the hip (Week 4, Week 8, and Week 12), knee (Week 4, Week 8, and Week 12), and ankle (Week 12). These findings demonstrate the importance of collecting and modeling the unaffected hindlimb during locomotion, providing insight into compensation strategies that a unilateral approach cannot fully elucidate.

TAR rats produced greater knee extension moments in both limbs at all post-surgical

time-points. Interestingly, there were minimal changes to affected limb joint moments at the hip or ankle, with the only other significant change being a slightly increased ankle plantarflexion moment during stance at Week 12. The significant increase in stance knee extension moment is surprising, as an impairment of the TA (ankle dorsiflexor) would not be expected to greatly alter joint moments during stance (Thota et. al, 2005). At Week 8, rats were walking significantly faster than at baseline, while they walked slightly faster than baseline at Week 12. This could offer some explanation to the increased knee extension moment, as increased walking speed has been shown to lead to higher peak knee extension moments (**Chapter 4, Table 3**). However, walking speed does not explain the significant increase in knee extension moments at Week 4, where rats maintained average walking speeds comparable to baseline values. In addition, changes in knee moment caused by increased walking speed are subtle, and the significant knee moment increases seen in the TAR group surpasses that which would be expected by the relatively small increase in velocity.

An examination of GRF and joint power curves can help elucidate the meaning of the increased knee moments observed in TAR rats (**Figure 26**). In humans, negative mechanical work (energy absorption) in the knee has been linked to the employment of "soft landing" techniques employed as a mechanism for injury prevention during landing (Tamura et al., 2021). Although TAR rats are demonstrating greater weight support with higher vertical ground reaction forces in mid stance (**Figure 25**, Week 8 and Week 12), it is likely that rats are employing this soft landing strategy as a mechanism to protect the previously sustained injury. However, energy absorbed at the knee must be returned to the system somewhere else in the gait cycle in order to maintain forward motion. This is demonstrated by increased power generation in the hip and, at later weeks, increased propulsive power at the ankle. In addition, animals

appear to employ this soft landing strategy in both the affected and unaffected hindlimbs. In fact, sagittal joint moment and power trajectories were largely similar between hindlimbs throughout the recovery period. Further investigation is needed to examine why this strategy was employed in the unaffected hindlimb.

These results provide robust information about systemic gait adaptations following TA VML injury and treatment with a regenerative therapeutic. In addition, the additional information provided by an examination of the contralateral hindlimb (TAR group) demonstrates the importance of a bilateral modeling approach during gait. Still, it is important that these results be combined with other metrics for quantifying recovery that examine muscle-level injury and recovery, such as force generating capacity of the affected muscle group and muscle histology. These techniques can provide insight into recovery at a local level, which can be combined with the systemic kinematic and kinetic approach to offer a deeper understanding of functional recovery.

5.5.2 LG VML Injury

Several spatiotemporal differences were found in the LGNR group, while the LGR group remained relatively consistent throughout the course of the experiment. Significant changes in speed and other STPs have been well documented across a number of injury paradigms (Batka et al., 2014; Hamers et al., 2001; Koopmans et al., 2005; Mountney et al., 2013; Vlamings et al., 2007). Still, it is surprising that the spatiotemporal changes observed in this study, such as increased stride length or increased speed, are typically associated with improved locomotor function, when a more detailed analysis of kinematics and kinetics suggest otherwise. There were minimal changes in STPs between the affected and unaffected limbs for the LGNR group, with only cadence (Week12, affected limb gait cycles higher) exhibiting significant differences

between the affected and unaffected limbs. The slight discrepancy between left and right limb STPs may be an indicator of limping compensation strategies employed in LGNR animals.

In the LGR group, there were minimal spatiotemporal changes at Weeks 4, 8, and 12. The minute differences in STPs contrast sharply with the extensive changes observed in LGR kinematics and kinetics. If a spatiotemporal analysis was the only evaluative metric in this study, the baseline animals would compare nearly identically to the treated group. Kinematics and kinetics demonstrate that treated animals are able to produce highly similar spatiotemporal results with distinctly different gait patterns. These findings highlight the importance of including a kinematic and kinetic analysis in order to provide a robust, comprehensive evaluation of treatment efficacy.

Kinematics and kinetics revealed significant deviations from baseline in the LGNR group throughout the recovery period. There were significant decreases in pelvic tilt (more anteriorly rotated), hip flexion, and knee flexion throughout the gait cycle, as well as significant increases in hip adduction during swing and hip external rotation in both stance and swing. Surprisingly, there were minimal changes in ankle kinematics in the LGNR group, with the only significant change being a slight increase in ankle plantarflexion at push-off in the left (unaffected) ankle at Week 4. It is possible that the rats are compensating by externally rotating and abducting to utilize the medial gastrocnemius instead of the injured LG. In humans, lateral gastrocnemius activation has been shown to decrease with greater external rotation while medial gastrocnemius activation increases (Cibulka et al., 2017; Riemann et al., 2011). In essence, these gait adaptations could be helping to redistribute the muscle work in stance away from the lateral gastrocnemius to other muscles in the posterior compartment. Joint kinetics were also different from baseline, with the largest difference being significantly greater knee extension moments

during stance in both hindlimbs. This increased moment was consistent, occurring at Weeks 4, 8, and 12 throughout the stance phase. It is interesting that there was an increased knee extension moment while sagittal plane moments stayed relatively unchanged in the hip and ankle. Importantly, these animals showed similar trends in kinematics and kinetics across the duration of the study, indicating that the functional deficit persists through time, negatively influencing the rats' return to normal movement.

LGR kinematics and kinetics were also significantly different from baseline throughout the recovery period. At all post-surgical time-points, the affected limb was more extended at the hip, knee, and ankle during both stance and swing, as well as more externally rotated at the hip. Unaffected limb kinematics were largely similar to affected limb kinematics, with the main distinction found in hip external rotation, which was significantly greater for the affected limb. This difference could be attributed to changes in pelvis motion between the affected and unaffected limb gait cycles, with kinematics indicative of pelvic hiking (obliquity) of the affected side and more acceptance on the unaffected side. This movement pattern is consistent with the rats favoring their unaffected leg. By Week 12, there is a general trend of returning to baseline kinematics, particularly in the sagittal plane. While there are still areas of significant differences from baseline, many of the supra-threshold clusters denoting significant changes have decreased in size or disappeared entirely. However, the remaining kinematic changes at Week 12 are still evidence of continued functional impairment. There were relatively few significant differences for joint moments during stance. Similar to the LGNR group, the LGR rats produced greater knee extension moments at all time-points. The rats also produced a greater peak ankle plantarflexion moment in their unaffected limb at Week 4, but this returns to normal at later time-points. An increased ankle plantarflexion moment produced by the unaffected limb could

be necessary earlier in the recovery period in order to provide a propulsive impulse during forward motion.

In both LGNR and LGR groups, the affected ankle joint was still able to produce a plantarflexion moment of comparable magnitude to baseline data. Similar results were noted in a study performed by Bennett et al. (2012), where they found that the ankle was able to produce an extensor moment of similar magnitude after medial gastrocnemius denervation. This study demonstrated that the ankle plantarflexion moment that develops in stance is likely attributable to passive stretch in the muscle and tendon rather than active contraction of the muscle, which raises questions about the normal function of the gastrocnemius during rodent gait. In rodent gait, the dorsiflexed posture of the ankle creates significant passive stretch of the Achilles tendon, storing more energy in the elastic tendon when compared to humans. At toe off, this energy is returned, producing propulsive power (Bennett et al., 2012; Dienes & Hicks et al., 2022) Thus, even following the introduction of LG VML injuries which decrease the active force production capability of the muscle, the ankle is still able to generate similar plantarflexion moments and propulsive power (**Figure 31**, **Figure 36**). In addition, prior studies have indicated that the LG is only comprised of approximately ~32% of the total mass of the ankle plantarflexor muscle group in rats (Charles et al., 2016). Thus, it is likely that the rats were able to compensate for the LG injury by re-distributing the load across other ankle plantarflexor muscles in order to achieve similar plantarflexor ability. As a result, it is possible that the currently implemented LG injury model is not severe enough to cause functional deficits during walking, and as such, is not a suitable injury paradigm for evaluating the efficacy of the TEMR treatment for restoring locomotor function.

While the reduced function of the LG appears to have minimal effects on the ankle, there

are clear implications at the knee. Similar to that observed in the TA injury model, both LGR and LGNR rats exhibited significantly greater knee extension moments during stance. Again, this increased knee extension moment results in significantly greater power absorption by the knee during early stance (**Figure 31**, **Figure 36**). Results from human studies demonstrate that negative mechanical work at the knee (power absorption) is effective in achieving a soft landing upon impact (Tamura et al., 2021). It is possible that LGR and LGNR rats are attempting to utilize soft-landing strategies to protect their injured limbs. In turn, however, this compensation significantly increases the load on the knees, which could negatively impact the joint by introducing secondary pathologies if the increased joint loading is prolonged.

Surprisingly, joint moment and joint power curves for the unaffected and affected limbs exhibited similar trends throughout the recovery period in both the LGNR and LGR groups. This contrasts work previously performed by Bennett et al. (2012), where they showed that affected limb and unaffected limb compensation strategies were largely different after medial gastrocnemius denervation, where reduced power generation in the affected hindlimb was compensated for by increased power generation by the unaffected hindlimb. Although the injury models for VML and peripheral nerve lesion are different, it is interesting that a different injury to the same muscle group produces such different compensation strategies. This could be due to differences in severity of the injuries sustained between studies, as LG VML injury reduced muscle strength but may maintain limited functionality, while muscle denervation results in complete inability to activate the injured muscle. In addition, functional deficits in the affected limb in Bennett's study may be have been exacerbated by the increased demands of trotting as compared to walking.

At Week 12, kinematic and kinetic changes are visibly reduced compared to previous

time-points in the LGR group, with the exception of a sustained increase in knee joint loading and external rotation in the affected hindlimb. While this demonstrates the potential of the TEMR construct as a treatment for LG VML injuries, more work needs to be done to fully quantify the treatment's efficacy. Changes in gait patterns between Week 8 and Week 12 indicate that the animals may not have reached a recovery plateau over the duration of the study. Thus, future work should look to evaluate changes in movement patterns over longer windows of recovery. Furthermore, these results should be contextualized with other metrics for quantifying functional recovery, such as force production capability and muscle histology, in order to provide a deeper understanding of recovery at the muscle level.

5.6 Conclusion

This study has demonstrated the potential of a comprehensive gait analysis for identifying and analyzing gait adaptations after VML injury, as well as the potential for evaluating the efficacy of different treatment strategies for restoration of function. Furthermore, this study has provided the first analysis of 3-D joint moments to evaluate volumetric muscle loss injuries in rodents and quantify functional recovery after treatment. By examining both kinematic and kinetic curves in 3-D, this data has provided novel information into hindlimb coordination in both the affected and unaffected hindlimb after VML injury. By applying the state-of-the-art methodologies in 3-D motion capture and musculoskeletal modeling to a pre-clinical model of VML injury, this study has taken a critical translational step toward developing therapies for use in the clinic. Further, this methodology for quantifying relevant functional deficits in rat models can be expanded beyond this specific use case for analyzing VML injuries. This study demonstrates the potential for future experiments geared toward providing insight that will accelerate the development of treatment strategies for a variety of neuromusculoskeletal pathologies.

Conclusions

6.1 Contributions of Thesis

This work:

- Developed a novel method to apply the gold-standard methodologies in 3-D motion capture and musculoskeletal modeling to quantify 3-D kinematics and kinetics of rodent gait during healthy, over-ground walking. This analysis demonstrated the importance of incorporating kinetics into analyses of rodent locomotion, as they provide novel insights into forces and loads experienced by the joints during gait.
- Developed a comprehensive normative database containing joint kinematics, kinetics, spatiotemporal parameters, ground reaction forces, and sagittal plane joint power for the rat hindlimbs during healthy, over-ground walking. This database provides valuable data for comparison for any study performing biomechanical analyses of rodent locomotion.
- Leveraged 3-D body scan data of fresh cadavers to generate regression equations based on measurable anthropometry (body mass, limb lengths) which can accurately predict body-segment inertial parameters for rats across a range of body sizes to enable accurate kinetic calculations.
- Expanded the capability of a publicly available unilateral model by adding contralateral (left) hindlimb. Musculoskeletal geometries, joints, and markers set necessary to drive the model were all added in order to produce bilateral modeling capability.
- Presented a case for the normalization of walking velocity based on rat limb lengths. Values for normal rat walking speeds vary widely in the literature, partially due to age/size differences across studies. Standardizing the presentation of velocity and other

anthropometry-dependent parameters (stride length, step width) allows for the comparison of spatiotemporal parameters among rats of different sizes, as well as provides context for the spatiotemporal variability observed in the literature.

- Characterized the effects of walking speed on rodent gait kinematics and kinetics, providing insights into the mechanisms rats use to modulate their walking speed. Furthermore, a method was presented to normalize the effects of walking speed on kinematics, kinetics, and spatiotemporal gait parameters by capitalizing on the relationship between walking speed and percent stance. This standardization of gait data was shown to minimize the impact of velocity on phasing and amplitude distortion in gait curves. By understanding the effects of walking speed on gait variables during normal walking, this information can be used in future studies to separate gait changes due to walking speed differences from gait changes due to gait pathology.
- Applied these data collection, modeling, and analysis methods to study gait changes after hindlimb muscle loss volumetric muscle loss injury and repair. This work demonstrates the potential of biomechanical analyses of rodent locomotion for quantifying functional deficits, evaluating treatment efficacies, and interpreting functional recovery. This analysis can be used to inform the development of more effective therapeutics to treat limb pathologies such as volumetric muscle loss. Furthermore, this analysis is a critical step toward developing these therapies for clinical applications, where the ultimate goal is improving the quality of life for impacted individuals.

6.2 Dissemination of Research

The work performed in this thesis is being disseminated into the scientific community in the form of journal publications and oral conference presentations.

Journal Publications

Dienes, J.*, **Hicks, B.***, Slater, C., Janson, K. D., Christ, G. J., & Russell, S. D. (2022). Comprehensive dynamic and kinematic analysis of the rodent hindlimb during over ground walking. Scientific Reports, 12(1), 19725. https://doi.org/10.1038/s41598-022-20288-3 *these authors contributed equally to this work

Hicks, B., Workman, A., Christ, G. J., Russell, S. D. (2023). Characterizing changes in rat gait kinematics and kinetics at different walking speeds. (In Prep)

Hicks, B., Nealon, C., Christ, G. J., Russell, S. D. (2023). A biomechanical analysis of rat gait to quantify functional deficits in response to volumetric muscle loss injury and repair. (In Prep)

Conference Presentations

Hicks, B., Dienes, J., Christ, G. C., Russell, S. D. Changes in rodent gait kinematics at different walking velocities. *North American Congress on Biomechanics (NACOB)*, Ottawa, Ontario, CN, August 2022

6.3 Future Work

This results from this thesis present many opportunities for future study into the modeling and analysis of rodent locomotion. The sections below present some ideas for future work that can be continued based on the results from this thesis.

6.3.1 Applying data collection and modeling methods to examine other pathologies

As previously stated, the methods developed in this work have primarily been applied to studies of volumetric muscle loss injury up to this point. However, it should be noted that VML injuries are typically accompanied by significant damage to peripheral nerve structures. Peripheral nerve injuries lead to a loss of sensory, motor, and autonomic signals conveyed to the denervated body segment, which can lead to significant atrophy in the affected muscle group (Menorca et al., 2013). Thus, more work should be done to investigate the impacts of muscle-nerve poly-traumas on locomotor function, in order to develop therapeutics targeted toward these more complex injuries.

In addition to VML, the rodent hindlimb is a common pre-clinical model system for evaluating a variety of other movement pathologies, including nerve injury, osteoarthritis, ligament injury, Parkinson's disease, and spinal cord injury. In each of these cases, varying forms of gait analysis have been used to gain insights into the various functional impacts of these pathologies. Applying the methods developed in this work to quantify 3-D kinetics would allow researchers to better analyze different compensation strategies by illuminating the driving forces behind movement patterns. Moreover, there is much work being done to optimize different therapies and treatment strategies for many of these pathologies. The methods developed herein provide unique insight into functional recovery, which will allow researchers to test and evaluate a variety of different treatments, therapies, and interventions in a pre-clinical setting.

6.3.2 Development of a gait deviation index for quantifying rodent locomotor function

3-D gait data (i.e. kinematics and kinetics) undoubtedly provides the most apt methodology for assessing overall gait pathology. However, the complex and intricate nature of gait data makes it difficult to interpret, as an evaluation of the motion of a limb over just a single stride requires the analysis of multiple joints and body segments, in multiple planes of motion, continuously over time (Schwartz & Rozumalski, 2008). In both humans and rats, many have attempted to simplify the interpretation of overall gait pathology via the use of locomotor scales or indices (Basso et al., 1995; Graham et al., 2004; Hillman et al., 2007; Novacheck et al., 2000). However, these methods are generally subjective in nature and often lack detail in their assessments of gait pathology. To address these concerns, several have worked to develop gait indices for humans which incorporate objective 3-D gait data into their locomotor rating systems, such as the Gillette Gait Index (GGI), Gait Deviation Index (GDI), or Gait Profile Score (GPS) (Baker et al., 2009; McMulkin & MacWilliams, 2015; Schutte et al., 2000; Schwartz & Rozumalski, 2008). While these analyses cannot provide specific insights into the causes and effects of gait pathologies at the joint level, they have been effective in quantifying deviations from normal gait in pathologic populations, such as in children with Cerebral Palsy (Schwartz & Rozumalski, 2008).

In this regard, it would be extremely useful to develop a Rodent Gait Deviation Index (RGDI) in order to provide a gross, interpretable metric for quantifying deviations in rodent gait. Furthermore, an RGDI could also be used to help contextualize functional recovery in studies evaluating different treatment efficacies. Typically, these gait indices require the acquisition of a large normative database to establish a reasonable estimate of the expected variance in gait parameters seen throughout the normal population. This work could leverage the expansive

normative database that was acquired throughout the completion of this thesis. More work would need to be done in order to identify the optimal set of gait parameters to be included in the RGDI. If completed, the RGDI could help provide an objective method with increased interpretability for quantifying gait deviations. It should be noted that this should not be used to replace a reporting of kinematics and kinetics, as a single numerical score is unable to fully address the many facets of pathologic gait adaptations.

6.3.3 Utilizing musculoskeletal modeling frameworks to gain muscle-level insights

Joint moments open the door for understanding neuromuscular motor control strategies at a new level. With joint moments as the launching pad, musculoskeletal modeling simulations such as static optimization or computed muscle control can further decompose joint moments to predict various muscle characteristics during gait, such as active fiber length, muscle force, and muscle activation (Crowninshield, 1978; Crowninshield & Brand, 1981; Seth et al., 2011; Thelen et al., 2003). Work done by Johnson et al. (2011) has elucidated many of the physiological parameters necessary to compute realistic muscle dynamics during simulations of rodent locomotion. In the future, this basis should be leveraged with the body-segment inertial parameters implemented herein, which are needed for the most accurate joint moment computations, to investigate muscle-tendon dynamics in the rodent hindlimb at a deeper level. The implications of this work are particularly exciting. Studies evaluating the effects of a particular pathology could adjust muscle properties to align with the injury in consideration. For instance, one could study changes in muscle recruitment after gastrocnemius denervation by dis-allowing gastrocnemius activation in the model during simulations. Ultimately, this work would provide deeper insight into the mechanisms behind compensatory movement patterns, which would be significant for developing treatments geared toward return to normal function.

6. References List

Akamatsu, F. E., Saleh, S. O., Teodoro, W. R., Silva, A. Q. da, Martinez, C. A. R., Duarte, R. J., Andrade, M. F. C. de, & Jacomo, A. L. (2014). Experimental model of Achilles tendon injury in rats. *Acta Cirurgica Brasileira*, *29*(7), 417–422. https://doi.org/10.1590/S0102-86502014000700002

Alexander, R. McN. (1984). The Gaits of Bipedal and Quadrupedal Animals. *The International Journal of Robotics Research*, *3*(2), 49–59. https://doi.org/10.1177/027836498400300205

Allbright, K. O., Bliley, J. M., Havis, E., Kim, D., Dibernardo, G. A., Grybowski, D., Waldner, M., James, I. B., Sivak, W. N., Rubin, J. P., & Marra, K. G. (2018). Delivery of adipose-derived stem cells in poloxamer hydrogel improves peripheral nerve regeneration. *Muscle & Nerve*, *58*(2), 251–260. https://doi.org/10.1002/mus.26094

Allen, K. D., Adams, S. B., Mata, B. A., Shamji, M. F., Gouze, E., Jing, L., Nettles, D. L., Latt, L. D., & Setton, L. A. (2011). Gait and behavior in an IL1β-mediated model of rat knee arthritis and effects of an IL1 antagonist. *Journal of Orthopaedic Research: Official Publication of the Orthopaedic Research Society*, *29*(5), 694–703. https://doi.org/10.1002/jor.21309

Allen, K. D., Mata, B. A., Gabr, M. A., Huebner, J. L., Adams, S. B., Kraus, V. B., Schmitt, D. O., & Setton, L. A. (2012). Kinematic and dynamic gait compensations resulting from knee instability in a rat model of osteoarthritis. *Arthritis Research & Therapy*, *14*(2), R78. https://doi.org/10.1186/ar3801

Alluin, O., Karimi-Abdolrezaee, S., Delivet-Mongrain, H., Leblond, H., Fehlings, M. G., & Rossignol, S. (2011). Kinematic study of locomotor recovery after spinal cord clip compression injury in rats. *Journal of Neurotrauma*, *28*(9), 1963–1981. https://doi.org/10.1089/neu.2011.1840

Amende, I., Kale, A., McCue, S., Glazier, S., Morgan, J. P., & Hampton, T. G. (2005). Gait dynamics in mouse models of Parkinson's disease and Huntington's disease. *Journal of NeuroEngineering and Rehabilitation*, *2*(1), 20. https://doi.org/10.1186/1743-0003-2-20

Andrada, E., Mämpel, J., Schmidt, A., Fischer, M. S., Karguth, A., & Witte, H. (2010). *Biomechanical analyses of rat locomotion during walking and climbing as a base for the design and construction of climbing robots*. 165–177. https://doi.org/10.2495/DN100151

Andrada, E., Mämpel, J., Schmidt, A., Fischer, M. S., Karguth, A., & Witte, H. (2013). From biomechanics of rats' inclined locomotion to a climbing robot. *International Journal of Design & Nature and Ecodynamics*, *8*(3), 192–212. https://doi.org/10.2495/DNE-V8-N3-192-212

Aurora, A., Garg, K., Corona, B. T., & Walters, T. J. (2014). Physical rehabilitation improves muscle function following volumetric muscle loss injury. *BMC Sports Science, Medicine and Rehabilitation*, *6*(1), 41. https://doi.org/10.1186/2052-1847-6-41

Baker, R., McGinley, J. L., Schwartz, M. H., Beynon, S., Rozumalski, A., Graham, H. K., & Tirosh, O. (2009). The Gait Profile Score and Movement Analysis Profile. *Gait & Posture*, *30*(3), 265–269. https://doi.org/10.1016/j.gaitpost.2009.05.020

Balbinot, G., Schuch, C. P., Jeffers, M. S., McDonald, M. W., Livingston-Thomas, J. M., & Corbett, D. (2018). Post-stroke kinematic analysis in rats reveals similar reaching abnormalities as humans. *Scientific Reports*, *8*(1), 8738. https://doi.org/10.1038/s41598-018-27101-0

Basso, D. M., Beattie, M. S., & Bresnahan, J. C. (1995). A Sensitive and Reliable Locomotor Rating Scale for Open Field Testing in Rats. *Journal of Neurotrauma*, *12*(1), 1–21. https://doi.org/10.1089/neu.1995.12.1

Batka, R. J., Brown, T. J., Mcmillan, K. P., Meadows, R. M., Jones, K. J., & Haulcomb, M. M. (2014). The Need for Speed in Rodent Locomotion Analyses: The Need for Speed. *The Anatomical Record*, *297*(10), 1839–1864. https://doi.org/10.1002/ar.22955

Bauman, J. M., & Chang, Y.-H. (2010). High-speed X-ray video demonstrates significant skin movement errors with standard optical kinematics during rat locomotion. *Journal of Neuroscience Methods*, *186*(1), 18–24. https://doi.org/10.1016/j.jneumeth.2009.10.017

Bauman, J. M., & Chang, Y.-H. (2013). Rules to limp by: Joint compensation conserves limb function after peripheral nerve injury. *Biology Letters*, *9*(5), 20130484. https://doi.org/10.1098/rsbl.2013.0484

Beare, J. E., Morehouse, J. R., DeVries, W. H., Enzmann, G. U., Burke, D. A., Magnuson, D. S. K., & Whittemore, S. R. (2009). Gait Analysis in Normal and Spinal Contused Mice Using the TreadScan System. *Journal of Neurotrauma*, *26*(11), 2045–2056. https://doi.org/10.1089/neu.2009.0914

Bennett, S. W., Lanovaz, J. L., & Muir, G. D. (2012). The biomechanics of locomotor compensation after peripheral nerve lesion in the rat. *Behavioural Brain Research*, *229*(2), 391–400. https://doi.org/10.1016/j.bbr.2012.01.040

Berryman, E. R., Harris, R. L., Moalli, M., & Bagi, C. M. (2009). *Digigait™ quantitation of gait dynamics in rat rheumatoid arthritis model*.

Bhimani, A. D., Kheirkhah, P., Arnone, G. D., Nahhas, C. R., Kumar, P., Wonais, M., Hidrogo, H., Aguilar, E., Spalinski, D., Gopalka, M., Roth, S., & Mehta, A. I. (2017). Functional gait analysis in a spinal contusion rat model. *Neuroscience & Biobehavioral Reviews*, *83*, 540–546. https://doi.org/10.1016/j.neubiorev.2017.09.007

Black, D. A., Lindley, S., Tucci, M., Lawyer, T., & Benghuzzi, H. (2011). A New Model for Repair of the Achilles Tendon in the Rat. *Journal of Investigative Surgery*, *24*(5), 217–221. https://doi.org/10.3109/08941939.2011.575915

Boettger, M. K., Weber, K., Schmidt, M., Gajda, M., Bräuer, R., & Schaible, H.-G. (2009). Gait abnormalities differentially indicate pain or structural joint damage in monoarticular antigen-induced arthritis. *Pain*, *145*(1–2), 142–150. https://doi.org/10.1016/j.pain.2009.06.006

Bonnet, C. S., Williams, A. S., Gilbert, S. J., Harvey, A. K., Evans, B. A., & Mason, D. J. (2015). AMPA/kainate glutamate receptors contribute to inflammation, degeneration and pain related behaviour in inflammatory stages of arthritis. *Annals of the Rheumatic Diseases*, *74*(1), 242–251. https://doi.org/10.1136/annrheumdis-2013-203670

Buchner, D. M., Cress, M. E., de Lateur, B. J., Esselman, P. C., Margherita, A. J., Price, R., & Wagner, E. H. (1997). The Effect of Strength and Endurance Training on Gait, Balance, Fall Risk, and Health Services Use in Community-Living Older Adults. *The Journals of Gerontology Series A: Biological Sciences and Medical Sciences*, *52A*(4), M218–M224. https://doi.org/10.1093/gerona/52A.4.M218

Burkholder, T. J., Fingado, B., Baron, S., & Lieber, R. L. (1994). Relationship between muscle fiber types and sizes and muscle architectural properties in the mouse hindlimb. *Journal of Morphology*, *221*(2), 177–190. https://doi.org/10.1002/jmor.1052210207

Canu, M.-H., & Garnier, C. (2009). A 3D analysis of fore- and hindlimb motion during overground and ladder walking: Comparison of control and unloaded rats. *Experimental*

Neurology, *218*(1), 98–108. https://doi.org/10.1016/j.expneurol.2009.04.009
Carnes, M. E., & Pins, G. D. (2020). Skeletal Muscle Tissue Engineering: Biomaterials-Based Strategies for the Treatment of Volumetric Muscle Loss. *Bioengineering*, *7*(3), 85. https://doi.org/10.3390/bioengineering7030085
Cendelín, J., Voller, J., & Vožeh, F. (2010). Ataxic gait analysis in a mouse model of the olivocerebellar degeneration. *Behavioural Brain Research*, *210*(1), 8–15. https://doi.org/10.1016/j.bbr.2010.01.035
Chang, Y.-H., Auyang, A. G., Scholz, J. P., & Nichols, T. R. (2009). Whole limb kinematics are preferentially conserved over individual joint kinematics after peripheral nerve injury. *Journal of Experimental Biology*, *212*(21), 3511–3521. https://doi.org/10.1242/jeb.033886
Charles, J. P., Cappellari, O., & Hutchinson, J. R. (2018). A Dynamic Simulation of Musculoskeletal Function in the Mouse Hindlimb During Trotting Locomotion. *Frontiers in Bioengineering and Biotechnology*, *6*, 61. https://doi.org/10.3389/fbioe.2018.00061
Choe, M.-A., Kyung Hwa Kim, Gyeong Ju An, Lee, K.-S., & Heitkemper, M. (2011). Hindlimb Muscle Atrophy Occurs From Peripheral Nerve Damage in a Rat Neuropathic Pain Model. *Biological Research For Nursing*, *13*(1), 44–54. https://doi.org/10.1177/1099800410382291
Cibulka, M., Wenthe, A., Boyle, Z., Callier, D., Schwerdt, A., Jarman, D., & Strube, M. J. (2017). VARIATION IN MEDIAL AND LATERAL GASTROCNEMIUS MUSCLE ACTIVITY WITH FOOT POSITION. *International Journal of Sports Physical Therapy*, *12*(2), 233–241.
Clarke, K. A., Heitmeyer, S. A., Smith, A. G., & Taiwo, Y. O. (1997). Gait analysis in a rat model of osteoarthrosis. *Physiology & Behavior*, *62*(5), 951–954. https://doi.org/10.1016/s0031-9384(97)00022-x
Clarke, K. A., & Parker, A. J. (1986). A quantitative study of normal locomotion in the rat. *Physiology & Behavior*, *38*(3), 345–351. https://doi.org/10.1016/0031-9384(86)90105-8
Cooney, D. S., Wimmers, E. G., Ibrahim, Z., Grahammer, J., Christensen, J. M., Brat, G. A., Wu, L. W., Sarhane, K. A., Lopez, J., Wallner, C., Furtmüller, G. J., Yuan, N., Pang, J., Sarkar, K., Lee, W. P. A., & Brandacher, G. (2016). Mesenchymal Stem Cells Enhance Nerve Regeneration in a Rat Sciatic Nerve Repair and Hindlimb Transplant Model. *Scientific Reports*, *6*, 31306. https://doi.org/10.1038/srep31306
Corona, B. T., Machingal, M. A., Criswell, T., Vadhavkar, M., Dannahower, A. C., Bergman, C., Zhao, W., & Christ, G. J. (2012). Further Development of a Tissue Engineered Muscle Repair Construct *In Vitro* for Enhanced Functional Recovery Following Implantation *In Vivo* in a Murine Model of Volumetric Muscle Loss Injury. *Tissue Engineering Part A*, *18*(11–12), 1213–1228. https://doi.org/10.1089/ten.tea.2011.0614
Corona, B. T., Ward, C. L., Baker, H. B., Walters, T. J., & Christ, G. J. (2013). Implantation of *In Vitro* Tissue Engineered Muscle Repair Constructs and Bladder Acellular Matrices Partially Restore *In Vivo* Skeletal Muscle Function in a Rat Model of Volumetric Muscle Loss Injury. *Tissue Engineering Part A*, 131219054609007. https://doi.org/10.1089/ten.tea.2012.0761
Coulthard, P., Simjee, S. U., & Pleuvry, B. J. (2003). Gait analysis as a correlate of pain induced by carrageenan intraplantar injection. *Journal of Neuroscience Methods*, *128*(1–2), 95–102. https://doi.org/10.1016/s0165-0270(03)00154-7
Crowninshield, R. D. (1978). Use of Optimization Techniques to Predict Muscle Forces. *Journal*

of Biomechanical Engineering, *100*(2), 88–92. https://doi.org/10.1115/1.3426197
Crowninshield, R. D., & Brand, R. A. (1981). A physiologically based criterion of muscle force prediction in locomotion. *Journal of Biomechanics*, *14*(11), 793–801. https://doi.org/10.1016/0021-9290(81)90035-x
Damiano, D. L., & Abel, M. F. (1998). Functional outcomes of strength training in spastic cerebral palsy. *Archives of Physical Medicine and Rehabilitation*, *79*(2), 119–125. https://doi.org/10.1016/S0003-9993(98)90287-8
Damiano, D. L., Arnold, A. S., Steele, K. M., & Delp, S. L. (2010). Can Strength Training Predictably Improve Gait Kinematics? A Pilot Study on the Effects of Hip and Knee Extensor Strengthening on Lower-Extremity Alignment in Cerebral Palsy. *Physical Therapy*, *90*(2), 269–279. https://doi.org/10.2522/ptj.20090062
Damiano, D. L., Prosser, L. A., Curatalo, L. A., & Alter, K. E. (2013). Muscle Plasticity and Ankle Control After Repetitive Use of a Functional Electrical Stimulation Device for Foot Drop in Cerebral Palsy. *Neurorehabilitation and Neural Repair*, *27*(3), 200–207. https://doi.org/10.1177/1545968312461716
DeLaurier, A., Burton, N., Bennett, M., Baldock, R., Davidson, D., Mohun, T. J., & Logan, M. P. (2008). The Mouse Limb Anatomy Atlas: An interactive 3D tool for studying embryonic limb patterning. *BMC Developmental Biology*, *8*(1), 83. https://doi.org/10.1186/1471-213X-8-83
Dellon, E. S., & Dellon, A. L. (1991). Functional Assessment of Neurologic Impairment: Track Analysis in Diabetic and Compression Neuropathies. *Plastic and Reconstructive Surgery*, *88*(4), 686–694. https://doi.org/10.1097/00006534-199110000-00020
Delp, S. L., Anderson, F. C., Arnold, A. S., Loan, P., Habib, A., John, C. T., Guendelman, E., & Thelen, D. G. (2007). OpenSim: Open-Source Software to Create and Analyze Dynamic Simulations of Movement. *IEEE Transactions on Biomedical Engineering*, *54*(11), 1940–1950. https://doi.org/10.1109/TBME.2007.901024
Dienes, J., Hicks, B., Slater, C., Janson, K. D., Christ, G. J., & Russell, S. D. (2022). Comprehensive dynamic and kinematic analysis of the rodent hindlimb during over ground walking. *Scientific Reports*, *12*(1), 19725. https://doi.org/10.1038/s41598-022-20288-3
Dienes, J., Hu, X., Janson, K. D., Slater, C., Dooley, E. A., Christ, G. J., & Russell, S. D. (2019). Analysis and Modeling of Rat Gait Biomechanical Deficits in Response to Volumetric Muscle Loss Injury. *Frontiers in Bioengineering and Biotechnology*, *7*, 146. https://doi.org/10.3389/fbioe.2019.00146
DiGiovanna, J., Dominici, N., Friedli, L., Rigosa, J., Duis, S., Kreider, J., Beauparlant, J., van den Brand, R., Schieppati, M., Micera, S., & Courtine, G. (2016). Engagement of the Rat Hindlimb Motor Cortex across Natural Locomotor Behaviors. *The Journal of Neuroscience: The Official Journal of the Society for Neuroscience*, *36*(40), 10440–10455. https://doi.org/10.1523/JNEUROSCI.4343-15.2016
Dutto, D. J., Hoyt, D. F., Clayton, H. M., Cogger, E. A., & Wickler, S. J. (2006). Joint work and power for both the forelimb and hindlimb during trotting in the horse. *Journal of Experimental Biology*, *209*(20), 3990–3999. https://doi.org/10.1242/jeb.02471
Dziki, J. L., Sicari, B. M., Wolf, M. T., Cramer, M. C., & Badylak, S. F. (2016). Immunomodulation and Mobilization of Progenitor Cells by Extracellular Matrix Bioscaffolds for Volumetric Muscle Loss Treatment. *Tissue Engineering Part A*, *22*(19–20), 1129–1139. https://doi.org/10.1089/ten.tea.2016.0340

Farris, D. J., & Sawicki, G. S. (2012). The mechanics and energetics of human walking and running: A joint level perspective. *Journal of the Royal Society, Interface*, *9*(66), 110–118. https://doi.org/10.1098/rsif.2011.0182

Ferland, C. E., Laverty, S., Beaudry, F., & Vachon, P. (2011). Gait analysis and pain response of two rodent models of osteoarthritis. *Pharmacology, Biochemistry, and Behavior*, *97*(3), 603–610. https://doi.org/10.1016/j.pbb.2010.11.003

Filipe, V. M., Pereira, J. E., Costa, L. M., Maurício, A. C., Couto, P. A., Melo-Pinto, P., & Varejão, A. S. P. (2006). Effect of skin movement on the analysis of hindlimb kinematics during treadmill locomotion in rats. *Journal of Neuroscience Methods*, *153*(1), 55–61. https://doi.org/10.1016/j.jneumeth.2005.10.006

Fu, S. C., Cheuk, Y. C., Hung, L. K., & Chan, K. M. (2012). Limb Idleness Index (LII): A novel measurement of pain in a rat model of osteoarthritis. *Osteoarthritis and Cartilage*, *20*(11), 1409–1416. https://doi.org/10.1016/j.joca.2012.08.006

Gambariẫn, P. P. (1974). *How mammals run: Anatomical adaptations*. Wiley.

Garg, K., Ward, C. L., Hurtgen, B. J., Wilken, J. M., Stinner, D. J., Wenke, J. C., Owens, J. G., & Corona, B. T. (2015). Volumetric muscle loss: Persistent functional deficits beyond frank loss of tissue: PERSISTENT FUNCTIONAL DEFICITS AFTER VML. *Journal of Orthopaedic Research*, *33*(1), 40–46. https://doi.org/10.1002/jor.22730

Garnier, C., Falempin, M., & Canu, M.-H. (2008). A 3D analysis of fore- and hindlimb motion during locomotion: Comparison of overground and ladder walking in rats. *Behavioural Brain Research*, *186*(1), 57–65. https://doi.org/10.1016/j.bbr.2007.07.023

Gillis, G. B., & Biewener, A. A. (2001). Hindlimb muscle function in relation to speed and gait: *In vivo* patterns of strain and activation in a hip and knee extensor of the rat (*Rattus norvegicus*). *Journal of Experimental Biology*, *204*(15), 2717–2731. https://doi.org/10.1242/jeb.204.15.2717

Górska, T., Chojnicka-Gittins, B., Majczyński, H., & Zmysłowski, W. (2007). Overground locomotion after incomplete spinal lesions in the rat: Quantitative gait analysis. *Journal of Neurotrauma*, *24*(7), 1198–1218. https://doi.org/10.1089/neu.2006.0219

Górska, T., Zmysłowski, W., & Majczyński, H. (1999). Overground locomotion in intact rats: Interlimb coordination, support patterns and support phases duration. *Acta Neurobiologiae Experimentalis*, *59*(2), 131–144.

Graham, H. K., Harvey, A., Rodda, J., Nattrass, G. R., & Pirpiris, M. (2004). The Functional Mobility Scale (FMS). *Journal of Pediatric Orthopedics*, *24*(5), 514–520. https://doi.org/10.1097/00004694-200409000-00011

Grasman, J. M., Zayas, M. J., Page, R. L., & Pins, G. D. (2015). Biomimetic scaffolds for regeneration of volumetric muscle loss in skeletal muscle injuries. *Acta Biomaterialia*, *25*, 2–15. https://doi.org/10.1016/j.actbio.2015.07.038

Gravel, P., Tremblay, M., Leblond, H., Rossignol, S., & de Guise, J. A. (2010). A semi-automated software tool to study treadmill locomotion in the rat: From experiment videos to statistical gait analysis. *Journal of Neuroscience Methods*, *190*(2), 279–288. https://doi.org/10.1016/j.jneumeth.2010.05.006

Grogan, B. F., & Hsu, J. R. (2011). Volumetric Muscle Loss: *American Academy of Orthopaedic Surgeon*, *19*, S35–S37. https://doi.org/10.5435/00124635-201102001-00007

Hamers, F. P. T., Lankhorst, A. J., van Laar, T. J., Veldhuis, W. B., & Gispen, W. H. (2001). Automated Quantitative Gait Analysis During Overground Locomotion in the Rat: Its Application to Spinal Cord Contusion and Transection Injuries. *Journal of Neurotrauma*,

18(2), 187–201. https://doi.org/10.1089/08977150150502613
Hamilton, C. B., Pest, M. A., Pitelka, V., Ratneswaran, A., Beier, F., & Chesworth, B. M. (2015). Weight-bearing asymmetry and vertical activity differences in a rat model of post-traumatic knee osteoarthritis. *Osteoarthritis and Cartilage*, *23*(7), 1178–1185. https://doi.org/10.1016/j.joca.2015.03.001
Herbin, M., Hackert, R., Gasc, J.-P., & Renous, S. (2007). Gait parameters of treadmill versus overground locomotion in mouse. *Behavioural Brain Research*, *181*(2), 173–179. https://doi.org/10.1016/j.bbr.2007.04.001
Hildebrand, M. (1980). The Adaptive Significance of Tetrapod Gait Selection. *American Zoologist*, *20*(1), 255–267. https://doi.org/10.1093/icb/20.1.255
Hildebrand, M. (1989). The Quadrupedal Gaits of Vertebrates. *BioScience*, *39*(11), 766–775. https://doi.org/10.2307/1311182
Hillman, S. J., Hazlewood, M. E., Schwartz, M. H., van der Linden, M. L., & Robb, J. E. (2007). Correlation of the Edinburgh Gait Score with the Gillette Gait Index, the Gillette Functional Assessment Questionnaire, and dimensionless speed. *Journal of Pediatric Orthopedics*, *27*(1), 7–11. https://doi.org/10.1097/BPO.0b013e31802b7104
Honert, E. C., & Pataky, T. C. (2021). Timing of gait events affects whole trajectory analyses: A statistical parametric mapping sensitivity analysis of lower limb biomechanics. *Journal of Biomechanics*, *119*, 110329. https://doi.org/10.1016/j.jbiomech.2021.110329
Howard, C. S., Blakeney, D. C., Medige, J., Moy, O. J., & Peimer, C. A. (2000). Functional assessment in the rat by ground reaction forces. *Journal of Biomechanics*, *33*(6), 751–757. https://doi.org/10.1016/S0021-9290(00)00023-3
Hoyt, D. F., & Taylor, C. R. (1981). Gait and the energetics of locomotion in horses. *Nature*, *292*(5820), 239–240. https://doi.org/10.1038/292239a0
Hruska, R. E., Kennedy, S., & Silbergeld, E. K. (1979). Quantitative aspects of normal locomotion in rats. *Life Sciences*, *25*(2), 171–179. https://doi.org/10.1016/0024-3205(79)90389-8
João, F., Amado, S., Veloso, A., Armada-da-Silva, P., & Maurício, A. C. (2010). Anatomical reference frame versus planar analysis: Implications for the kinematics of the rat hindlimb during locomotion. *Reviews in the Neurosciences*, *21*(6), 469–485.
Johnson, W. L., Jindrich, D. L., Hui Zhong, Roy, R. R., & Edgerton, V. R. (2011). Application of a Rat Hindlimb Model: A Prediction of Force Spaces Reachable Through Stimulation of Nerve Fascicles. *IEEE Transactions on Biomedical Engineering*, *58*(12), 3328–3338. https://doi.org/10.1109/TBME.2011.2106784
Johnson, W. L., Jindrich, D. L., Roy, R. R., & Reggie Edgerton, V. (2008). A three-dimensional model of the rat hindlimb: Musculoskeletal geometry and muscle moment arms. *Journal of Biomechanics*, *41*(3), 610–619. https://doi.org/10.1016/j.jbiomech.2007.10.004
Kappos, E. A., Sieber, P. K., Engels, P. E., Mariolo, A. V., D'Arpa, S., Schaefer, D. J., & Kalbermatten, D. F. (2017). Validity and reliability of the CatWalk system as a static and dynamic gait analysis tool for the assessment of functional nerve recovery in small animal models. *Brain and Behavior*, *7*(7), e00723. https://doi.org/10.1002/brb3.723
Kaufman, K. R., An, K. W., Litchy, W. J., & Chao, E. Y. (1991). Physiological prediction of muscle forces—I. Theoretical formulation. *Neuroscience*, *40*(3), 781–792. https://doi.org/10.1016/0306-4522(91)90012-d
Kemp, S. W. P., Phua, P. D., Stanoulis, K. N., Wood, M. D., Liu, E. H., Gordon, T., & Borschel, G. H. (2013). Functional recovery following peripheral nerve injury in the transgenic

Thy1 -GFP rat. *Journal of the Peripheral Nervous System*, *18*(3), 220–231. https://doi.org/10.1111/jns5.12035

Kloefkorn, H. E., Jacobs, B. Y., Loye, A. M., & Allen, K. D. (2015). Spatiotemporal gait compensations following medial collateral ligament and medial meniscus injury in the rat: Correlating gait patterns to joint damage. *Arthritis Research & Therapy*, *17*, 287. https://doi.org/10.1186/s13075-015-0791-2

Komatsu, I., Wang, J. H.-C., Iwasaki, K., Shimizu, T., & Okano, T. (2016). The effect of tendon stem/progenitor cell (TSC) sheet on the early tendon healing in a rat Achilles tendon injury model. *Acta Biomaterialia*, *42*, 136–146. https://doi.org/10.1016/j.actbio.2016.06.026

Koopmans, G. C., Deumens, R., Brook, G., Gerver, J., Honig, W. M. M., Hamers, F. P. T., & Joosten, E. A. J. (2007). Strain and locomotor speed affect over-ground locomotion in intact rats. *Physiology & Behavior*, *92*(5), 993–1001. https://doi.org/10.1016/j.physbeh.2007.07.018

Koopmans, G. C., Deumens, R., Honig, W. M. M., Hamers, F. P. T., Steinbusch, H. W. M., & Joosten, E. A. J. (2005). The Assessment of Locomotor Function in Spinal Cord Injured Rats: The Importance of Objective Analysis of Coordination. *Journal of Neurotrauma*, *22*(2), 214–225. https://doi.org/10.1089/neu.2005.22.214

Lakes, E. H., & Allen, K. D. (2016). Gait analysis methods for rodent models of arthritic disorders: Reviews and recommendations. *Osteoarthritis and Cartilage*, *24*(11), 1837–1849. https://doi.org/10.1016/j.joca.2016.03.008

Machingal, M. A., Corona, B. T., Walters, T. J., Kesireddy, V., Koval, C. N., Dannahower, A., Zhao, W., Yoo, J. J., & Christ, G. J. (2011). A Tissue-Engineered Muscle Repair Construct for Functional Restoration of an Irrecoverable Muscle Injury in a Murine Model. *Tissue Engineering Part A*, *17*(17–18), 2291–2303. https://doi.org/10.1089/ten.tea.2010.0682

Maerz, T., Kurdziel, M. D., Davidson, A. A., Baker, K. C., Anderson, K., & Matthew, H. W. T. (2015). Biomechanical Characterization of a Model of Noninvasive, Traumatic Anterior Cruciate Ligament Injury in the Rat. *Annals of Biomedical Engineering*, *43*(10), 2467–2476. https://doi.org/10.1007/s10439-015-1292-9

McIlwain, K. L., Merriweather, M. Y., Yuva-Paylor, L. A., & Paylor, R. (2001). The use of behavioral test batteries: Effects of training history. *Physiology & Behavior*, *73*(5), 705–717. https://doi.org/10.1016/S0031-9384(01)00528-5

McMulkin, M. L., & MacWilliams, B. A. (2015). Application of the Gillette Gait Index, Gait Deviation Index and Gait Profile Score to multiple clinical pediatric populations. *Gait & Posture*, *41*(2), 608–612. https://doi.org/10.1016/j.gaitpost.2015.01.005

Menorca, R. M. G., Fussell, T. S., & Elfar, J. C. (2013). Nerve physiology: Mechanisms of injury and recovery. *Hand Clinics*, *29*(3), 317–330. https://doi.org/10.1016/j.hcl.2013.04.002

Merritt, E. K., Hammers, D. W., Tierney, M., Suggs, L. J., Walters, T. J., & Farrar, R. P. (2010). Functional assessment of skeletal muscle regeneration utilizing homologous extracellular matrix as scaffolding. *Tissue Engineering. Part A*, *16*(4), 1395–1405. https://doi.org/10.1089/ten.TEA.2009.0226

Mintz, E. L., Passipieri, J. A., Lovell, D. Y., & Christ, G. J. (2016). Applications of In Vivo Functional Testing of the Rat Tibialis Anterior for Evaluating Tissue Engineered Skeletal Muscle Repair. *Journal of Visualized Experiments: JoVE*, *116*, 54487.

https://doi.org/10.3791/54487
Mountney, A., Leung, L. Y., Pedersen, R., Shear, D., & Tortella, F. (2013). Longitudinal assessment of gait abnormalities following penetrating ballistic-like brain injury in rats. *Journal of Neuroscience Methods*, *212*(1), 1–16. https://doi.org/10.1016/j.jneumeth.2012.08.025
Muir, G. D., & Whishaw, I. Q. (1999a). Ground reaction forces in locomoting hemi-parkinsonian rats: A definitive test for impairments and compensations. *Experimental Brain Research*, *126*(3), 307–314. https://doi.org/10.1007/s002210050739
Muir, G. D., & Whishaw, I. Q. (1999b). Complete locomotor recovery following corticospinal tract lesions: Measurement of ground reaction forces during overground locomotion in rats. *Behavioural Brain Research*, *103*(1), 45–53. https://doi.org/10.1016/S0166-4328(99)00018-2
Nakahata, A., Iijima, H., Tanima-Nagai, M., Ito, A., Tajino, J., Kyan, W., Zang, J., Ji, X., Wang, T., Aoyama, T., Nishitani, K., & Kuroki, H. (2018). Gait kinematics changes in post traumatic knee osteoarthritis with destabilized medial meniscus in rat. *Osteoarthritis and Cartilage*, *26*, S390. https://doi.org/10.1016/j.joca.2018.02.759
Neckel, N. D. (2015). Methods to quantify the velocity dependence of common gait measurements from automated rodent gait analysis devices. *Journal of Neuroscience Methods*, *253*, 244–253. https://doi.org/10.1016/j.jneumeth.2015.06.017
Neckel, N. D., Dai, H., & Bregman, B. S. (2013). Quantifying changes following spinal cord injury with velocity dependent locomotor measures. *Journal of Neuroscience Methods*, *214*(1), 27–36. https://doi.org/10.1016/j.jneumeth.2013.01.008
Nica, I., Deprez, M., Nuttin, B., & Aerts, J.-M. (2017). Automated Assessment of Endpoint and Kinematic Features of Skilled Reaching in Rats. *Frontiers in Behavioral Neuroscience*, *11*, 255. https://doi.org/10.3389/fnbeh.2017.00255
Novacheck, T. F., Stout, J. L., & Tervo, R. (2000). Reliability and validity of the Gillette Functional Assessment Questionnaire as an outcome measure in children with walking disabilities. *Journal of Pediatric Orthopedics*, *20*(1), 75–81.
Passipieri, J. A., Baker, H. B., Siriwardane, M., Ellenburg, M. D., Vadhavkar, M., Saul, J. M., Tomblyn, S., Burnett, L., & Christ, G. J. (2017). Keratin Hydrogel Enhances *In Vivo* Skeletal Muscle Function in a Rat Model of Volumetric Muscle Loss. *Tissue Engineering Part A*, *23*(11–12), 556–571. https://doi.org/10.1089/ten.tea.2016.0458
Passipieri, J. A., Hu, X., Mintz, E., Dienes, J., Baker, H. B., Wallace, C. H., Blemker, S. S., & Christ, G. J. (2019). *In Silico* and *In Vivo* Studies Detect Functional Repair Mechanisms in a Volumetric Muscle Loss Injury. *Tissue Engineering Part A*, *25*(17–18), 1272–1288. https://doi.org/10.1089/ten.tea.2018.0280
Pataky, T. C. (2012). One-dimensional statistical parametric mapping in Python. *Computer Methods in Biomechanics and Biomedical Engineering*, *15*(3), 295–301. https://doi.org/10.1080/10255842.2010.527837
Pereira, J. E., Cabrita, A. M., Filipe, V. M., Bulas-Cruz, J., Couto, P. A., Melo-Pinto, P., Costa, L. M., Geuna, S., Maurício, A. C., & Varejão, A. S. P. (2006). A comparison analysis of hindlimb kinematics during overground and treadmill locomotion in rats. *Behavioural Brain Research*, *172*(2), 212–218. https://doi.org/10.1016/j.bbr.2006.04.027
Perrot, O., Laroche, D., Pozzo, T., & Marie, C. (2011). Kinematics of obstacle clearance in the rat. *Behavioural Brain Research*, *224*(2), 241–249. https://doi.org/10.1016/j.bbr.2011.05.027

Riemann, B. L., Limbaugh, G. K., Eitner, J. D., & LeFavi, R. G. (2011). Medial and lateral gastrocnemius activation differences during heel-raise exercise with three different foot positions. *Journal of Strength and Conditioning Research*, *25*(3), 634–639. https://doi.org/10.1519/JSC.0b013e3181cc22b8

Robbins, S. M., Birmingham, T. B., Jones, I. C., Sischek, E. L., Dietzsch, M., & Giffin, J. R. (2016). Comparison of Gait Characteristics Between Patients With Nontraumatic and Posttraumatic Medial Knee Osteoarthritis. *Arthritis Care & Research*, *68*(9), 1215–1223. https://doi.org/10.1002/acr.22822

Roemhildt, M. L., Gardner-Morse, M., Rowell, C., Beynnon, B. D., & Badger, G. J. (2010). Gait alterations in rats following attachment of a device and application of altered knee loading. *Journal of Biomechanics*, *43*(16), 3227–3231. https://doi.org/10.1016/j.jbiomech.2010.07.036

Schmidt, A., & Fischer, M. S. (2011). The kinematic consequences of locomotion on sloped arboreal substrates in a generalized (*Rattus norvegicus*) and a specialized (*Sciurus vulgaris*) rodent. *Journal of Experimental Biology*, *214*(15), 2544–2559. https://doi.org/10.1242/jeb.051086

Schutte, L. M., Narayanan, U., Stout, J. L., Selber, P., Gage, J. R., & Schwartz, M. H. (2000). An index for quantifying deviations from normal gait. *Gait & Posture*, *11*(1), 25–31. https://doi.org/10.1016/S0966-6362(99)00047-8

Schutte, L. M., Rodgers, M. M., Zajac, F. E., & Glaser, R. M. (1993). Improving the efficacy of electrical stimulation-induced leg cycle ergometry: An analysis based on a dynamic musculoskeletal model. *IEEE Transactions on Rehabilitation Engineering*, *1*(2), 109–125. https://doi.org/10.1109/86.242425

Schwartz, M. H., & Rozumalski, A. (2008). The gait deviation index: A new comprehensive index of gait pathology. *Gait & Posture*, *28*(3), 351–357. https://doi.org/10.1016/j.gaitpost.2008.05.001

Seth, A., Sherman, M., Reinbolt, J. A., & Delp, S. L. (2011). OpenSim: A musculoskeletal modeling and simulation framework for in silico investigations and exchange. *Procedia IUTAM*, *2*, 212–232. https://doi.org/10.1016/j.piutam.2011.04.021

Simjee, S., Jawed, H., Quadri, J., & Saeed, S. (2007). Quantitative gait analysis as a method to assess mechanical hyperalgesia modulated by disease-modifying antirheumatoid drugs in the adjuvant-induced arthritic rat. *Arthritis Research & Therapy*, *9*(5), R91. https://doi.org/10.1186/ar2290

Slater, L. V., Hart, J. M., Kelly, A. R., & Kuenze, C. M. (2017). Progressive Changes in Walking Kinematics and Kinetics After Anterior Cruciate Ligament Injury and Reconstruction: A Review and Meta-Analysis. *Journal of Athletic Training*, 1062-6050.52.6.06. https://doi.org/10.4085/1062-6050.52.6.06

Tamura, A., Akasaka, K., & Otsudo, T. (2021). Contribution of Lower Extremity Joints on Energy Absorption during Soft Landing. *International Journal of Environmental Research and Public Health*, *18*(10), 5130. https://doi.org/10.3390/ijerph18105130

Thelen, D. G., & Anderson, F. C. (2006). Using computed muscle control to generate forward dynamic simulations of human walking from experimental data. *Journal of Biomechanics*, *39*(6), 1107–1115. https://doi.org/10.1016/j.jbiomech.2005.02.010

Thelen, D. G., Anderson, F. C., & Delp, S. L. (2003). Generating dynamic simulations of movement using computed muscle control. *Journal of Biomechanics*, *36*(3), 321–328. https://doi.org/10.1016/S0021-9290(02)00432-3

Thota, A. K., Watson, S. C., Knapp, E., Thompson, B., & Jung, R. (2005). Neuromechanical control of locomotion in the rat. *Journal of Neurotrauma*, *22*(4), 442–465. https://doi.org/10.1089/neu.2005.22.442

Topp, R., Mikesky, A., Wigglesworth, J., Holt, W., & Edwards, J. E. (1993). The Effect of a 12-week Dynamic Resistance Strength Training Program on Gait Velocity and Balance of Older Adults. *The Gerontologist*, *33*(4), 501–506. https://doi.org/10.1093/geront/33.4.501

Vincelette, J., Xu, Y., Zhang, L.-N., Schaefer, C. J., Vergona, R., Sullivan, M. E., Hampton, T. G., & Wang, Y.-X. (2007). Gait analysis in a murine model of collagen-induced arthritis. *Arthritis Research & Therapy*, *9*(6), R123. https://doi.org/10.1186/ar2331

Vlamings, R., Visser-Vandewalle, V., Koopmans, G., Joosten, E. A. J., Kozan, R., Kaplan, S., Steinbusch, H. W. M., & Temel, Y. (2007). High frequency stimulation of the subthalamic nucleus improves speed of locomotion but impairs forelimb movement in Parkinsonian rats. *Neuroscience*, *148*(3), 815–823. https://doi.org/10.1016/j.neuroscience.2007.06.043

Webb, A. A., Kerr, B., Neville, T., Ngan, S., & Assem, H. (2011). Kinematics and Ground Reaction Force Determination: A Demonstration Quantifying Locomotor Abilities of Young Adult, Middle-aged, and Geriatric Rats. *Journal of Visualized Experiments*, *48*, 2138. https://doi.org/10.3791/2138

Wehner, T., Wolfram, U., Henzler, T., Niemeyer, F., Claes, L., & Simon, U. (2010). Internal forces and moments in the femur of the rat during gait. *Journal of Biomechanics*, *43*(13), 2473–2479. https://doi.org/10.1016/j.jbiomech.2010.05.028

Winter, D. A. (2009). *Biomechanics and motor control of human movement* (4th ed). Wiley.

Wooley, C. M., Xing, S., Burgess, R. W., Cox, G. A., & Seburn, K. L. (2009). Age, experience and genetic background influence treadmill walking in mice. *Physiology & Behavior*, *96*(2), 350–361. https://doi.org/10.1016/j.physbeh.2008.10.020

Wu, G., & Cavanagh, P. R. (1995). ISB recommendations for standardization in the reporting of kinematic data. *Journal of Biomechanics*, *28*(10), 1257–1261. https://doi.org/10.1016/0021-9290(95)00017-c

Wu, X., Corona, B. T., Chen, X., & Walters, T. J. (2012). A Standardized Rat Model of Volumetric Muscle Loss Injury for the Development of Tissue Engineering Therapies. *BioResearch Open Access*, *1*(6), 280–290. https://doi.org/10.1089/biores.2012.0271

Zajac, F. E. (1989). Muscle and tendon: Properties, models, scaling, and application to biomechanics and motor control. *Critical Reviews in Biomedical Engineering*, *17*(4), 359–411.